1996

Molecular dynamics simulations of multiple-layer thin film growth on fcc(001) metal surfaces

Cynthia Lynne Kelchner
Iowa State University

INFORMATION TO USERS

This manuscript has been reproduced from the microfilm master. UMI films the text directly from the original or copy submitted. Thus, some thesis and dissertation copies are in typewriter face, while others may be from any type of computer printer.

The quality of this reproduction is dependent upon the quality of the copy submitted. Broken or indistinct print, colored or poor quality illustrations and photographs, print bleedthrough, substandard margins, and improper alignment can adversely affect reproduction.

In the unlikely event that the author did not send UMI a complete manuscript and there are missing pages, these will be noted. Also, if unauthorized copyright material had to be removed, a note will indicate the deletion.

Oversize materials (e.g., maps, drawings, charts) are reproduced by sectioning the original, beginning at the upper left-hand corner and continuing from left to right in equal sections with small overlaps. Each original is also photographed in one exposure and is included in reduced form at the back of the book.

Photographs included in the original manuscript have been reproduced xerographically in this copy. Higher quality 6" x 9" black and white photographic prints are available for any photographs or illustrations appearing in this copy for an additional charge. Contact UMI directly to order.

UMI

A Bell & Howell Information Company
300 North Zeeb Road, Ann Arbor, MI 48106-1346 USA
313/761-4700 800/521-0600

Molecular dynamics simulations of multiple-layer thin film growth on fcc(001) metal surfaces

by

Cynthia Lynne Kelchner

A dissertation submitted to the graduate faculty

in partial fulfillment of the requirements for the degree of

DOCTOR OF PHILOSOPHY

Department: Chemistry

Major: Physical Chemistry

Major Professor: Andrew E. DePristo

Iowa State University

Ames, Iowa

1996

Graduate College
Iowa State University

This is to certify that the doctoral dissertation of

Cynthia Lynne Kelchner

has met the dissertation requirements of Iowa State University

Signature was redacted for privacy.

Major Professor

Signature was redacted for privacy.

For the Major Department

Signature was redacted for privacy.

For the Graduate College

TABLE OF CONTENTS

ABSTRACT

Molecular dynamics simulations are a valuable tool for understanding thin film growth since individual deposition events and atomic growth mechanisms cannot be studied with current experimental techniques. In this dissertation, multiple-layer homoepitaxial thin film growth is studied in detail using reliable interatomic potentials for fcc metals from corrected effective medium theory. The development of these potentials from experimental data on the bulk and on the diatomic molecule is described.

Two features are observed to be important during the growth of 50-layer thin films by deposition of single atoms of Pd on Pd(001) and Cu on Cu(001) at 80 K. First, a fourfold hollow site that is missing one or more of its four supporting atoms on the surface (i.e., an overhang site) can be stable. This increases the surface roughness by allowing defects in the growing surface. Second, multiatom rearrangements occur during growth and decrease the local surface roughness by filling deep holes in the surface. Neither of these features is included in currently used kinetic growth models.

The growth behavior of the thin film changes after deposition of the first 5-10 layers: more overhanging atoms are present, the surface is rougher, and multiple-layer events begin to occur. The formation of large voids in the film and the mechanism of multiatom rearrangement events are discussed. There is no clear difference between Pd and Cu thin film growth at this low temperature.

Results are also presented for the deposition of 5- and 10-atom clusters during growth of 20-layer homoepitaxial films on Pd(001) and Cu(001) at 80 K, along with initial deposition results for 100-atom clusters. The growth of these thin films by low energy cluster deposition

is much rougher than that of films grown by single atom deposition. This can be attributed to two factors: (1) most deposition events add atoms to two or more layers; and (2) the growth of (111) facets on the surface produces many partially exposed atoms. Thin films grown by deposition of larger clusters tend to be rougher than those produced by smaller clusters.

GENERAL INTRODUCTION

Dissertation Organization

This dissertation contains four papers which have been prepared for publication in scholarly journals. The majority of the research and writing in each paper was performed by the first author (C. L. Kelchner). The problem of interest and the necessary background material are detailed in the general introduction. The first paper, "Construction and evaluation of embedding functions," has been published in Surface Science. The second paper, "Molecular dynamics simulation of multilayer homoepitaxial deposition on fcc(100) metal surfaces," has been accepted for publication by the Journal of Vacuum Science and Technology A. The third paper, "Molecular dynamics simulations of multilayer homoepitaxial thin film growth," has been submitted to Surface Science. The fourth paper, "Molecular dynamics simulations of homoepitaxial thin film growth via cluster deposition," has been prepared for submission to Nanostructured Materials. A general conclusion chapter is included at the end of the dissertation.

Literature Review

Thin films are used in many industrial applications such as electronic devices, printed circuit boards, and optical coatings. The properties of a thin film can differ substantially from the properties of the bulk material, often leading to novel materials and applications. Many of these new properties are quite sensitive to the microscopic structure of the film as well as to the film thickness.

The microscopic structure of a thin film is to a large extent determined by the conditions under which the film is grown.[1] Molecular beam epitaxy is an important experimental technique used to deposit atoms from the vapor phase onto a substrate under carefully controlled conditions. This method requires an ultrahigh vacuum system and yields high purity films.[2,3] Varying the deposition conditions (e.g., temperature and flux) can greatly change the microstructure of the growing thin film, and the necessary conditions for a desired film structure are typically determined empirically. The fundamental question of how the experimental conditions affect the deposition dynamics and growth mechanisms is vital to both understanding thin film growth and predicting results for thin films with different materials and deposition conditions.

Three distinct modes of thin film growth have been observed experimentally for epitaxial growth.[4] The simplest growth mode is layer-by-layer (Frank-van der Merwe [FV] growth) where one layer is completely filled before atoms begin to fill the next layer. This results in an atomically smooth surface. The roughest growth mode is three dimensional (Volmer-Weber [VW] growth) where the deposited atoms form three-dimensional (3D) clusters on the surface and may not completely cover the substrate until many atoms have been deposited. The third growth mode (Stranski-Krastanov [SK] growth) is a combination of the other two modes where the growth is layer-by-layer for the first few layers and then begins to form 3D clusters. Layer-by-layer growth is in general the most desirable since many thin film applications require films which are atomically smooth on the surface. It is also the least common growth mode, particularly for heteroepitaxial systems.

A surface at equilibrium has distinct thermodynamic properties defined separately from bulk properties, including the surface energy, surface entropy, and surface total free energy.[5] The equilibrium growth mode (FV, VW, or SK) of a thin film can be determined from the comparison of surface free energies for the substrate, adsorbate, and substrate-adsorbate interface,[4] although these free energies are often unknown. A surface can reach its equilibrium state by surface diffusion or other atom transport mechanisms given enough time and adatom mobility, whether the surface was originally cleaved from a bulk crystal or recrystallized from the melt or grown by deposition of atoms on a substrate.

Under typical growth conditions, however, the deposition and growth of a thin film do not occur at equilibrium. This means that the growth is limited by the kinetics of the deposition process, surface diffusion, and other events. The thermodynamics of the system (e.g., surface free energies of substrate and adsorbate) are not relevant when the growing film does not have enough time or energy to reach the most energetically stable configuration but is locked into a metastable state by the kinetics of the system.[1,6] Therefore one must use caution in applying descriptions and explanations of equilibrium surface behavior and energetics to the non-equilibrium growth of thin films.

Many experimental studies have explored the early stages of thin film growth.[7,8,9] The results often show interesting island shapes which depend on the growth conditions. For example, at high flux one can produce dendritic islands while decreasing the flux yields fractal islands for the same system.[8] It has also been shown that the islands on a Pt (111) surface tend to become more compact as the temperature increases and can be hexagonal or triangular depending on the temperature and coverage.[9]

A number of kinetic and statistical models have been developed to help explain the experimental results.[3,10] For example, the diffusion limited aggregation (DLA) model describes the behavior of adsorbed atoms diffusing on the surface at very low coverage.[3,11] The random deposition (RD) model[10,12] describes deposition when atoms do not move after hitting the surface. Variations of the RD model specify the sites where atoms can stick, e.g., in ballistic deposition[10] the depositing atoms stick wherever they find a nearest neighbor. The solid-on-solid model[10] and kinetic Monte Carlo (KMC) simulations[13] can include a variety of rules and rate equations regarding the deposition and subsequent diffusion of atoms. The downward funneling model[14] describes how a depositing atom first reaches a stable adsorption site. Some of these models are intended to describe only the initial growth of a film (e.g., DLA) while others have no explicit limit on their validity range. These simple models can include the large numbers of atoms necessary for the study of surfaces and film growth.

Each of these models explicitly states the processes which are allowed to occur during deposition. Some of the models can be fine-tuned to reproduce experimental results, e.g., varying the rates of various events in KMC.[15] However, none of the models are truly predictive because they cannot predict events which are completely unknown. These unknown types of events are likely to be more complicated or very rare events, perhaps involving a large number of atoms, multiple layers of the film, or some other unusual mechanism.

There is one further theoretical method which does not require the user to define the types of processes that can occur during deposition and which can still handle a large number of atoms. This method is classical molecular dynamics (MD) and consists of calculating the

forces on every atom then moving the atoms according to Newton's equations of motion.[16] An MD simulation puts no restrictions on the allowed processes and can be thought of as a "numerical experiment" where the system is followed for a length of time to observe what happens. This is a significant improvement over the simpler models described above.

The great advantage of doing a molecular dynamics simulation rather than an actual experiment is the ease of analysis of individual atomic motions during thin film growth. Current experimental techniques are not able to follow the motion of individual atoms in such detail and often cannot distinguish between the various processes which may be occurring on the surface. The disadvantage of MD is the limited time scale of the simulation. The total length of a simulation is currently limited by computational constraints to nanoseconds whereas typical experiments require minutes or hours. Therefore careful consideration must be given to the choice of systems and deposition conditions studied with MD.

The MD method does make some assumptions about how the atoms in the system interact via interatomic potentials. The accuracy of these potentials determines the reliability of the MD simulation results. (The most accurate MD simulations involve quantum mechanical descriptions, rather than classical, of the interactions between atoms and are prohibitively expensive for the many atoms needed to model thin film growth.[17]) One of the earliest and most general interatomic potentials was the Lennard-Jones (L-J) pair potential.[18] This potential determines the interaction between two spherically symmetric atoms and can be used to model a class of effects rather than processes specific to a given system. The L-J potential form has been used to study a wide range of systems (e.g., Ar, Si, and Cu).[19]

Another type of interatomic potential which has seen widespread use is that from the embedded atom method (EAM).[20] These semiempirical potentials include a many-body contribution to the energy which is important for the description of surfaces and metallic systems. Similar interatomic potentials have been developed in effective medium (EM) theory.[21] The interatomic potentials used in the present work have been developed within corrected effective medium (CEM) theory which will be discussed in the following section. The first chapter of this dissertation describes the development of these interatomic potentials from experimental data on the bulk and on the diatomic molecule for a number of fcc metals.

One problem with the kinetic and statistical models mentioned above is that they have been developed from data on the early stages of thin film growth. This low coverage regime is certainly important and can greatly influence the structure of a thin film. However, there may be more information to obtain when many layers have been deposited in a thin film since the atomic growth mechanisms may change as a function of the film thickness. A good example of this is the SK growth mode described earlier, where the growth is initially layer-by-layer and then changes to 3D growth at some film thickness. These growth mode changes cannot be predicted by simple models which only contain information from the low coverage regime of thin film growth. There have been many experimental studies on the growth of thin films during deposition of many layers[22] but little is known about the atomic growth mechanisms specific to this regime. (One recent model[23] does include information regarding the transition to multilayer growth.)

Molecular dynamics is an effective tool for studying atomic interactions during thin film growth. A number of MD simulations with reliable interatomic potentials for fcc metals (from

CEM, EM, and EAM) have been used to study surface events at low coverage[24] as well as during the growth of a few layers.[25] Simulations of thin film growth involving multiple layers have been performed using a simple Lennard-Jones potential nominally fit to a metal[19] and also for covalent materials such as Si and Ge.[26] The research presented in the second and third chapters of this dissertation represents the first molecular dynamics simulations of multiple-layer (> 10) homoepitaxial thin film growth using reliable interatomic potentials for fcc metals.

There is also a great deal of interest in depositing clusters of atoms instead of single atoms to grow thin films.[27, 28] Two different results are anticipated from cluster deposition. One possibility is that the clusters will create a good, strongly adhering thin film. This can happen by depositing high energy clusters,[28] where the energy is localized on the surface upon cluster adsorption and promotes annealing of defects and epitaxial growth. Another possible result, particularly from low energy cluster deposition, is that the film will retain some of the original cluster structure and properties, leading to new types of materials.[29] Experimental evidence has been seen for both of these situations.

Thin film growth by cluster deposition is a relatively new field and not much is known about the growth mechanisms.[27] A number of MD studies have explored the deposition of one cluster on a clean surface[30] but few have studied the full deposition process of many clusters during thin film growth.[31] The final chapter of this dissertation presents MD simulations of the growth of multiple-layer thin films during the low energy deposition of small clusters.

Corrected Effective Medium Theory

The details of CEM theory have been presented previously,[32] including a recent critical review,[33] and the theory is briefly outlined here. For a system of atoms, $\{A_i, i=1,...,N\}$, the CEM interaction energy is

$$\Delta E\left(\{A_i\}\right) = \sum_{i=1}^{N} \Delta E_J\left(A_i; n_i\right) + \sum_{i=1}^{N}\sum_{j>i}^{N} V_c(i,j) + \Delta G\left(\{A_i\}\right) \qquad \textbf{Eq. 1}$$

The jellium density, n_i, is

$$n_i = \frac{1}{2}\sum_{j\neq i}^{N} \int \frac{n\left(A_i; \bar{r} - \bar{R}_i\right)}{Z_i} n\left(A_j; \bar{r} - \bar{R}_j\right) d\bar{r} \qquad \textbf{Eq. 2}$$

where $n(A_i;\boldsymbol{r} - \boldsymbol{R}_i)$ is the atomic electron density distribution as taken from Hartree-Fock calculations[34] and represented in even-tempered Gaussians[35] for computational ease. Z_i and $\boldsymbol{R}_i$ are the atomic number and nuclear position, respectively. The underlying approximation leading to Eq.(1) is that the total system electron density is equal to the superposition of atomic electron densities.

The first right-hand-side (RHS) term in Eq.(1) is the sum of the embedding energy for each atom, where the embedding energy is solely a function of the average electron density environment of that particular type of atom. The average electron (jellium) density is provided by Eq.(2). The subscript "J" in Eq.(1) stands for jellium. It is worthwhile to emphasize that the only unknown part of the interaction energy expression in Eq.(1) is the embedding function. Once this is specified for each atom type, the CEM theory can be used to predict the interaction energies for a system in any geometry.

The second RHS term consists of pairwise additive Coulomb energies: $V_c(i,j)$ is the sum of electron-electron, electron-nuclear, and nuclear-nuclear Coulomb interactions between atoms A_i and A_j. These are determined from the electron densities of each atom.[36]

The last RHS term is the difference in kinetic-exchange-correlation energy between the N-atom and atom-in-jellium systems and is given by the explicit expression

$$\Delta G\left(\{A_i\}\right) = \left[G\left(\{A_i\}\right) - \sum_{i=1}^{N} G\left(A_i\right)\right] - \sum_{i=1}^{N}\left[G\left(A_i + n_i\right) - G\left(A_i\right) - G\left(n_i\right)\right] \qquad \textbf{Eq. 3}$$

It is a many body correction. The $G(S)$ term is a complicated functional of the electron density and its gradient that is completely specified by the atomic electron densities for a system S.

This final term, ΔG, is computationally intensive and limits the application of CEM theory to small systems (< 200 atoms). It is therefore this quantity that must be approximated in Eq.(1) in order to study large systems or to perform simulations using molecular dynamics or Monte Carlo methods. One approximation, known as MD/MC-CEM, was developed by assuming that ΔG is simply a function of the jellium density.[37] The value of ΔG is determined from the bulk system and incorporated into new "effective" embedding functions, $\Delta F_J(A_i;n_i)$, leading to the following equation for the MD/MC-CEM interaction energy.

$$\Delta E\left(\{A_i\}\right) = \sum_{i=1}^{N} \Delta F_J\left(A_i;n_i\right) + \sum_{i=1}^{N}\sum_{j>i}^{N} V_c\left(i,j\right) \qquad \textbf{Eq. 4}$$

The MD/MC-CEM approximation has been used successfully in a number of applications[38] and is the method used in the research presented here.

A different approximation has been made to CEM theory by replacing ΔG with a two-body function[39] rather than with the bulk value. This method has some advantages and

disadvantages compared to the MD/MC-CEM method. Further details of the approximation and sample applications can be found in Ref. [39].

References

[1] E. S. Machlin, *Materials Science in Microelectronics: The relationships between thin film processing and structure* (Giro Press, Croton-on-Hudson, NY, 1995).

[2] M. Ohring, *The Materials Science of Thin Films* (Academic Press, San Diego, CA, 1992) ch. 7;
K. J. Klabunde, *Thin Films from Free Atoms and Particles* (Academic Press, Orlando, FL, 1985) ch. 5.

[3] A.-L. Barabási and H. E. Stanley, *Fractal Concepts in Surface Growth* (Cambridge University Press, Cambridge, 1995).

[4] A. Zangwill, *Physics at Surfaces*, (Cambridge University Press, Cambridge, 1988) ch. 16.

[5] G. A. Somorjai, *Introduction to Surface Chemistry and Catalysis* (John Wiley & Sons, New York, 1994) ch. 3.

[6] J. Lapujoulade, Surf. Sci. Rep. **20**, 191 (1994).

[7] H. Brune, H. Röder, C. Boragno, and K. Kern, Phys. Rev. Lett. **73**, 1955 (1994);
J.-K. Zuo, J. F. Wendelken, H. Dürr, and C.-L. Liu, Phys. Rev. Lett. **72**, 3064 (1994);
R. Q. Hwang, C. Günther, J. Schröder, S. Günther, E. Kopatzki, and R. J. Behm, J. Vac. Sci. Tech. A **10**, 1970 (1992);
R. Q. Hwang, J. Schröder, C. Günther, and R. J. Behm, Phys. Rev. Lett. **67**, 3279 (1991).

[8] H. Brune, C. Romainczyk, H. Röder, and K. Kern, Nature **369**, 469 (1994).

[9] T. Michely, M. Hohage, M. Bott, and G. Comsa, Phys. Rev. Lett. **70**, 3943 (1993).

[10] F. Family, Physics A **168**, 561 (1990).

[11] L. M. Sander, in *Solids Far From Equilibrium*, ed. C. Godrèche (Cambridge University Press, Cambridge, 1991) ch. 5.

[12] J. W. Evans, Phys. Rev. B **39**, 5655 (1989).

[13] P. Nielaba, V. Privman, and J.-S. Wang, J. Phys. A: Math. Gen. **23**, L1187 (1990).

[14] J. W. Evans, D. E. Sanders, P. A. Thiel, and A. E. DePristo, Phys. Rev. B **41**, 5410 (1990);
D. E. Sanders and J. W. Evans, in *The Structure of Surfaces III*, Springer Series in Surface Sciences, vol. **24**, ed. S. Y. Tong, M. A. Van Hove, K. Takayanagi, and X. D. Xie (Springer-Verlag, Berlin, 1991), 38;
J. W. Evans, Phys. Rev. B **43**, 3897 (1991).

[15] I. K. Marmorkos and S. Das Sarma, Surf. Sci. Lett. **237**, L411 (1990).

[16] B. W. Dodson, Crit. Rev. Solid State Mater. Sci. **16**, 115 (1990).

[17] A. P. Sutton, P. D. Godwin, and A. P. Horsfield, MRS Bulletin, 42 (Feb. 1996).

[18] J. E. Lennard-Jones, Trans. Faraday Soc. **28**, 333 (1932);
J. H. Harding, in *Computer Simulation in Materials Science*, ed. M. Meyer and V. Pontikis (Kluwer Academic Publishers, Dordrecht, 1991) 159;
K. M. Nelson, S. T. Smith, and L. T. Wille, Mater. Res. Soc. Symp. Proc. **278** (*Computational Methods in Materials Science*), 231 (1992).

[19] K.-H. Müller, Phys. Rev. B **35**, 7906 (1987);
K.-H. Müller, Surf. Sci. **184**, L375 (1987);
M. Schneider, A. Rahman, and I. K. Schuller, Superlattices Microstruct. **7**, 39 (1990);
M. Schneider, A. Rahman, and I. K. Schuller, Phys. Rev. Lett. **55**, 604 (1985);
M. Matsui, M. Ohyabu, and H. Toyoda, *Int. Conf. Process. Mater. Prop., 1st*, ed. H. Henein and T. Oki. (Miner. Met. Mater. Soc., 1993) 1229;
H. Toyoda, M. Ohyabu, S. Mitani, M. Matsui, and M. Doyama, *Comput. Aided Innovation New Mater. 2*, Proc. Int. Conf. Exhib. Comput. Appl. Mater. Mol. Sci. Eng., 2nd, Issue Pt. 1, ed. M. Doyama (North-Holland, Amsterdam, 1993) 351;
Y. Sasajima, S. Ozawa, and R. Yamamoto, Mater. Res. Soc. Symp. Proc. **187** (*Thin Film Structures and Phase Stability*), 177 (1990).

[20] A. F. Voter, in *Intermetallic Compounds: Vol. 1, Principles*, ed. J. H. Westbrook and R. L. Fleischer (John Wiley & Sons, Chichester, 1994) ch. 4.

[21] J. K. Nørskov, K. W. Jacobsen, P. Stoltze, and L. B. Hansen, Surf. Sci. **283**, 277 (1993).

[22] J. A. Stroscio, D. T. Pierce, and R. A. Dragoset, Phys. Rev. Lett. **70**, 3615 (1993);
G. L. Nyberg, M. T. Kief, and W. F. Egelhoff, Jr., Phys. Rev. B **48**, 14509 (1993);
W. F. Egelhoff, Jr. and I. Jacob, Phys. Rev. Lett. **62**, 921 (1989);
B. Poelsema, A. F. Becker, R. Kunkel, G. Rosenfeld, L. K. Verheij, and G. Comsa, Springer Proc. Phys. **73** (*Surface Science*), 95 (1993);
B. Poelsema, A. F. Becker, G. Rosenfeld, R. Kunkel, N. Nagel, L. K. Verheij, and G. Comsa, Surf. Sci. **272**, 269 (1992);

M. Bott, T. Michely, and G. Comsa, Surf. Sci. **272**, 161 (1992);
M. Henzler, T. Schmidt, and E. Z. Luo, in *The Structure of Surfaces IV*, ed. X. Xie, S. Y. Tong, and M. A. Van Hove (World-Scientific, Singapore, 1994);
J.-K. Zuo and J. F. Wendelken, Phys. Rev. Lett. **70**, 1662 (1993);
H. J. Ernst, F. Fabre, and J. Lapujoulade, Surf. Sci. **275**, L682 (1992);
J. Chevrier, V. Le Thanh, R. Buys, and J. Derrien, Europhys. Lett. **16**, 737 (1991);
B. L. Evans and S. Xu, Proc. SPIE-Int. Soc. Opt. Eng. **1324** (*Model. Opt. Thin Films 2*), 90 (1990).

[23] M. C. Bartelt and J. W. Evans, Phys. Rev. Lett. **75**, 4250 (1995).

[24] Y. Li, T. J. Raeker, and A. E. DePristo, Phys. Rev. B **50**, 14742 (1994);
G. Bilalbegovic and A. E. DePristo, Surf. Sci. **302**, L299 (1994);
T. J. Raeker and A. E. DePristo, Surf. Sci. **317**, 283 (1994);
S. Liu, Z. Zhang, J. Nørskov, and H. Metiu, Surf. Sci. **321**, 161 (1994);
J. C. Hamilton, M. S. Daw, and S. M. Foiles, Phys. Rev. Lett. **74**, 2760 (1995).

[25] C. M. Gilmore and J. A. Sprague, J. Vac. Sci. Tech. A **13**, 1160 (1995);
J. A. Sprague and C. M. Gilmore, Surf. Coat. Technol. **65**, 71 (1994);
J. A. Sprague and C. M. Gilmore, Mater. Res. Soc. Symp. Proc. **268** (*Materials Modification by Energetic Atoms and Ions*), 115 (1992);
C. M. Gilmore and J. A. Sprague, Surf. Coat. Technol. **51**, 324 (1992);
C. M. Gilmore and J. A. Sprague, Phys. Rev. B **44**, 8950 (1991);
T. D. Andreadis, M. Rosen, M. I. Haftel, and J. A. Sprague, Mater. Res. Soc. Symp. Proc. **202** (*Evolution of Thin Film and Surface Microstructure*), 283 (1991);
M. Villarba and H. Jonsson, Phys. Rev. B **49**, 2208 (1994);
M. Breeman, G. T. Barkema, and D. O. Boerma, Surf. Sci. **307-309**, 526 (1994);
P. Stoltze and J.K. Nørskov, Phys. Rev. B **48**, 5607 (1993).

[26] M. O. Kaukonen and R. M. Nieminen, Surf. Sci. **331-333**, 975 (1995);
H. P. Kaukonen and R. M. Nieminen, Phys. Rev. Lett. **68**, 620 (1992);
J. Lampinen, R. M. Nieminen, and K. Kaski, Surf. Sci. **203**, 201 (1988);
A. Spinelli and L. Colombo, Mater. Sci. Eng. B **26**, 61 (1994);
M. F. Crowley, D. Srivastava, and B. J. Garrison, Surf. Sci. **284**, 91 (1993);
D. Srivastava, B.J. Garrison, and D. W. Brenner, Langmuir **7**, 683 (1991);
D. Srivastava and B. J. Garrison, J. Vac. Sci. Tech. A **8**, 3506 (1990);
S. Ethier and L. J. Lewis, J. Mater. Res. **7**, 2817 (1992);
B. A. Pailthorpe and P. Knight, Mater. Res. Soc. Symp. Proc. **223** (*Low Energy Ion Beam and Plasma Modification of Materials*), 29 (1991);
B. A. Pailthorpe, J. Appl. Phys. **70**, 543 (1991);
R. Biswas, G. S. Grest, and C. M. Soukoulis, Phys. Rev. B **38**, 8154 (1988);
M. Schneider, I. K. Schuller, and A. Rahman, Phys. Rev. B **36**, 1340 (1987).

[27] W. L. Brown and M. Sosnowski, Nuc. Instr. and Meth. B **102**, 305 (1995).

[28] H. Haberland, M. Karrais, M. Mall, and Y. Thurner, J. Vac. Sci. Tech. A **10**, 3266 (1992);
H. Haberland, Z. Insepov, M. Karrais, M. Mall, M. Moseler, and Y. Thurner, Mater. Sci. Eng. B **19**, 31 (1993);
H. Haberland, M. Lever, M. Moseler, Y. Qiang, O. Rattunde, T. Reiners, and Y. Thurner, Mater. Res. Soc. Symp. Proc. **388** (*Film Synthesis and Growth Using Energetic Beams*), 207 (1995).

[29] P. Melinon, V. Paillard, V. Dupuis, A. Perez, P. Jensen, A. Hoareau, J. P. Perez, J. Tuaillon, M. Broyer, J. L. Vialle, M. Pellarin, B. Baguenard, and J. Lerme, Int. J. Mod. Phys. B **9**, 339 (1995);
A. Perez, P. Melinon, V. Paillard, V. Dupuis, P. Jensen, A. Hoareau, J. P. Perez, J. Tuaillon, M. Broyer, J. L. Vialle, M. Pellarin, B. Baguenard, and J. Lerme, Nanostruct. Mater. **6**, 43 (1995);
J. D. Bielefeld and R. P. Andres, Mater. Res. Soc. Symp. Proc. **317** (*Mechanisms of Thin Film Evolution*), 155 (1994).

[30] L. Rongwu, P. Zhengying, and H. Yukun, Phys. Rev. B **53**, 4156 (1996);
H. Hsieh and R. S. Averback, Phys. Rev. B **45**, 4417 (1992);
Z. Insepov, M. Sosnowski, G. H. Takaoka, and I. Yamada, Mater. Res. Soc. Symp. Proc. **316** (*Materials Synthesis and Processing Using Ion Beams*), 999 (1994);
H.-P. Cheng and U. Landman, J. Phys. Chem. **98**, 3527 (1994);
C. L. Cleveland and U. Landman, Science **257**, 355 (1992);
A. Miyamoto, R. Yamauchi, and M. Kubo, App. Surf. Sci. **75**, 51 (1994);
P. Blandin, C. Massobrio, and J. Buttet, Mater. Res. Soc. Symp. Proc. **278** (*Computational Methods in Materials Science*), 249 (1992).

[31] K.-H. Müller, J. Appl. Phys. **61**, 2516 (1987);
H. Haberland, Z. Insepov, and M. Moseler, Phys. Rev. B **51**, 11061 (1995);
R. Biswas, G. S. Grest, and C. M. Soukoulis, Phys. Rev. B **38**, 8154 (1988).

[32] T. J. Raeker and A. E. DePristo, Int. Rev. Phys. Chem. **10**, 1 (1991) and references therein;
J. D. Kress, M. S . Stave, and A. E. DePristo, J. Phys. Chem. **93**, 1556 (1989);
J. D. Kress and A. E. DePristo, J. Chem. Phys. **88**, 2596 (1988).

[33] A. E. DePristo, in *Recent Advances in Density Functional Theory*, vol. 1, Part 1, ed. D. Chong (World-Scientific, Singapore, 1996) ch. 6.

[34] E. Clementi, IBM J. Res. Develop. Suppl. **9** (1965);
P. S. Bagus, T. L. Gilbert, and C. J. Roothan, J. Chem. Phys. **56**, 5159 (1972).

[35] M. Schmidt and K. Ruedenberg, J. Chem. Phys. **71**, 3951 (1979).

[36] S. Huzinaga, Prog. Theor. Physics Suppl. **40**, 279 (1967).

[37] M. S. Stave, D. E. Sanders, T. J. Raeker, and A. E. DePristo, J. Chem. Phys. **93**, 4413 (1990);
S. B. Sinnott, M. S. Stave, T. J. Raeker, and A. E. DePristo, Phys. Rev. B **44**, 8927 (1991).

[38] D. M. Halstead and A. E. DePristo, Surf. Sci. **286**, 275 (1993);
D. E. Sanders and A. E. DePristo, Surf. Sci. **260**, 116 (1992);
D. E. Sanders, D. M. Halstead, and A. E. DePristo, J. Vac. Sci. Tech. A **10**, 1986 (1992);
D. E. Sanders and A. E. DePristo, Surf. Sci. **254**, 341 (1991);
T. J. Raeker, D. E. Sanders, and A. E. DePristo, J. Vac. Sci. Tech. A **8**, 3531 (1990).

[39] S. B. Sinnott, C. L. Kelchner, and A. E. DePristo, J. Chem. Phys. **99**, 1816 (1993).

CONSTRUCTION AND EVALUATION OF EMBEDDING FUNCTIONS

A paper published in Surface Science[†]

Cynthia L. Kelchner, David M. Halstead, Leslie S. Perkins, Nora M. Wallace,
and Andrew E. DePristo

Abstract

Non-self-consistent density functional theories require specification of the embedding energy for an atom in a reference system. We combine the embedding energies determined from linear muffin tin orbital (LMTO) calculations of the bulk cohesive energy curves with those determined from the experimental diatomic binding curve. These new embedding functions contain information about the variation of binding with both coordination and separation between atomic centers. These are shown to be superior to embedding functions determined solely from bulk cohesive energy curves through tests on structures and energies of small metal clusters, self-diffusion of adatoms on metal surfaces, and scattering of metal atoms from metal surfaces.

Introduction

Non-self-consistent density functional based theoretical methods have become prevalent in computational physics, chemistry, and materials science. The conceptual model in these methods involves embedding an atom in jellium, which describes the delocalized bonding in metals. The energy of embedding each atom in jellium provides the zeroth order term in the

---

[†] Reprinted with permission from Surface Science **310** (1994), 425-435.

expression for the interaction energy. The more localized interactions in real N-atom systems are included in a variety of ways. The simplest approaches use localized empirical two-body interactions and empirical embedding functions, and are known as the embedded atom,[1-4] Finnis-Sinclair,[5] and "glue"[6] methods. More sophisticated (and thus more computationally demanding) semi-empirical methods include explicit calculations of the corrections to the zeroth order model via either 1-electron tight binding energies in the effective medium approach[7] or kinetic-exchange-correlation functionals of the electron density in the corrected effective medium (CEM) method.[8-11]

The purpose of the present paper is to describe the construction of embedding functions which include information on both the diatomic binding and the bulk cohesive energy curves. Since the embedding energy is a major component of the system interaction energy, it is important to determine an accurate embedding function which describes the variation of bonding both with coordination (i.e., change from bulk to dimer) and with atomic separation. We use the CEM theory as the formalism, and also show results for the simpler MD/MC-CEM approach which is analogous to the EAM but with non-empirical two-body interactions. The construction method presented is applicable to the embedding function in any theory. The only difficulty will occur for theories that are intrinsically inaccurate for the low coordination binding in the dimer, since the embedding curve will then not be single valued. However, this is advantageous since it provides a consistency test on such a theory.

To evaluate these new embedding functions, we compare results using different embedding functions. The comparisons include energies and geometries for small clusters and

surfaces, diffusion of metal atoms on metal substrates, and scattering of metal atoms from defect structures on metal substrates.

Theory

The CEM theory has been presented in detail previously.[8-11] For a system of atoms, $\{A_i, i=1,...,N\}$, the CEM interaction energy is

$$\Delta\bar{E}\left(\{A_i\}\right) = \sum_{i=1}^{N} \Delta\bar{E}_J\left(A_i; n_i\right) + \sum_{i=1}^{N}\sum_{j>i}^{N} V_c(i,j) + \Delta G\left(\{A_i\}\right) \qquad \textbf{Eq. 1}$$

The jellium density, n_i, is

$$n_i = \frac{1}{2}\sum_{j\neq i}^{N} \int \frac{n\left(A_i; \bar{r} - \bar{R}_i\right)}{Z_i} n\left(A_j; \bar{r} - \bar{R}_j\right) d\bar{r} \qquad \textbf{Eq. 2}$$

where $n(A_i;\boldsymbol{r} - \boldsymbol{R}_i)$ is the atomic electron density distribution as taken from Hartree-Fock calculations[12] and represented in even-tempered Gaussians[13] for computational ease. Z_i and $\boldsymbol{R}_i$ are the atomic number and nuclear position, respectively. The underlying approximation leading to Eq.(1) is that the total system electron density is equal to the superposition of atomic electron densities.

The first right-hand-side (RHS) term in Eq.(1) is the sum of the embedding energy for each atom, where the embedding energy is solely a function of the average electron density environment of that particular type of atom. The average electron (jellium) density is provided by Eq.(2). The subscript "J" in Eq.(1) stands for jellium. It is worthwhile to emphasize that the only unknown part of the interaction energy expression in Eq.(1) is the embedding function. Once this is specified for each atom type, the CEM theory can be used to predict the interaction energies for a system in any geometry.

The second RHS term consists of pairwise additive Coulomb energies: $V_c(i,j)$ is the sum of electron-electron, electron-nuclear, and nuclear-nuclear Coulomb interactions between atoms A_i and A_j. These are determined from the electron densities of each atom.[14]

The last RHS term is the difference in kinetic-exchange-correlation energy between the N-atom and atom-in-jellium systems and is given by the explicit expression

$$\Delta G\left(\{A_i\}\right) = \left[G\left(\{A_i\}\right) - \sum_{i=1}^{N} G\left(A_i\right)\right] - \sum_{i=1}^{N}\left[G\left(A_i + n_i\right) - G\left(A_i\right) - G\left(n_i\right)\right] \qquad \textbf{Eq. 3}$$

It is a many body correction. The $G(S)$ term is a complicated functional of the electron density and its gradient that is completely specified by the atomic electron densities.

To determine the embedding functions, we write down explicit expressions for the homonuclear bulk and dimer systems. Using 3D periodicity, Eq.(1) produces the following expression for the cohesive energy of a monatomic solid with one atom per unit cell:

$$\Delta E_{coh}\left(A_b\right) = \Delta E_J\left(A_b; n_b\right) + \frac{1}{2}\sum_{j \neq b} V_c\left(b, j\right) + \Delta G_{WS(b)}, \quad \textbf{monatomic bulk} \qquad \textbf{Eq. 4}$$

A_b labels any equivalent (bulk) atom in the system and n_b is its jellium density. The subscript WS indicates that the integration extends only over the Wigner-Seitz cell of atom A_b. Knowledge of $\Delta E_{coh}(A_b)$ at various lattice constants yields $\Delta E_J(A_b;n_b)$ at various n_b. The analogous expression for a homonuclear diatom is

$$\Delta E\left(A_1, A_2\right) = 2\Delta E_J\left(A_1; n_1\right) + V_c(1,2) + \Delta G\left(A_1, A_2\right), \quad \textbf{homonuclear dimer} \qquad \textbf{Eq. 5}$$

Knowledge of $\Delta E(A_1,A_2)$, the dimer interaction energy, at various bond lengths provides $\Delta E_J(A_1;n_1)$ at various n_1. Clearly, either Eq.(4) or Eq.(5) could yield the entire embedding function by sufficient expansion and contraction of the internuclear separations.

An important point about these expressions is that for the same nearest neighbor separation, n_b in Eq.(4) is much larger than n_l in Eq.(5) because an atom in the bulk system has twelve nearest (and many further) neighbors while each atom in the dimer has only one. As an example, we show the jellium density for a range of nearest neighbor distances in Cu bulk and Cu dimer in Figure 1. The jellium density at R_e for the dimer corresponds to the jellium density at a 27% expansion of the bulk Cu lattice from equilibrium. Thus, Eqs.(4) and (5) will give embedding functions at different electron densities for similar internuclear separations.

In a previous article,[10] we presented embedding functions generated from Eq.(4) using ΔE_{coh} obtained from linear muffin tin orbital (LMTO) calculations involving lattice constants from a 30% expansion to a 10% contraction of the bulk equilibrium. Calculated values of ΔE_{coh} were used because experimental data are not available for such an extended range, since contractions of more than a few percent require extremely high pressure and stretching more than a few percent leads to fracture. This procedure determined the embedding functions for coordinations approaching that of the bulk. For example, the (111), (100), (110), (331), (311), and (210) surfaces have jellium densities that are lower than the equilibrium bulk electron density due to the loss of neighbors. These electron densities correspond to approximately a 10-15% expansion of the lattice from the equilibrium bulk lattice constant, with the more close-packed faces corresponding to the smaller expansions (higher electron densities) and the open faces corresponding to the larger expansions (lower electron densities). These embedding functions are denoted as $\Delta E_{LMTO}(A_i;n_l)$ and are shown in Figure 2 for Al, Ni, Cu, Pd, Ag, Pt, and Au.

The problem with $\Delta E_{LMTO}(A_i;n_j)$ occurs for very low electron densities which correspond to an extremely expanded bulk. These low electron densities also correspond to lower-coordination bonding near equilibrium. Unfortunately, these two situations are not equivalent. Thus, we must supplement the LMTO determined curves with information on the homonuclear dimer. We do this by using Eq.(5) with the experimental dimer data, setting $\Delta E(A_1,A_2)=V(R)$ where $V(R)$ is a Morse potential fit to the experimental binding energy, bond length, and vibrational frequency.[15] An embedding function determined in this way is denoted by $\Delta E_{Morse}(A_i;n_j)$; these functions are shown in Figure 3 for Al, Ni, Cu, Pd, Ag, Pt, and Au. The range of bond lengths used in all cases was 2.00 - 15.00 bohr.

The two different methods for finding the embedding function do not yield identical results but this does not cause a fundamental problem for the following reasons. First, the very expanded bulk region (low jellium density) is unimportant physically except for much lower coordination bonds than those in the bulk. Second, the high jellium density region is unimportant physically for lower coordination bonds because it corresponds to very repulsive interaction energies. A change in the interaction energies in this high electron density region requires only a very small change in interatomic separation and thus the exact high electron density embedding function is unimportant for compressed low coordination structures.

For the new embedding functions, $\Delta E_{Morse}(A_i;n_j)$ will be used at very low n_i (at least below the electron density corresponding to the dimer equilibrium distance) while $\Delta E_{LMTO}(A_i;n_j)$ will be used at larger n_i. The resulting embedding function is denoted by $\Delta E_{EXLM}(A_i;n_j)$, from experimental data fit to a Morse potential and LMTO generated embedding energies. The

process of smoothly joining the two curves over some electron density interval [$n_<$,$n_>$] requires consideration of two cases.

In the first case, $\Delta E_{Morse}(A_i;n_i)$ does not intersect $\Delta E_{LMTO}(A_i;n_i)$ as n_i increases beyond the jellium density at the dimer equilibrium separation. This occurs for Ag and Pd. The two curves are then joined by the following interpolation formula:

$$\Delta E_{EXLM}(A_i;n_i) = \Delta E_{Morse}(A_i;n_i)\cos^2\left(\frac{n_i - n_<}{n_> - n_<}\frac{\pi}{2}\right) + \Delta E_{LMTO}(A_i;n_i)\sin^2\left(\frac{n_i - n_<}{n_> - n_<}\frac{\pi}{2}\right) \quad \textbf{Eq. 6}$$

The jellium density interval [$n_<$,$n_>$] is chosen so that the transition between the LMTO and Morse embedding functions is gradual and monotonic. This formula provides a continuous function and first derivative. We show the three embedding functions versus jellium density for Ag in Figure 4 with a mixing interval of [0.0008 a.u., 0.004 a.u.]. (Note that the crossing in the Ag case occurs at a jellium density that is much smaller than that at the dimer equilibrium.)

In the second case, $\Delta E_{Morse}(A_i;n_i)$ intersects $\Delta E_{LMTO}(A_i;n_i)$ as n_i increases. This occurs for Al, Ni, Cu, Pt, and Au. The two curves are then joined by the following interpolation formula:

$$\Delta E_{EXLM}(A_i;n_i) = \frac{1}{2}\left[\Delta E_{Morse}(A_i;n_i) + \Delta E_{LMTO}(A_i;n_i)\right] - \frac{1}{2}\left\{\left[\Delta E_{Morse}(A_i;n_i) - \Delta E_{LMTO}(A_i;n_i)\right]^2 - 4Q^2\right\}^{\frac{1}{2}} \quad \textbf{Eq. 7}$$

where Q is a mixing parameter which determines how far the EXLM embedding function curve will lie below the value of the LMTO and Morse curves when they cross. This formula also provides a continuous function and derivatives. We show the three embedding functions versus jellium density for Cu in Figure 5, where the Morse and LMTO curves cross at

0.00365 a.u. In general, the actual transition from the Morse to the LMTO curve occurs over a much smaller jellium density range if the two curves cross.

The reader will notice that these interpolation formulas have, respectively, the form of mixing the squares of two wavefunctions (Eq.(6)) and the formation of an adiabatic potential from two diabatic ones (Eq.(7)).

The same interpolation formula can be used for any other method using embedding functions, and we have done so for the more approximate MD/MC-CEM theory[10,11a] in which the energy expression equivalent to Eq.(1) is

$$\Delta E\left(\{A_i\}\right) = \sum_{i=1}^{N} \Delta F_J\left(A_i; n_i\right) + \sum_{i=1}^{N}\sum_{j>i}^{N} V_c(i,j) \qquad \textbf{Eq. 8}$$

The "effective" embedding functions, $\Delta F_{EXLM}(A_i;n_i)$, can be constructed by the same procedure used for $\Delta E_{EXLM}(A_i;n_i)$ in the full CEM theory.

Results and Discussion

In Table I we present the parameters for construction of the new EXLM embedding functions for Al, Ni, Cu, Pd, Ag, Pt, and Au, using CEM. If the Morse and LMTO curves cross for a particular metal, these parameters include the jellium density at the crossing point and the mixing parameter, Q. If the curves do not cross, the jellium densities at the endpoints of the mixing range are given. Table II shows the same information for MD/MC-CEM. There is no correlation in these parameters between the CEM and MD/MC-CEM embedding functions. Note also that Q is always rather small, indicating that the deviation of the EXLM curve at the crossing of the LMTO and Morse embedding functions is small.

For homonuclear diatomic molecules, the error in the LMTO results is substantial when compared to experimental data. A typical case is Ag, where the LMTO binding energy is too large by 0.3 eV, the equilibrium distance is too large by 0.1 bohr, and the vibrational frequency is too large by 80 cm^{-1}. Cu is an extreme case, where the binding energy is too small by 1.1 eV, the equilibrium distance is too small by 0.7 bohr, and the frequency is too large by 220 cm^{-1} when using the LMTO embedding function. By contrast, the EXLM embedding functions reproduce the dimer binding energy, equilibrium separation, and vibrational frequency to within 0.02 eV, 0.01 bohr, and 10-15 cm^{-1} by construct.

For Pd_3 clusters, Table III presents the equilibrium binding energy, bond length, and corresponding electron density for the equilateral triangle structure. The Morse and LMTO curves for Pd do not cross, indicating that the EXLM embedding function makes a gradual transition between the two curves over the chosen mixing range (Table I). The electron density for Pd_3 is well within this mixing range and thus the LMTO and EXLM results differ considerably, as seen in Table III. The structures and energies of small Pd clusters are very sensitive to the embedding function because the Pd dimer has a large bond length and is weakly bound relative to bulk Pd, in comparison to other metals. Small Pd clusters require information on both the coordination and electron density variation of the embedding function. The comparison to the SCF-DF values in Table III does not provide unequivocal evidence to favor either embedding function, as the binding energy for Pd_3 is midway between the LMTO and EXLM values.

The results for small Cu clusters in Table IV likewise exhibit substantial differences between the LMTO and EXLM results from CEM calculations for both binding energy and

bond length. However, for Cu the EXLM results agree better with the SCF-DF values in every case. The EXLM and LMTO curves are well-separated at low jellium densities, as seen in Figure 5, and the jellium density at the crossing point (Table I) is higher than the jellium density of the small Cu clusters using EXLM. Thus, the equilibrium bond energy and distance of small Cu clusters are very sensitive to the very low jellium density region.

The results for Ni in Table V provide another type of situation. The differences between the LMTO and EXLM results from CEM calculations are very small for Ni_3. The Morse and LMTO curves for Ni cross, meaning that the EXLM embedding function connects the two curves over a very small jellium density range near the crossing point. The equilibrium jellium density predicted for Ni_3 (0.00441 a.u. using EXLM) is much higher than the jellium density where the Morse and LMTO curves cross (Table I), so for Ni_3 the EXLM curve is already nearly identical to the LMTO curve. The equilibrium bond energy and distance of small Ni clusters are thus insensitive to the very low jellium density region.

Based upon the above results, we expect that, for systems with higher coordination of atoms, the EXLM and LMTO embedding functions will produce nearly identical results. For example, we have tested surface energies and interlayer spacings due to surface relaxations of the simple cubic faces. The two embedding functions yield results that agree to better than 1.5% for the (111), (100), and (110) faces of Al, Ni, Cu, Pd, Ag, Pt, and Au, with the exceptions of Ag(100) and Ag(110). In these cases, the EXLM values of the surface energy are 5% larger for Ag(100) and 10% larger for Ag(110). Similarly, the first layer contraction is 13.8% for Ag(110) using ΔE_{EXLM} and 7.3% for ΔE_{LMTO}. Apart from these two exceptions,

the results generally indicate that the two different embedding functions obtain nearly the same surface energies and relaxations.

It is worthwhile to emphasize that even for large systems there are processes that may involve lower coordination atoms and these cases will be sensitive to the embedding function. We examined the influence of the embedding function on the activation barrier to self-diffusion for two mechanisms on fcc(100) surfaces. In bridge-hopping, the adatom hops from one four-fold hollow site to an adjacent four-fold hollow site, over the intervening two-fold bridge site. In replacement or exchange, the adatom displaces an atom in the first substrate layer, and the displaced substrate atom then moves to the four-fold hollow site diagonal from the adatom's original four-fold site. (For further information concerning diffusion barriers, see reference [19].)

Using the LMTO embedding function, the CEM values for the bridge and replacement diffusion barriers are 0.70 eV and 0.44 eV on Cu(100). Using the EXLM embedding function, the analogous values are 0.47 eV and 0.43 eV. The bridge-hopping transition state involves a low coordinated Cu atom while the replacement transition state does not. For this system and others not shown, we have found that the electron density region that controls bridge-hopping is in the transition region between the Morse and LMTO embedding functions. The combination of low coordination and low electron density indicates that the EXLM embedding function must be used to describe diffusion on metal surfaces. For this reason, Ref. [19] only reported the barriers calculated using the EXLM embedding functions.

As a final example, we consider the dynamics of Cu atom adsorption on clean Cu surfaces and on Cu surfaces with Cu island defects. For large scale dynamics simulations, it is necessary to use the faster MD/MC-CEM approximation rather than the full CEM theory.

Our results for adsorption on the clean fcc(100) face of Cu at 80 K showed that 99.9% of depositing atoms localize in the first unit cell encountered for both the EXLM and LMTO "effective" embedding functions. This arises from the fact that the repulsive potential felt by the adsorbate as it strikes the clean surface is essentially identical for both "effective" embedding functions, since the electron density is greater than 0.005 a.u. (Table II) in this region. It is this coupling to the surface that determines the final adsorption site.

When the adsorbate interacts with an island defect, however, the electron density encountered during the collision is substantially lower than that for the clean surface, and the simulation results for the two "effective" embedding functions are no longer identical. The geometry of the island was a 14-atom pyramid on the fcc(100) face. This has a square nine-atom base, four atoms in the second layer and a single apex atom in the third layer above the plane of the substrate surface atoms.[11g,11h] The right-hand panels of Figs. 6a and 6b show the interaction energies between a Cu gas atom and the pyramidal defect/fcc(100) substrate for a cut through the center of the pyramid, using the LMTO and EXLM "effective" embedding functions, respectively. The LMTO results predict a less stable adsorption site on the pyramid face by 0.19 eV and a larger barrier to diffusion out of this site by 0.24 eV than that encountered in the EXLM results.

The left panel of each figure shows some sample trajectories at normal incidence to the surface with initial energy of 0.25 eV on a 0 K surface. Two out of the five trajectories result

in adsorption to the side of the pyramid in the LMTO case, but only one out of five for the EXLM case. To obtain statistically reliable results, we ran 325 trajectories over the irreducible triangular octant of the pyramid on an 80 K surface. These showed that the probability of adhering to the pyramid facet is more than four times greater for the LMTO results, giving a capture cross section of 37.2 $Å^2$ compared with 9.0 $Å^2$ for the EXLM results. (The area of sites blocked by the 14 atom pyramid is 104.3 $Å^2$.) Thus the inability of the adsorbing Cu atom to reach the more stable base sites in the LMTO case is caused by the relative instability of the low electron density transition state, which must be surmounted to reach the base. The EXLM embedding function predicts a more stable facet site compared with the LMTO embedding function and exhibits a lower barrier to reaching the base, leading to a smoother growth mode. Failure to reach the vacant sites around the pyramid base is therefore a kinetic limitation, as these sites are energetically the most stable for both "effective" embedding functions with an adsorption energy of 3.11 eV in both cases.

The deposition process samples the low electron density region as the adsorbing atom begins to interact with the surface atoms, and it is this interaction region which is critical in determining the outcome of growth deposition processes. This illustrates that for deposition studies involving the growth of incomplete overlayers and small structures, it is essential to treat the entire jellium density range of the embedding function as accurately as possible, and not rely on embedding functions that solely extrapolate from bulk or even clean surface properties.

Conclusions

There are two distinct electron density and coordination regions in metal systems: the high electron density, high coordination region which corresponds to the bulk system and the low electron density, low coordination region which corresponds to the dimer. The LMTO embedding function does a good job of describing the bulk region,[10] and the Morse embedding function describes the dimer region well.

For many systems it is essential to use an embedding function that describes both the high and low electron density regions accurately, since the lower electron density regions can play an important role in determining the outcome of a calculation. This has been illustrated for self-diffusion on metal surfaces and for homoepitaxial deposition on metal surfaces with island defects. Neither the LMTO nor the Morse embedding function is adequate here, and we have shown how to smoothly join these two into a new EXLM embedding function which mixes these two curves in the mid-electron density range. Thus, the EXLM embedding function combines the best features of the LMTO and Morse embedding functions over the entire electron density range of interest.

We should emphasize that a more comprehensive approach would allow the embedding function to depend upon both a jellium density and a bond coordination parameter. The dimer would then determine an embedding function over the entire jellium density regime for a one-fold coordination, while the bulk would do so for 12-fold coordination. Determination of the embedding function for intermediate coordinations and even the definition of the bond coordination parameter pose outstanding challenges to this theoretical development.

Acknowledgements

This work was supported by NSF grants CHE-8921099 and CHE-9224884. Calculations were performed on a Silicon Graphics 4D/380S purchased by an NSF instrumentation grant and a nCUBE 2 hypercube at the Scalable Computing Laboratory, Ames Laboratory (which is operated for the U.S. DOE by Iowa State University under Contract No. W-7405-Eng-82). L.S. Perkins thanks the Amoco Chemical Corporation for their funding through the Amoco Fellowship in the Department of Chemistry at Iowa State University.

References

1. a) M. S. Daw and M. I. Baskes, Phys. Rev. B **29** (1984) 6443.
   b) S. M. Foiles, M. I. Baskes, and M. S. Daw, Phys. Rev. B **33** (1986) 7983.
   c) M. S. Daw, Phys. Rev. B **39** (1989) 7441.

2. T. Ning, Q. Yu, and Y. Ye, Surf. Sci. **206** (1988) L857.

3. C. L. Liu, J. M. Cohen, J. B. Adams, and A. F. Voter, Surf. Sci. **253** (1991) 334.

4. M.S. Daw, S. M. Foiles, and M. I. Baskes, Materials Science Reports, **9** (1993) 251.

5. a) M. W. Finnis and J. E. Sinclair, Phil Mag. A **50** (1984) 45.
   b) G. J. Ackland, G. Tichy, V. Vitek, and M. W. Finnis, Philos. Mag. A **56** (1987) 735.
   c) M. W. Finnis, A. T. Paxton, D. G. Pettifor, A. P. Sutton, and Y. Ohta, Philos. Mag. A **58** (1988) 143.
   d) G. J. Ackland and V. Vitek, Phys. Rev. B **41** (1990) 10324.

6. a) F. Ercolessi, M. Parrinello, and E. Tosatti, Philos. Mag. A **58** (1988) 213 and references therein.
   b) G. Bilalbegovic, F. Ercolessi, and E. Tosatti, Surf. Sci. **258** (1991) L676.

7. a) J. K. Nørskov and N. D. Lang, Phys. Rev. B **21** (1980) 2131.
   b) K. W. Jacobsen, J. K. Nørskov, and M. J. Puska, Phys. Rev. B **35** (1987) 7423.
   c) K. W. Jacobsen and J. K. Nørskov, Phys. Rev. Lett. **59** (1987) 764.
   d) K. W. Jacobsen and J. K. Nørskov, Phys. Rev. Lett. **60** (1988) 2496.
   e) J. K. Nørskov, Prog. in Surf. Sci. **38** (1991) 103.

f) L. Hansen, P. Stoltze, K. W. Jacobsen, and J. K. Nørskov, Phys. Rev. B **44** (1991) 6523.

8. a) J. D. Kress and A. E. DePristo, J. Chem. Phys. **88** (1988) 2596.
   b) T. J. Raeker and A. E. DePristo, Int. Rev. Phys. Chem. **10** (1991) 1 and references therein.

9. a) J. D. Kress, M.S . Stave, and A. E. DePristo, J. Phys. Chem. **93** (1989) 1556.
   b) M. S. Stave and A. E. DePristo, J. Chem. Phys. **97** (1992) 3386.

10. S. B. Sinnott, M. S. Stave, T. J. Raeker, and A. E. DePristo, Phys. Rev. B **44** (1991) 8927.

11. a) M. S. Stave, D. E. Sanders, T. J. Raeker, and A. E. DePristo, J. Chem. Phys. **93** (1990) 4413.
   b) T. J. Raeker, D. E. Sanders, and A. E. DePristo, J. Vac. Sci. Tech. A **8** (1990) 3531.
   c) T. J. Raeker and A. E. DePristo, Surf. Sci. **248** (1991) 134.
   d) D. E. Sanders and A. E. DePristo, Surf. Sci. **254** (1991) 341.
   e) D. E. Sanders and A. DePristo, Surf. Sci. **260** (1992) 116.
   f) T. J. Raeker and A. E. DePristo, J. Vac. Sci. Tech. A **10** (1992) 2396.
   g) D. E. Sanders, D. M. Halstead, and A. E. DePristo, J. Vac. Sci. Tech. A **10** (1992) 1986.
   h) D. M. Halstead and A. E. DePristo, Surf. Sci. **286** (1993) 275.

12. a) E. Clementi, IBM J. Res. Develop. Suppl. **9** (1965).
   b) P. S. Bagus, T. L. Gilbert, and C. J. Roothan, J. Chem. Phys. **56** (1972) 5159.

13. M. Schmidt and K. Ruedenberg, J. Chem. Phys. **71** (1979) 3951.

14. S. Huzinaga, Prog. Theor. Physics Suppl. **40** (1967) 279.

15. a) K. P. Huber and G. Herzberg, in *Molecular Spectra and Molecular Structure, Vol. 4, Constants of Diatomic Molecules* (Van Nostrand, Princeton, 1979).
   b) M. Morse, Chem. Rev. **86** (1986) 1049.

16. N. M. Wallace and A. E. DePristo (unpublished results).

17. a) A. St-Amant, Thèse de doctorat, Université de Montréal (1992).
   b) A. St-Amant and D. R. Salahub, Chem. Phys. Lett. **169**, 387 (1990).

18. a) J. P. Perdew, Phys. Rev. Lett. **55**, 1665 (1985).
   b) J. P. Perdew and Y. Wang, Phys. Rev. B **33**, 8800 (1986).

19. L.S. Perkins and A.E. DePristo, Surf. Sci. **294**, 67 (1993).

Table I. Parameters used in the construction of $\Delta E_{EXLM}(A_i;n_i)$ via Eqs.(6) and (7) for CEM.

Metal	curve crossing (a.u.)	$[n_<,n_>]$ (a.u.)	Q (eV)
Al	0.00168	NA[a]	0.01
Ni	0.00293	NA	0.06
Cu	0.00365	NA	0.065
Pd	no	0.0005 - 0.005	NA
Ag	no	0.0008 - 0.004	NA
Pt	0.00214	NA	0.03
Au	0.00208	NA	0.06

[a] The mixing range only enters when the curves do not cross, using Eq.(6). The mixing parameter, Q, enters when the curves do cross via the interpolation formula in Eq.(7).

Table II. Parameters used in the construction of $\Delta F_{EXLM}(A_i;n_i)$ via Eqs.(6) and (7) for the MD/MC-CEM approximation in Eq.(8) to the CEM expression in Eq.(1).

metal	curve crossing (a.u.)	$[n_<,n_>]$ (a.u.)	Q (eV)
Al	no	0.0015 - 0.0045	NA[a]
Ni	0.00274	NA	0.04
Cu	no	0.003 - 0.005	NA
Pd	no	0.001 - 0.004	NA
Ag	no	0.0018 - 0.0025	NA
Pt	0.00223	NA	0.01
Au	0.00226	NA	0.04

[a] The mixing range only enters when the curves do not cross, using Eq.(6). The mixing parameter, Q, enters when the curves do cross via the interpolation formula in Eq.(7).

Table III. Equilibrium results for highly symmetric Pd clusters, calculated with the LMTO and EXLM embedding functions for CEM and MD/MC-CEM. SCF-DF results are all electron *ab initio* density functional calculations[16] using the program deMon[17] with non-local exchange correlation functionals.[18]

	CEM			MD/MC-CEM		
	interaction energy (eV)	atomic separation (bohr)	jellium density (a.u.)[a]	interaction energy (eV)	atomic separation (bohr)	jellium density (a.u.)
Pd_2						
experiment	-1.04	5.01		-1.04	5.01	
LMTO	-1.04	4.46	0.00150	-1.54	5.03	0.00074
EXLM	-1.04	5.01	0.00077	-1.04	5.01	0.00076
SCF-DF	-0.78	5.00		-0.78	5.00	
Pd_3						
LMTO	-3.12	4.44	0.00294	-3.05	4.81	0.00191
EXLM	-2.52	4.22	0.00381	-2.46	4.42	0.00299
SCF-DF	-2.85	5.2		-2.85	5.2	

[a] For comparison, the jellium density for a bulk Pd atom at equilibrium is 0.00775 a.u.

Table IV. Equilibrium results for highly symmetric Cu clusters, calculated with the LMTO and EXLM embedding functions for CEM and MD/MC-CEM. SCF-DF results are all electron *ab initio* density functional calculations[16] using the program deMon[17] with non-local exchange correlation functionals.[18]

	CEM			MD/MC-CEM		
	interaction energy (eV)	atomic separation (bohr)	jellium density (a.u.)[a]	interaction energy (eV)	atomic separation (bohr)	jellium density (a.u.)
Cu_2						
experiment	-2.05	4.20		-2.05	4.20	
LMTO	-0.98	3.49	0.00354	-1.16	4.25	0.00135
EXLM	-2.06	4.19	0.00146	-2.05	4.19	0.00145
SCF-DF	-2.91	4.3		-2.91	4.3	
Cu_3						
LMTO	-3.21	3.85	0.00449	-2.95	4.17	0.00301
EXLM	-3.96	4.54	0.00187	-3.99	4.43	0.00215
SCF-DF	-4.35	4.56		-4.35	4.56	
Cu_4						
LMTO	-5.86	4.07	0.00508	-5.32	4.32	0.00373
EXLM	-6.09	4.74	0.00217	-6.31	4.54	0.00279
SCF-DF	-6.34	4.58		-6.34	4.58	

[a] For comparison, the jellium density for a bulk Cu atom at equilibrium is 0.00818 a.u.

Table V. Equilibrium results for highly symmetric Ni clusters, calculated with the LMTO and EXLM embedding functions for CEM and MD/MC-CEM. SCF-DF results are all electron *ab initio* density functional calculations[16] using the program deMon[17] with non-local exchange correlation functionals.[18]

	CEM			MD/MC-CEM		
	interaction energy (eV)	atomic separation (bohr)	jellium density (a.u.)[a]	interaction energy (eV)	atomic separation (bohr)	jellium density (a.u.)
Ni_2						
experiment	-2.09	4.16		-2.09	4.16	
LMTO	-1.66	3.58	.00330	-1.82	3.89	.00225
EXLM	-2.11	4.15	.00163	-2.11	4.14	.00165
SCF-DF	-3.13	4.05		-3.13	4.05	
Ni_3						
LMTO	-4.31	3.90	.00443	-4.20	4.23	.00298
EXLM	-4.33	3.91	.00441	-4.30	4.33	.00262
SCF-DF	-5.98	4.25		-5.98	4.25	

[a] For comparison, the jellium density for a bulk Ni atom at equilibrium is 0.01049 a.u.

Figure Captions

Figure 1. Jellium density versus nearest neighbor distance for Cu dimer and Cu bulk. The bands represent 10% expansion and contraction around the equilibrium nearest neighbor distance for the dimer (4.195 bohr) and the bulk (4.824 bohr).

Figure 2. $\Delta E_{LMTO}(A_i;n_j)$ generated from LMTO calculations of the bulk cohesive energy from 10% contraction to 30% expansion via Eq.(4).[10] The values for the equilibrium bulk and dimer systems are marked on each curve.

Figure 3. $\Delta E_{Morse}(A_i;n_j)$ generated from Morse potential representation of the dimer binding energy curve from 2.0 - 15.0 bohr via Eq.(5). The values for the equilibrium bulk and dimer systems are marked on each curve.

Figure 4. LMTO, Morse and EXLM embedding functions for Ag. The jellium densities for equilibrium bulk, fcc(110) surface and dimer atoms are indicated. Note that $\Delta E_{EXLM}(Ag;n_j)$ smoothly joins $\Delta E_{Morse}(Ag;n_j)$ at low jellium densities with $\Delta E_{LMTO}(Ag;n_j)$ at high jellium densities via Eq.(6).

Figure 5. Same as Figure 4 but for Cu and using Eq.(7) to generate $\Delta E_{EXLM}(Cu;n_i)$.

Figure 6. **(a)** A plot through a (010) plane cut through the Cu pyramid center (bisected atoms shown in cross hatched) for the LMTO embedding function. The left side shows the path of five trajectories on a 0 K surface with the final site indicated by the numerated arrows. The right panel shows the potential energy contours for this embedding function in decrements of 0.5 eV starting at zero (dashed line). The energies of six sites of interest are also shown (in eV).

(b) Same as Fig. 6a but using the EXLM embedding function. Both figures reproduced from Ref. [11g] with permission.

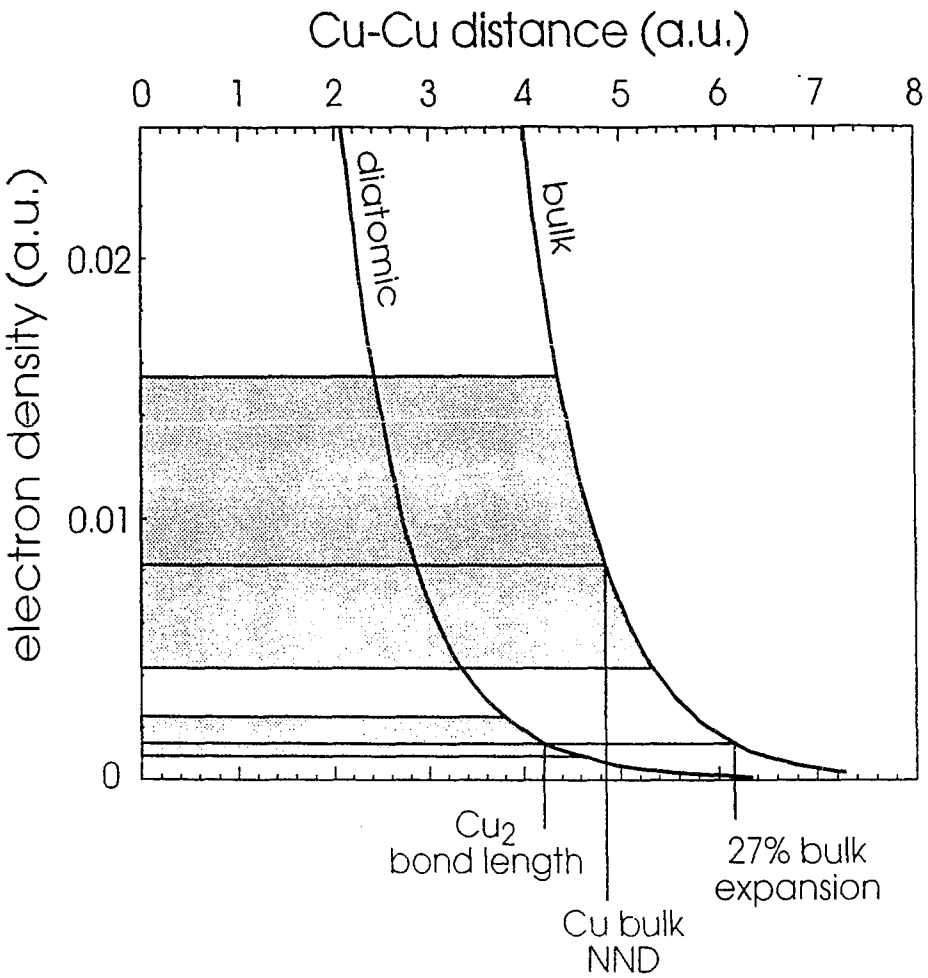
Cu-Cu distance (a.u.)
0
1
2
3
4
5
6
7
8
electron density (a.u.)
0.02
0.01
0
diatomic
bulk
Cu2
bond length
Cu bulk
NND
27% bulk
expansion

Figure 1.

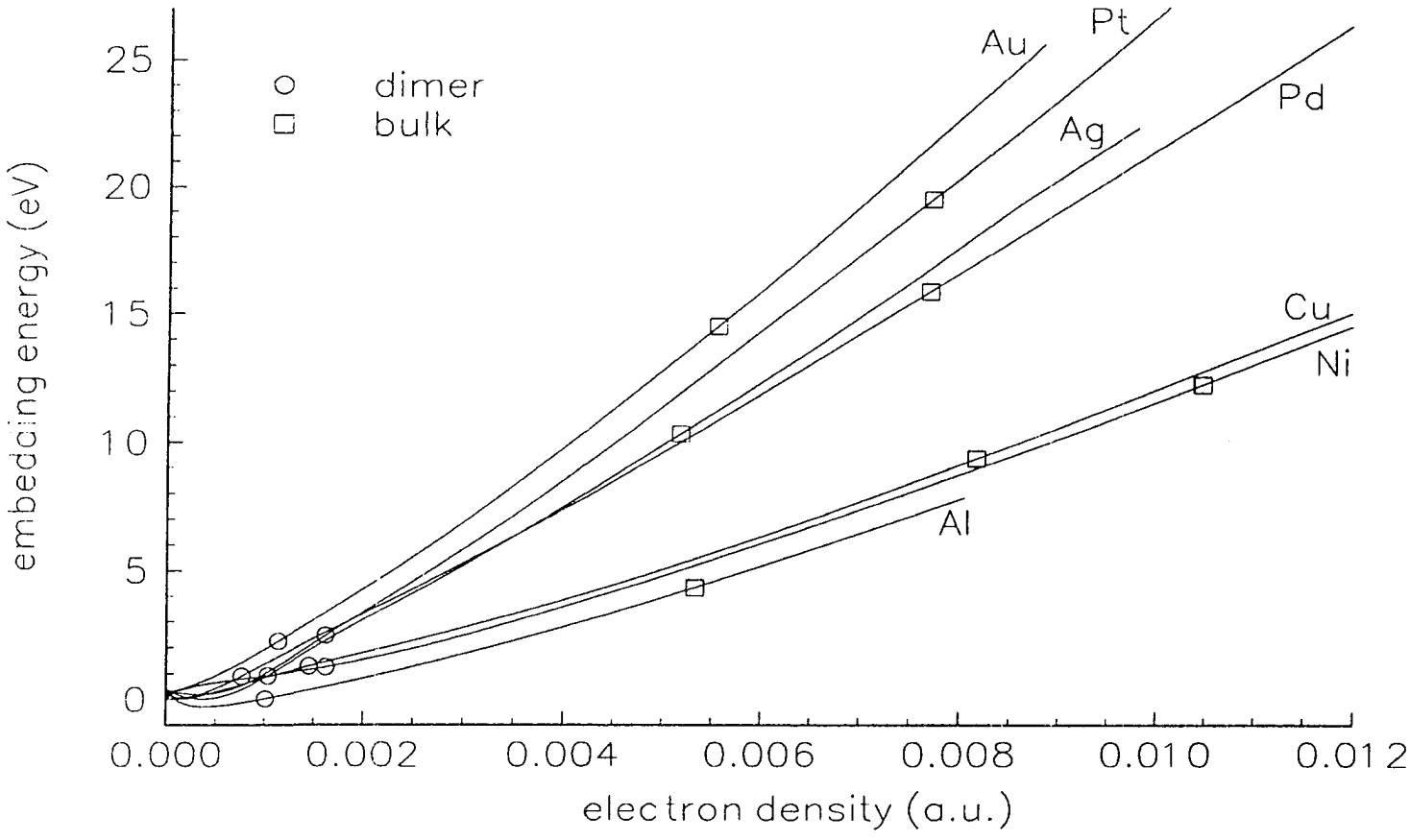
embedding energy (eV)
25
20
15
10
5
0
0.000
0.002
0.004
0.006
0.008
0.010
0.012
electron density (a.u.)
dimer
bulk
Au
Pt
Ag
Pd
Cu
Ni
Al

Figure 2.

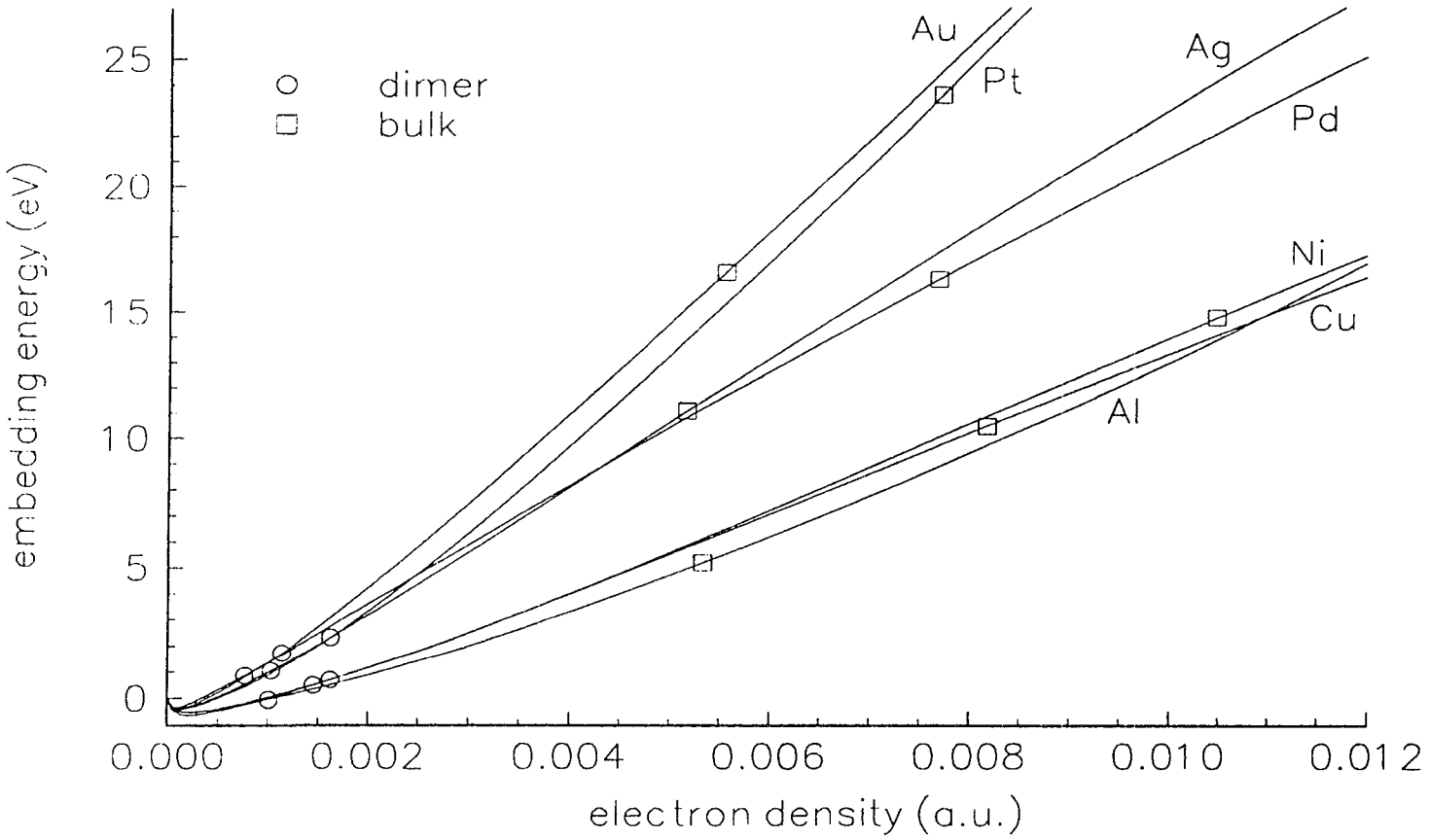
embedding energy (eV)
25
20
15
10
5
0
0.000
0.002
0.004
0.006
0.008
0.010
0.012
electron density (a.u.)
dimer
bulk
Au
Pt
Ag
Pd
Ni
Cu
Al

Figure 3.

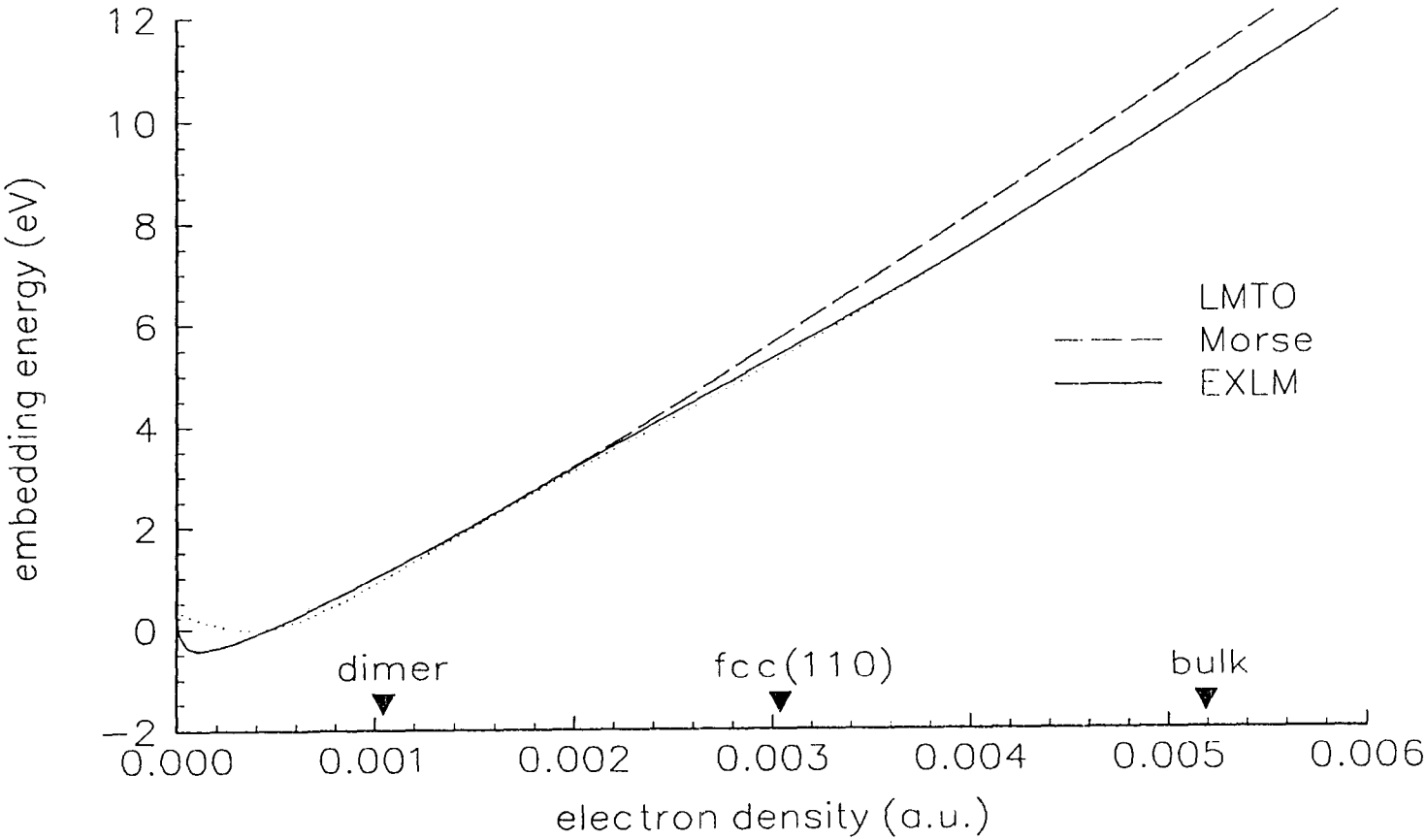
12
10
8
6
4
2
0
−2
embedding energy (eV)
LMTO
Morse
EXLM
dimer
fcc(110)
bulk
0.000
0.001
0.002
0.003
0.004
0.005
0.006
electron density (a.u.)

Figure 4.

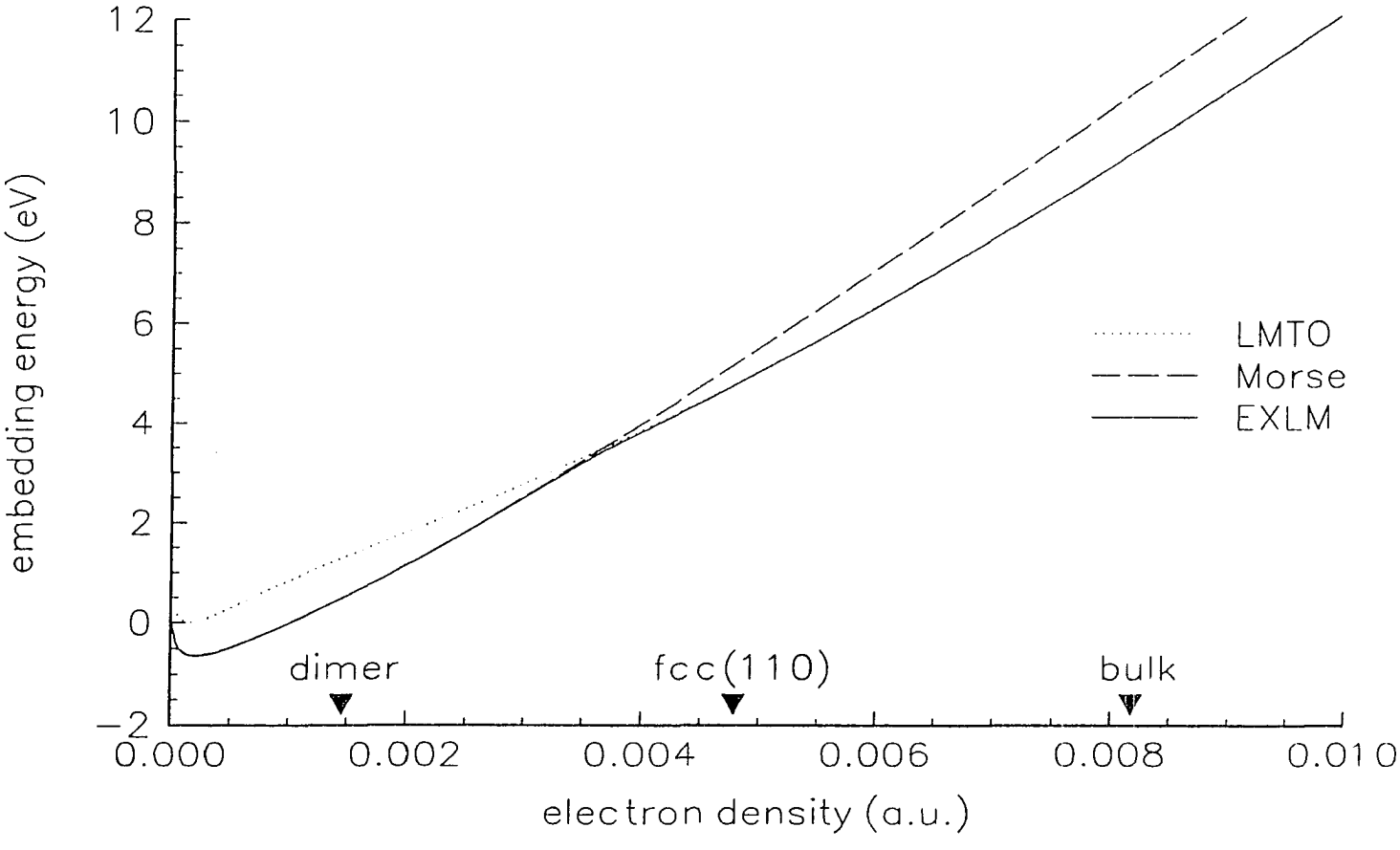
12
10
8
6
4
2
0
−2
embedding energy (eV)
dimer
fcc(110)
bulk
0.000
0.002
0.004
0.006
0.008
0.010
electron density (a.u.)
LMTO
Morse
EXLM

Figure 5.

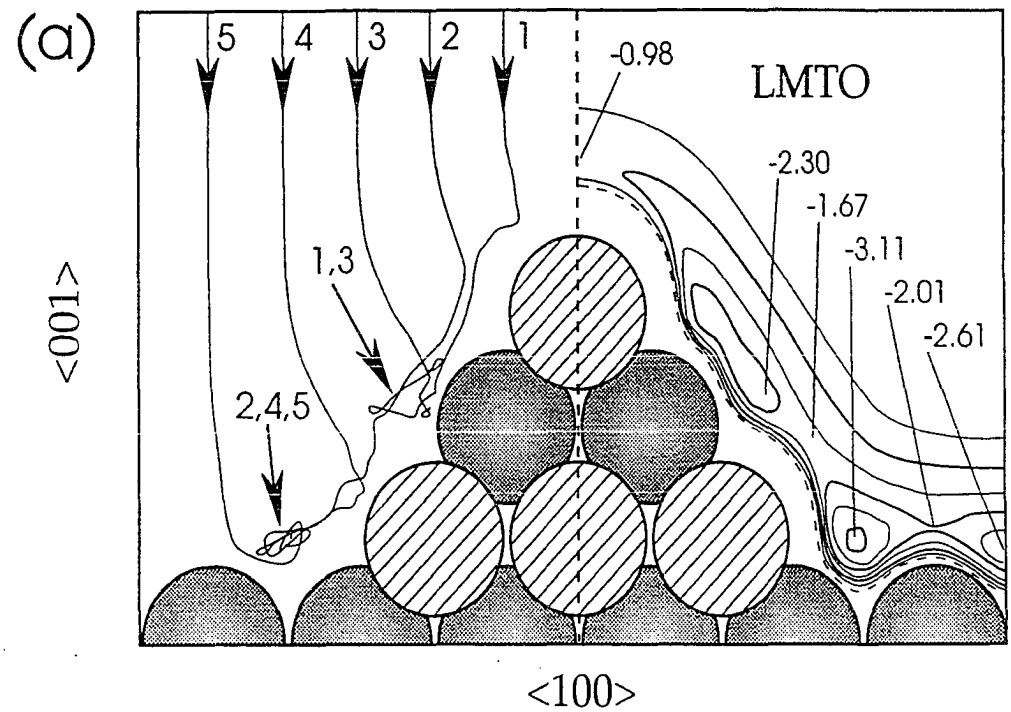
(a)
5
4
3
2
1
-0.98
LMTO
-2.30
-1.67
-3.11
-2.01
-2.61
1,3
2,4,5
<001>
<100>
(b)
5
4
3
2
1
-1.18
EXLM
-2.49
-2.10
-3.11
-2.27
-2.65
3
1,2,4,5
<001>
<100>

Figure 6.

MOLECULAR DYNAMICS SIMULATION OF MULTILAYER HOMOEPITAXIAL DEPOSITION ON FCC(100) METAL SURFACES

A paper accepted by the Journal of Vacuum Science and Technology A

Cynthia L. Kelchner and Andrew E. DePristo

Abstract

Two features are observed to be important in the homoepitaxial deposition of 50 monolayers on Pd(100) and Cu(100) at 80 K. First, a fourfold hollow site that is missing one or more of its four supporting atoms on the surface (i.e., an overhang site) can be stable. This increases the surface roughness by allowing defects in the growing surface. Second, multiatom rearrangements occur during growth. These events decrease the local surface roughness by filling deep holes in the surface. Neither of these two features is included in currently used kinetic growth models.

Introduction

The growth of thin films is a topic of great interest to experimentalists and theorists for both fundamental and applied reasons. Thin films are often grown by a sequential deposition process such as molecular beam epitaxy, and the final structure of a film can range from a smooth, uniform thin film to a very rough or amorphous film. Applications include a wide variety of electronic devices as well as the development of new materials.

The film structure can often be selected by an appropriate choice of experimental parameters, e.g., deposition rate (flux) and temperature. Insight into how and why thin films

grow under different experimental conditions can be provided by molecular dynamics (MD) simulations of the deposition process which explore the atomic growth mechanism(s) of the film during deposition. Such detailed information is impossible to obtain with current experimental techniques since it entails following the motion of individual atoms as they are deposited and determining the various processes involved as the atoms equilibrate with the surface. Furthermore, MD simulations make no assumptions about the type of processes allowed during deposition and growth, and thus can provide more complete information about the growth behavior than found in the currently available kinetic and statistical models of thin film growth.

A great deal of theoretical and experimental work has been done on submonolayer film growth for metals.[1] However, the growth of multiple layer thin films has not been as well studied, especially by theoretical methods. Since applications often use films containing many layers, it is important to understand how the growth behavior changes with the film thickness as well as the mechanisms behind such changes. Toward this end, we have studied two very simple yet realistic metal systems in order to elucidate the basic processes occurring during the deposition of multiple layers. This article presents the initial findings for homoepitaxial deposition of Pd and Cu on the fcc(100) surface.

We have designed and performed numerical experiments using MD to study the low temperature deposition of multiple layers in metal systems, specifically homoepitaxial deposition of 50 monolayers (ML) of Pd and Cu on the fcc(100) surface at 80 K. To our knowledge, the only earlier articles in this area are MD simulations by Gilmore and Sprague that studied the deposition of up to 3 ML Ag on (100) and (111) Ag surfaces using embedded

atom method (EAM) potentials[2,3] and a brief mention of void formation during deposition of about 8 ML Ni/Ni(100) by Andreadis, et al.[4] using MD with EAM potentials. The latter article did not give any details and we are not aware of any other MD simulations of multiple layer deposition in metal systems with reliable interaction potentials.

The primary concern when simulating deposition processes is the incompatible time scales of the experiment and the simulation. Whereas deposition experiments typically run for minutes with a slow deposition rate such as 0.01 ML/s, MD simulations can only model up to a few nanoseconds due to computational limits and necessarily use a much higher deposition rate such as 0.01 ML/ps. One way to avoid the experiment/theory time scale discrepancy is to study systems in which the only important processes occur on a very fast (picosecond) time scale. This permits the simulation and the experiment to observe the same events. At 80 K, thermally activated surface diffusion for the Pd/Pd(100) and Cu/Cu(100) systems is extremely slow, e.g., 1 atomic hop per 10^5 years for an activation energy of 0.4 eV. The film growth is then determined solely by the deposition dynamics which persist for only picoseconds after a deposition event. MD is therefore an appropriate method to study these systems. (It is interesting to note that, if only long-time scale processes involving a few atoms are important, one can also simulate the problem using kinetic Monte Carlo methods. The difficulty occurs when both short-time deposition dynamics and long-time diffusion are important.)

Simulation Details

These MD simulations use the simplest form of corrected effective medium (CEM) theory, known as MD/MC-CEM, which provides accurate interaction potentials for metals.[5-7] Briefly, CEM theory determines the interaction energy of a system in any geometry by calculating the

energy of each atom in a reference system plus correction terms, a non-self consistent approximation to density functional theory. This method has been extensively described elsewhere[5,6] including a recent critical review,[7] and no further details will be given here. The present study is the first use of this method for sequential deposition and the subsequent growth of thin films.

The MD simulations use periodic boundary conditions in the surface plane (in x and y). The square fcc(100) surface is modeled by 11 x 11 atoms in each layer, with three active layers and one fixed layer at the start of the simulation. The surface is initialized from a Boltzmann distribution at 80 K, and the lowest active layer (i.e., the one closest to the fixed layer) is treated by Langevin dynamics during the simulation to mimic a constant temperature heat bath. One new atom is placed out of the interaction range above the surface (+ z direction) with random x and y coordinates and an initial kinetic energy of 0.25 eV directed toward the surface. This kinetic energy is sufficiently small to be of no consequence compared to the large energy of adsorption. After 1 ps, another new atom is placed above the surface and the deposition process is repeated until the desired number of atoms have been deposited. All atoms follow Newton's equations (with local Langevin dynamics for the lowest active layer) throughout the simulation (except for the initial fixed layer which remains fixed, of course). The deposition of 50 ML with these simulation parameters requires eight weeks on a single MIPS R4400 150 MHz processor on an SGI Challenge-L computer.

Results

The morphology of the growing surface can suggest some of the possible mechanisms by which deposited atoms find stable adsorption sites on the surface. For instance, an atomically

smooth surface implies that the deposited atoms move to find the lowest empty sites on the surface, rather than staying very close to where they land and presumably creating an atomically rough surface. One way to measure the roughness of the surface is to calculate the interface width, w. (The interface referred to here is that of the surface with the surrounding vacuum. The adsorbate-substrate interface has little significance in homoepitaxial systems.) The interface width is defined to be the standard deviation of the distribution of the exposed layers' height in units of the ideal layer spacing, and is calculated from the following equation:[8]

$$w^2 = \sum_{j=0}^{\infty} \left(j - \bar{j}\right)^2 N_j \qquad (1)$$

N_j is the net number of exposed atoms in layer j where j=0 is the top substrate layer. The mean height of the surface is $\bar{j}$. The standard method[8] of calculating the net number of atoms in each layer that is exposed to the vacuum, i.e., $N_j = \theta_j - \theta_{j+1}$, where θ_j is the coverage in ML of layer j, assumes that no vacancies are present in the deposited adsorbate layers so that $\theta_j \geq \theta_{j+1}$ and $N_j \geq 0$. However, we find many vacancies in our MD simulations, as we shall discuss, and therefore must explicitly consider each atom rather than use the layer coverages to calculate N_j.

The interface width during deposition of 50 ML Pd/Pd(100) and 50 ML Cu/Cu(100) is shown in Figures 1 and 2. These results are from a single MD simulation of each system. In general, the interface width increases as more layers are deposited, indicating a continual roughening of the surface with coverage. The abrupt drop in the Pd/Pd(100) interface width just after deposition of 20 ML (Figure 1) reflects a dramatic change in the surface structure

leading to a smoother surface. This particular structural transformation is caused by a large number of adsorbed atoms moving to fill a deep hole in the surface, as can be seen by visual animation of the MD simulation results (not shown). A similar rearrangement event in the Cu/Cu(100) system is marked by the sharp decrease in the interface width at 34 ML (Figure 2). Several other decreases in the interface width are observed in each system as well. The magnitude of the interface width decrease is not necessarily related to the number of atoms involved in the rearrangement. For example, covering two partially exposed atoms in lower layers can greatly decrease the interface width, as occurs in the Pd/Pd(100) system at 49 ML coverage. The exposed atoms in lower layers (far from the average surface height, $\bar{j}$) are weighted quadratically in the interface width calculation (Eq. 1) and thus contribute much more to the width than those in higher layers (closer to $\bar{j}$).

It is not yet clear what initiates a rearrangement event. Perhaps an unstable structure simply collapses, or an impinging atom hits a rough portion of the surface in a certain way, or some other multiatom mechanism appears. It is also unclear if the multiatom events are due to a true concerted motion or to a chain reaction of the involved atoms. We are presently working to further understand these interesting reorganizations. Nonetheless, it is obvious that the rearrangement events significantly decrease the surface roughness, at least on a local scale.

By the end of 50 ML deposition, there are 55 occupied adsorbate layers in both the Pd and Cu systems. In the Pd/Pd(100) system, these consist of 20 completely filled and 35 incomplete adsorbate layers, including 12 layers which have atoms exposed to the vacuum. In the Cu/Cu(100) system, there are 14 complete and 41 incomplete layers, including nine

exposed layers. The Cu/Cu(100) system is likely a little smoother than the Pd/Pd(100) one since it has fewer exposed layers and generally a smaller interface width (compare Figures 1 and 2). However, the complex variation of interface width with deposition coverage makes such a comparison difficult.

Most of the incomplete layers contain vacancies which are covered by atoms in higher layers, i.e., bulk vacancies. The Pd/Pd(100) system has an equivalent of 1.24 ML bulk vacancies after deposition of 50 ML, and Cu/Cu(100) has 1.67 ML bulk vacancies. Single bulk vacancies are found as well as small voids containing several vacancies. Most of the vacancies, however, are found in large voids with 30-100 or more connected bulk vacancies. A bulk vacancy or void is formed when depositing atoms remain in overhang sites instead of moving down to fill an empty site. An overhang site is defined as a fourfold hollow site that is missing one or more of its four supporting atoms. The fourfold hollow sites are usually considered to be the only energetically stable adsorption sites on fcc(100) surfaces. However, the overhang sites are clearly stable in these MD simulations, with up to 15% of the atoms in some layers missing at least one of their four supporting atoms. This stability is presumably due to interactions with neighboring atoms in the same layer as the overhanging atom. The presence of atoms in overhang sites increases the surface roughness by leaving more layers of atoms partially exposed than if the overhanging atoms moved down to fill the lower empty sites.

These vacancy observations are in general agreement with those reported by Sprague and Gilmore for MD deposition of 3 ML Ag/Ag(100).[2] They stated that the "undersupported" (overhang) sites are stabilized by neighboring atoms on the (100) surface, although this was

not the case on the triangular (111) surface where overhanging atoms quickly moved to fill an empty site. They also saw small voids and single bulk vacancies form. Similarly, Andreadis et al.[4] observed "ribbon-like voids" of 5-10 vacancies across in an MD simulation of Ni/Ni(100). The occupied fractions of the adsorbate layers after 3 ML deposition are given in Table I. The results from the Ag/Ag(100) simulation[2] indicate a noticeably rougher surface after deposition of 3 ML than do our MD results for either Pd/Pd(100) or Cu/Cu(100). We do not see any bulk vacancies at this early stage of the deposition process. This difference is almost certainly due to the inadequacy of the EAM interactions used in Ref. 2 which overbind the low coordination atoms, a well-known failing of EAM potentials.[6]

Growth Models

Several kinetic and statistical models have been developed for epitaxial growth. In layer-by-layer growth,[9] each layer is completely filled before the next layer begins to fill. In the downward funneling model,[9] impinging atoms "funnel down" the side of existing structures to reach an adsorption site at the base. In the random deposition (RD) model,[10,11] atoms deposit onto atop sites in a simple cubic lattice, i.e., column growth. In the more sophisticated random deposition onto fourfold hollow sites (RD-4FH) model,[12] atoms may only deposit in fourfold hollow sites on an fcc(100) surface with any atom not deposited in an allowed site being deflected from the surface. Defects are not allowed in any of these models. The predicted interface width scales as $w = \{\theta(1-\theta)\}^{1/2}$ for the layer-by-layer model, where θ is the total coverage in ML and the restriction $0 \leq \theta \leq 1$ holds since each layer fills completely before another is started in this model. For the other models, one has $w \sim \{\log\theta\}^{1/2}$, $w = \theta^{1/2}$, and $w \sim \theta^{1/4}$ for funneling, RD, and RD-4FH models, respectively. In the ballistic deposition

model,[10,13] defects can form since each impinging atom is required to stay in the first site it reaches with one or more nearest neighbors. This results in a large number of vacancies and overhangs since no supporting atoms are needed when an atom has a nearest neighbor in the same layer. The predicted interface width scales as $w \sim \theta^{1/4}$ for three-dimensional ballistic deposition onto a simple cubic lattice.[13] Each overhanging atom in this simple cubic lattice model completely covers an empty site as well as the atoms exposed by the empty site, and therefore it does not increase the surface roughness as an overhanging atom does on the fcc(100) surface.

The predicted interface width from these models is plotted in Figures 1 and 2 for comparison with the MD results. Layer-by-layer growth results in the smoothest possible growing surface and hence the smallest interface width, with the model's predictions bearing little resemblance to the detailed MD simulations. By contrast, the downward funneling model's interface width is similar to the MD results for about the first 5 ML deposition in both the Pd and Cu systems but is much too small at higher coverages compared to the MD values. The reason for the funneling model's failure is that a deposited atom cannot occupy an overhang site but always continues down to a complete fourfold hollow site, thereby eliminating vacancies and overhangs. The RD-4FH model's interface width is similar to the MD results for up to about 10 ML in Pd and 16 ML in Cu. This is surprising since this model allows only those atoms landing directly in a complete fourfold hollow site to stay on the surface and thus has a sticking coefficient that is less than one, a physically unreasonable result for metals. Eventually, since no overhanging atoms are allowed, the RD-4FH model produces a smaller interface width (smoother surface) than in the MD simulations. Lastly, the RD

model predicts perhaps the roughest possible growth (assuming no upward motion of atoms), corresponding to a Poisson distribution of the column heights.

We fit our interface width results to a power law of the coverage: $w = A\ \theta^{\beta}$, where β is the growth exponent in accordance with the dynamic scaling theory.[14] This yields $\beta = 0.45$, $A = 0.44$ for 50 ML Pd/Pd(100), and $\beta = 0.40$, $A = 0.47$ for 50 ML Cu/Cu(100). If the first 15 ML of the Cu simulation in Figure 2 is considered, we find $\beta = 0.26$, which is similar to the RD-4FH and ballistic deposition models ($\beta = 0.25$). In contrast to the Cu/Cu(100) system, the Pd/Pd(100) interface width in Figure 1 increases more quickly during deposition of the first 15 ML (β=0.44) indicating the continuous roughening of the surface. The rougher growth of the Pd vs. Cu system is in accord with simple arguments[15] based upon the funneling model, even though such arguments lose validity after about 5 ML in these MD results since the funneling model is not accurate there. The steep increases and decreases in the interface width from our MD simulations in Figures 1 and 2 suggest the difficulties in accurately modeling the complicated growth mechanisms and multiatom structural rearrangements taking place on the growing surface.

Conclusions

Two significant features are observed in the homoepitaxial deposition of 50 ML Pd/Pd(100) and Cu/Cu(100) at 80 K. First, the overhang sites on the surface can be stable, in contrast to the common view that only complete fourfold hollow sites are stable on the fcc(100) surface. This can greatly increase the surface roughness by allowing defects in the growing surface. Most growth models do not include defects of any kind. An exception is the ballistic deposition model on the simple cubic lattice but this lattice structure prevents the

defects from increasing the surface roughness as in the fcc(100) systems. Second, multiatom rearrangement events occur during growth. These fill or cover deep holes in the surface and thus tend to decrease the local surface roughness. Such multiatom processes are not included in any of the current growth models, and indeed may be too difficult to do so and retain any simplicity in the model.

Acknowledgements

We thank Professor J. W. Evans for helpful discussions. This work was supported by NSF grant CHE-9224884.

References

[1] J.-K. Zuo, J. F. Wendelken, H. Dürr, and C.-L. Liu, Phys. Rev. Lett. **72**, 3064 (1994); H. Brune, Ch. Romainczyk, H. Röder, and K. Kern, Nature **369**, 469 (1994); A. Zangwill, Mater. Res. Soc. Symp. Proc. **280** (*Evolution of Surface and Thin Film Microstructure)*, 121 (1993).

[2] J. A. Sprague and C. M. Gilmore, Mater. Res. Soc. Symp. Proc. **268** (*Materials Modification by Energetic Atoms and Ions*), 115 (1992).

[3] C. M. Gilmore and J. A. Sprague, Surf. Coat. Technol. **51**, 324 (1992); C. M. Gilmore and J. A. Sprague, Phys. Rev. B **44**, 8950 (1991).

[4] T. D. Andreadis, M. Rosen, M. I. Haftel, and J. A. Sprague, Mater. Res. Soc. Symp. Proc. **202** (*Evolution of Thin Film and Surface Microstructure*), 283 (1991).

[5] S. W. Rosencrance, J. S. Burnham, D. E. Sanders, C. He, B. J. Garrison, N. Winograd, Z. Postawa, and A. E. DePristo, Phys. Rev. B **52**, 6006 (1995); Y. Li and A. E. DePristo, Surf. Sci. **319**, 141 (1994); T. J. Raeker and A. E. DePristo, Phys. Rev. B **49**, 8663 (1994); C. L. Kelchner, D. M. Halstead, L. S. Perkins, N. M. Wallace, and A. E. DePristo, Surf. Sci. **310**, 425 (1994); M. S. Stave and A. E. DePristo, J. Chem. Phys. **97**, 3386 (1992); S. B. Sinnott, M. S. Stave, T. J. Raeker, and A. E. DePristo, Phys. Rev. B **44**, 8927 (1991).

[6] T. J. Raeker and A. E. DePristo, Int. Rev. Phys. Chem. **10**, 1 (1991).

[7] A. E. DePristo, in *Recent Advances in Density Functional Theory*, vol. 1, Part 1, ed. D. Chong (World-Scientific, Singapore, 1996), ch. 6.

[8] J. W. Evans, Phys. Rev. B **43**, 3897 (1991).

[9] J. W. Evans, D. E. Sanders, P. A. Thiel, and A. E. DePristo, Phys. Rev. B **41**, 5410 (1990).

[10] J. W. Evans, Phys. Rev. B **39**, 5655 (1989).

[11] F. Reif, *Fundamentals of Statistical and Thermal Physics* (McGraw-Hill, New York, 1965), p. 42.

[12] H. C. Kang and J. W. Evans, Surf. Sci. **271**, 321 (1992).

[13] P. Meakin, CRC Crit. Rev. Solid State Mater. Sci. **13**, 143 (1988).

[14] L. M. Sander, in *Solids Far From Equilibrium: Growth Morphology and Defects*, ed. C. Godrèche (Cambridge University Press, Cambridge, 1991); F. Family and T. Vicsek, J. Phys. A **18**, L75 (1985).

[15] D. M. Halstead and A. E. DePristo, Surf. Sci. **286**, 275 (1993).

Table I. Occupied layer fractions after 3 ML deposition for adsorbate layers 1-5. The Pd and Cu results are from the MD simulations presented in this article. The Ag results are from MD simulations in Ref. 2.

	layer				
system	1	2	3	4	5
Pd/Pd(100)	1.00	0.99	0.82	0.17	0.02
Cu/Cu(100)	1.00	1.00	0.75	0.24	0.01
Ag/Ag(100)	0.92	0.86	0.74	0.40	0.08

Figure Captions

Figure 1. Interface width for Pd/Pd(100) during homoepitaxial deposition at 80 K. The predicted interface widths from several models are labeled and plotted for comparison.

Figure 2. Same as Figure 1 but for Cu/Cu(100).

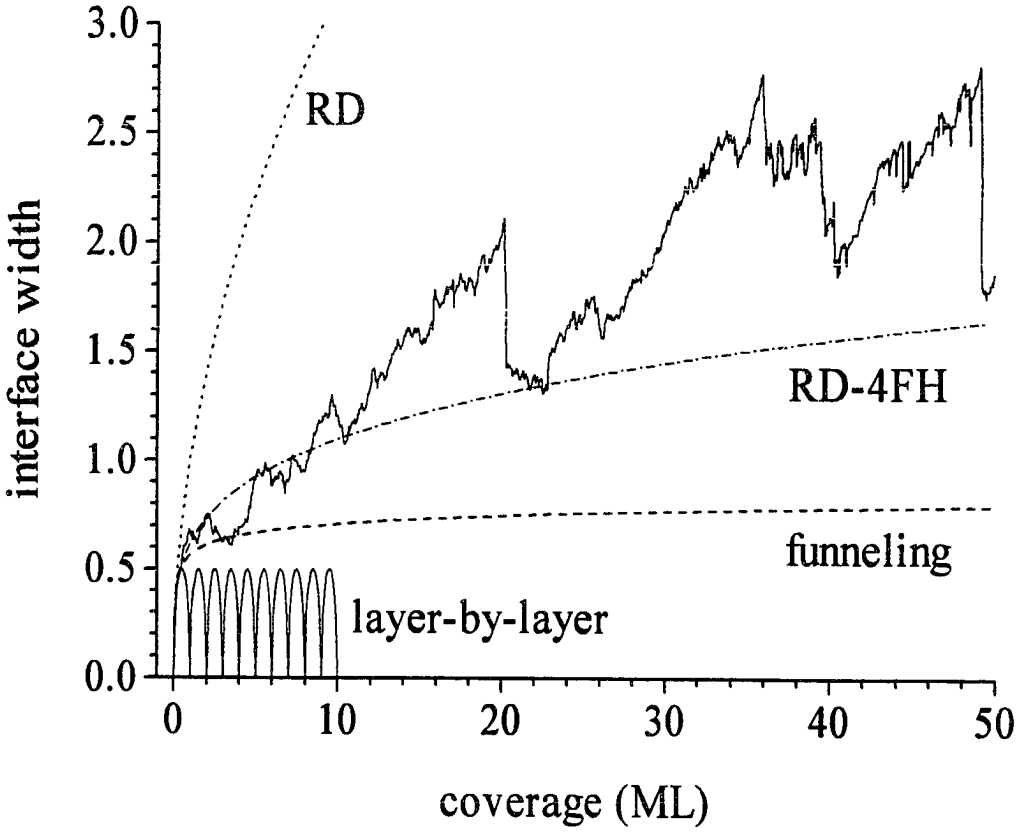
3.0
2.5
2.0
1.5
1.0
0.5
0.0
interface width
RD
RD-4FH
funneling
layer-by-layer
0
10
20
30
40
50
coverage (ML)

Figure 1.

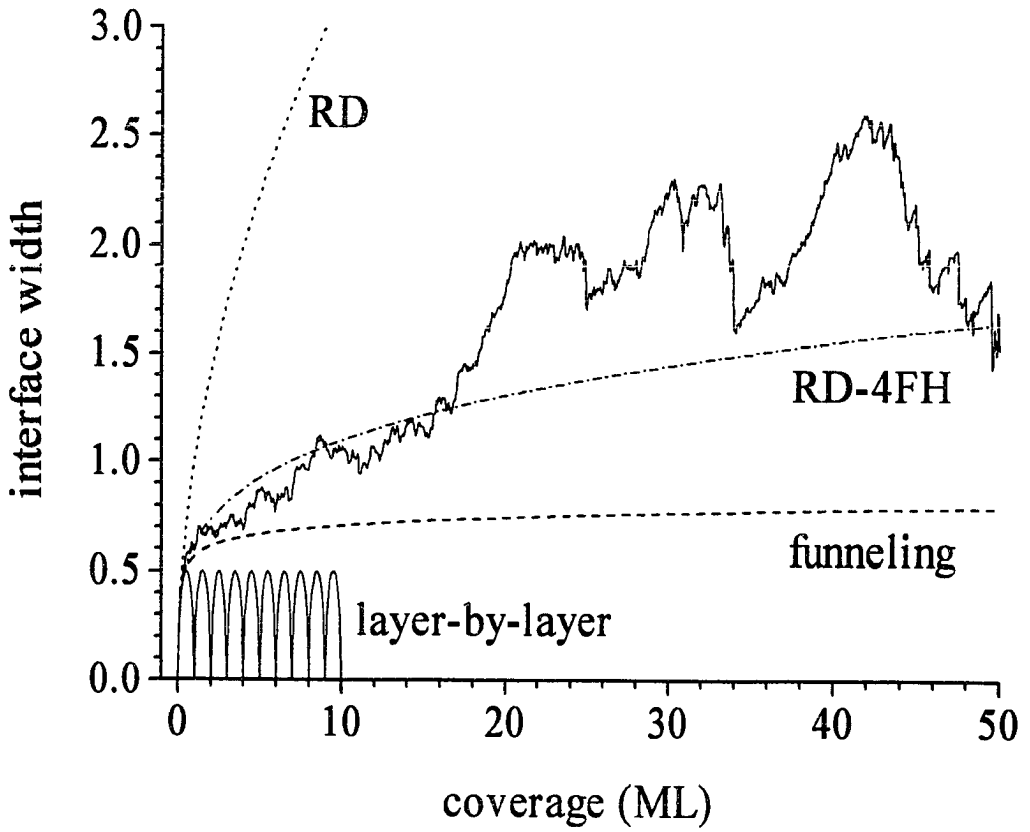
3.0
2.5
2.0
1.5
1.0
0.5
0.0
interface width
RD
RD-4FH
funneling
layer-by-layer
0
10
20
30
40
50
coverage (ML)

Figure 2.

MOLECULAR DYNAMICS SIMULATIONS OF MULTILAYER HOMOEPITAXIAL THIN FILM GROWTH

A paper submitted to Surface Science

Cynthia L. Kelchner and Andrew E. DePristo

Abstract

Molecular dynamics simulations permit multiple-layer thin film growth to be studied in detail, using reliable interatomic potentials for fcc metals from corrected effective medium theory. Results are presented for the homoepitaxial deposition of 50 ML on Pd(001) and Cu(001) at 80 K. We find that atoms in overhang sites are stable, and this stability leads to many of the observed results. The growth behavior of the thin film changes after deposition of the first 5-10 monolayers: more overhanging atoms are present, the surface is rougher, and multiple-layer events begin to occur. The formation of large voids in the film and the mechanism of multiatom rearrangement events which decrease the surface roughness are discussed. Several simulation parameters have been varied (e.g., deposition rate, system size, random aiming points of the deposited atoms) to study their effects on the results. There is no clear difference between Pd and Cu thin film growth at this low temperature.

Introduction

The properties of thin films are often very different from those of bulk materials and can lead to new materials and applications. Varying the way in which the films are grown can further modify the electrical, magnetic, optical, and mechanical properties. The physical

structure of a thin film affects many of these properties through the roughness of the film surface and the concentration of defects such as dislocations, voids or porosity, grain boundaries, and impurities.[1] Precise control of the growth of thin films is therefore critical in many applications of thin film technology.

Thin films are typically grown by a sequential deposition process such as molecular beam epitaxy, and the surface of a deposited film can range from smooth and uniform to very rough or amorphous. Insight into how and why thin films grow under different experimental conditions enables production of the desired film structure in a controlled manner. This insight can be provided by molecular dynamics (MD) simulations of the deposition process. MD simulations identify the atomic growth mechanism(s) of the film by following the motion of individual atoms as they are deposited and determining the various processes involved as the atoms adsorb on the surface. Current experimental techniques do not allow such detailed observations of individual atomic movements or atomic growth mechanisms. Furthermore, MD simulations make no assumptions about the type of processes allowed during deposition and growth, and thus can provide more complete information about the growth behavior than found in the currently available kinetic and statistical models of thin film growth.[2] A major disadvantage to MD simulations is the time scale which is at least 10 orders of magnitude shorter than experimental time scales. This limitation can be obviated by choosing systems where only short time scale (picosecond) processes are important so that the MD simulation and the experiment can observe the same events.

While a great deal of theoretical and experimental work has been done on submonolayer film growth for metals,[3] the growth of multiple-layer thin films has not been well studied,

especially by theoretical methods. Some theoretical work has been done on the growth of films with up to three layers,[4] but we are unaware of any theoretical studies in three dimensions detailing the growth of thicker metal films with reasonably accurate interatomic potentials (e.g., describing coordination dependence of bonding). It is important to understand how the growth behavior changes with the film thickness and the mechanisms behind such changes, since applications typically use films containing many layers.

With this in mind, we have studied two homoatomic fcc(001) metal systems at very low temperature in order to elucidate the basic processes occurring during the deposition of multiple layers. Low coordination sites are important on the surface, particularly during deposition when the atom is first approaching the surface and near defects. The two fcc metals chosen, Pd and Cu, have very different dimer binding energies compared to their bulk cohesive energies. For Pd, the bond energy drops by 73% from the bulk to the dimer, whereas the corresponding bond energy drop is only 41% for Cu. The variation of bonding with coordination will therefore differ for the two metals.[5]

Previous work predicted that Pd would prefer to grow more roughly than Cu on the fcc(001) surface at low temperature due to kinetic limitations, in spite of the lower stability of Pd in low coordination sites.[6] These results were based on multiple trajectories of the deposition of a single atom onto a prepared pyramidal defect. In the present study, we consider sequential deposition of many single atoms to determine if the thin film growth does indeed agree with this prediction. We follow the growth of ultrathin films up to 50 monolayers (ML) thick, about 100 Å or 10 nm.

An earlier paper[7] presented our initial findings for homoepitaxial deposition of Pd and Cu on the fcc(001) surface at 80 K. This low temperature was chosen to eliminate any effects of thermally activated surface diffusion on the (001) surface. Results from a single simulation of the deposition of 50 ML Cu/Cu(001) and one of 50 ML Pd/Pd(001) emphasized the presence of bulk vacancies and voids in the deposited films and the occurrence of multiatom rearrangements during thin film growth. Several kinetic and statistical models of thin film growth were examined but none of them agreed with the MD simulation results.[7] In the present paper, we extend the analysis and discussion of such "numerical experiments" and include the effects of varying the deposition parameters.

The next section describes the MD simulations and the calculation of the surface roughness. The effects of varying the deposition parameters are then explored in order to control any computational artifacts. The important results from these simulations are presented in the Results section for comparison to experiment, and conclusions are given in the final section.

Simulation Procedure

The MD simulations use the simplest form of corrected effective medium (CEM) theory, known as MD/MC-CEM, which provides accurate interaction potentials for metals.[8, 9, 10] CEM theory determines the interaction energy of a system in any geometry by calculating the energy of each atom in a reference system plus correction terms for the difference in Coulomb and kinetic-exchange-correlation energies between the interacting system and the atom-in-reference system. This method has been extensively described elsewhere,[8, 9] including a recent critical review,[10] and no further details are given here.

Periodic boundary conditions are used in the surface plane (in x and y). The square fcc(001) surface has three active layers and one fixed layer at the start of the simulation. The surface is initialized from a Boltzmann distribution at 80 K, and the lowest active layer (i.e., the one closest to the fixed layer) is treated by Langevin dynamics during the simulation to mimic a constant temperature heat bath. One new atom is placed out of the interaction range above the surface (+ z direction) with random x and y coordinates and a small initial kinetic energy of 0.25 eV directed toward the surface. After a specified time, another new atom is placed above the surface and the deposition process is repeated until the desired number of atoms have been deposited. All atoms follow Newton's equations (with local Langevin dynamics for the lowest active layer) throughout the simulation, except for the initial fixed layer which remains fixed. An MD simulation with 11 x 11 atoms in each layer and 1 ps between depositions corresponds to a deposition rate of 8×10^9 ML/s. Allowing 2 ps between depositions decreases the deposition rate to 4×10^9 ML/s.

The morphology of the growing film can suggest possible mechanisms by which deposited atoms find stable adsorption sites on the surface. One way to measure the roughness of the surface is to calculate the interface width, w. The interface width is defined to be the standard deviation of the distribution of the exposed layers' height in units of the ideal layer spacing, and is calculated from the following equation:[11]

$$w^2 = \sum_{j=0}^{\infty} \left(j - \bar{j}\right)^2 N_j \qquad \textbf{Eq. 1}$$

N_j is the net number of exposed atoms in layer j where j=0 is the top substrate layer. The mean height of the surface is $\bar{j}$. Other notation in this paper includes θ_{tot}, the total coverage

in ML, and θ_j which is the fractional coverage in ML of any layer j such that layer j is completely filled when $\theta_j = 1$.

The interface width, w, is calculated from the surface structure at the end of each deposition event throughout the simulation. However, not every deposited atom reaches a stable site before the next atom is deposited, particularly if the atom's aiming point is located in a deep hole on the surface. At $\theta_{tot} > 40$ ML in Figure 1, the interface width in the top curve displays many steep decreases consisting of a single point. These negative spikes in w are caused by a depositing atom that is temporarily covering atoms exposed in a deep hole. The exposed atoms in lower layers (far from $\bar{j}$) are weighted quadratically in the interface width calculation (Eq. 1) and thus contribute much more to the width than those in higher layers (closer to $\bar{j}$). When the depositing atom reaches a stable adsorption site, w assumes its previous value or close to it.

In experimental measurements, the interface width and other surface data are not evaluated after deposition of every atom but after deposition of a large number of atoms. The interface width from our MD simulations can be evened out by averaging w over multiple deposition events. Figure 1 presents the results for one simulation from averaging w over 10, 100, 500, and 1000 deposition events (i.e., 0.08, 0.83, 4.13, and 8.26 ML), as well as the original w calculated after each deposition event. The averaged curves are shifted for clarity. Virtually no details are lost when averaging over 10 deposition events (0.08 ML) and the negative spikes are for the most part removed. Averaging over a larger coverage range flattens out the features of the interface width. Very few features remain when averaging over 1000 deposition events (8.26 ML). This is similar to bulk type experiments in that much of

the surface information has been lost. All other interface width figures in this paper plot w averaged over 10 deposition events.

Effects of Varying the Deposition Parameters

Random aiming points

The growth of a thin film at very low temperature is essentially a random process. The structure of the film in any small surface region is highly dependent upon the random aiming points of the depositing atoms since there is no mechanism (such as site hopping) for atoms to move after they adsorb on the surface. On a large surface, the random growth should average out to produce a surface structure which is more uniform. We look only at small-scale structures and the local effects of the random aiming points.

We compare two simulations for a Pd(001) surface with 11 x 11 atoms per layer at 80 K and identical deposition parameters except for the set of random aiming points for the deposited atoms. One Pd atom is deposited every 1 ps until a total of 50 ML have been deposited. The interface widths, plotted in Figure 2, show that the surface in simulation B remains smoother than that in simulation A. This holds throughout the deposition process except near a multiatom rearrangement event which occurs in simulation A at $\theta_{tot} = 20.1$ ML, about 5 ML earlier than in simulation B. (Rearrangement events are indicated by a sudden decrease in the interface width.) This is consistent with the idea that the surface must develop a certain degree of roughness before a rearrangement is likely to take place. The two simulations are fairly similar until $\theta_{tot} \approx 35$-40 ML where there are several rearrangement events in simulation B. The surface roughness in simulation B then remains nearly constant

during deposition of another 10 ML. This is the only simulation we have seen with a constant interface width over such a large coverage range.

Details about these two thin films at the end of 50 ML deposition are given in Table 1. Simulation B has less than half as many bulk vacancies and one-third fewer incomplete layers as compared to simulation A. However, the most striking difference, not evident from these numbers, is the initiation and propagation of an edge dislocation during film growth in simulation B. The dislocation is first observed on the surface at θ_{tot} = 25.8 ML, where two adjacent atoms are located in twofold bridge sites instead of fourfold hollow sites. This dislocation appears at the end of a multiatom rearrangement which covers (rather than completely fills) a narrow hole in the surface. Overhanging atoms in distorted positions cover the hole, which is only 3 sites wide here, and induce the dislocation by providing distorted adsorption sites for atoms in higher layers. Subsequent deposited layers each contain one or more rows shifted by one-half of a unit cell with respect to neighboring rows. The atoms in a single dislocated row have six nearest neighbors (hexagonal) in the same layer and create threefold sites for two rows of atoms in the next higher layer, propagating the dislocation. As the film grows, the dislocated row(s) move one unit cell across the surface with each additional layer.

It is difficult to determine if the dislocation is directly responsible for the relatively smooth surface during thin film growth in simulation B. The large decrease in w during deposition of 36-39 ML reflects several multiatom rearrangements, possibly influenced by the presence of the edge dislocation. The dislocation may also help prevent large holes from forming in the surface by destabilizing the overhang sites around a hole, i.e., by lowering the energetic barrier

to interlayer diffusion. This would make it easier for an atom to move down to fill an empty site.

The comparisons in Figure 2 and Table 1 clearly show that the random deposition process can exert great influence on the short-range surface structure of a thin film. As we will see in the following sections, the random deposition itself can have more effect on the surface roughness than changing the parameters of the simulation.

Deposition rate

The deposition rate in an MD simulation is limited by the available computational resources. The small timestep in an MD simulation (10^{-14} s) restricts the total length of the simulation to 5-10 ns and forces a very fast deposition rate when studying thin film growth. If the deposition rate is too fast, one deposition event may affect the next and produce results not seen in experiments where the slower rate ensures isolation of deposition events.

There are two ways to measure the effect of the deposition rate on film growth. One way is to look at the structure of the surface at the end of deposition, and the other is to determine the surface temperature during deposition. If the surface structure is similar for different rates, then there is no practical effect of varying the deposition rate in the growth regime being studied and the more convenient rate may be used. The surface temperature indicates how quickly the adsorption energy of each deposited atom is dissipated into the bulk for a given set of parameters and whether one deposition event can affect the next through changing the surface temperature.

First we consider the surface structure. Figure 3 shows the fraction of atoms in the first adsorbate layer (θ_1) after deposition of 1 ML for various deposition rates of Pd/Pd(001) and

Cu/Cu(001). This value does not depend on the deposition rate, suggesting that the surface structure does not depend on the rate during film growth. The same is true for θ_3 after deposition of 3 ML for Cu/Cu(001), as seen in the inset of Figure 3.

The interface width gives further information about the surface structure, and w is plotted in Figure 4 for two simulations of 50 ML Pd/Pd(001) with different deposition rates. There is no clear distinction between the two curves. One might expect the faster deposition rate (1 ps between depositions) to produce a smoother surface due to local heating or ballistic effects of two or more atoms depositing in the same area within a short time. However, the opposite seems to be true for both Pd (Figure 4) and Cu (not shown), although the differences are small. It appears that the slower deposition rate (2 ps) may allow w to increase more slowly. This would explain the multiatom rearrangement event occurring roughly 4 ML later than in the 1 ps simulation in Figure 4 since, as we shall discuss in the Results section, the interface width must reach a certain value before rearrangement is likely to take place. On the other hand, the differences in w could easily be due to the different sets of random aiming points in the two simulations rather than to the deposition rates. Unfortunately, this cannot be resolved since statistics are unavailable for these extremely long simulations. (Each 50 ML simulation requires 8 to 15 weeks on a single MIPS R4400 150 MHz processor on an SGI Power Challenge-L computer.)

Next we consider the surface temperature during deposition. Figures 5 and 6 show that the temperature does depend upon the deposition rate. The adsorption energy of a deposited atom quickly dissipates away from the point of impact and disperses through all active atoms in the system.[12] Any excess energy is removed from the system via the Langevin atoms,

located in the bottom active layer. If the next deposition event occurs before the system returns to the bulk temperature, energy is being put in faster than it can be removed. This delay in energy removal is simply due to the time required for the adsorption energy to be transferred through the layers of the film and substrate. (Equilibration with the heat bath is completed within 1 ps after the excess energy reaches the Langevin atoms.) The rate of energy transport in a metal depends on the motion of the conduction electrons and the frequency of the atomic vibrations in the system.[13] Since CEM is based on ground state density functional theory with no coupling to electronic states, all energy transport in the MD simulations is due to the atomic vibrations. The adsorption energy dissipates faster in Cu than in Pd, as indicated by the lower temperatures for Cu in Figures 5 and 6, because Cu has a higher Debye frequency than Pd[13] (0.421 vs. 0.357 in 10^{14} s^{-1}). In all materials, however, the local surface temperature will be higher than the bulk temperature for some time after a deposition event.

Figure 5 shows the total system temperature during several 50 ML simulations. As the film thickness increases, the adsorption energy has farther to travel before it can equilibrate with the heat bath. The longer distance increases the time required for complete energy dissipation and hence the total temperature increases as θ_{tot} increases. The temperature increases more quickly for the surface (Figure 6) than for the total system (Figure 5) and this difference continues to increase with coverage, particularly for the faster deposition rate. The high temperature at low θ_{tot} in Figure 6 is due to the small number of adsorbate atoms. The surface temperature has been defined here as the temperature of the top 10 adsorbate layers. At θ_{tot} < 10 ML, the most recently deposited, and hottest, atoms are weighted more heavily in

the temperature calculation, particularly for very low θ_{tot}. As the deposition rate decreases (longer time between depositions), the temperature at a given θ_{tot} is noticeably smaller. For example, at θ_{tot} = 10 ML for Cu/Cu(001), the adsorbate temperature from Figure 6 is 132 K for 1 ps between depositions, decreases to 104 K for 2 ps, and is only 87 K when 5 ps are allowed between subsequent deposition events.

In this study, a very low temperature was chosen specifically to prevent surface diffusion on the time scale of both the MD simulation and experiment. A "hot" surface may provide enough extra energy for some atoms to overcome energetic barriers for processes which do not occur at the bulk temperature. The increased temperature in Figures 5 and 6 suggests that this may occur, again raising the issue of the time scale difference between simulation and experiment and the ensuing difficulty of simulating long-time scale processes such as surface diffusion. However, the high temperature is in fact an artifact of the very fast deposition rate in the simulations combined with the intrinsic thermal transport properties of the material. Therefore the possibility of surface diffusion and its corresponding difficulties for the MD simulations can be dismissed since diffusion does not occur in the real systems maintained at a very low temperature.

The increased temperature in the MD simulations has no obvious effect on the morphology of the surface, as seen in the earlier discussion regarding w for differing deposition rates. If anything, the surface should be smoother than the real system since deposition processes with higher energetic barriers may be more available. We conclude that the increased temperature in the MD simulations, while not reproducing the experimental

temperature, is explainable and does not affect the value of the simulations in understanding the mechanisms and events occurring during deposition.

System size

We now discuss the effect of varying the size of the system. A smaller system with periodic boundary conditions is preferred computationally since the size of the system determines how long it takes to calculate each timestep, as well as the number of atoms in one monolayer. If the system size is too small, however, surface defects may cover most of the surface and interact with one another through the periodic boundary conditions, unlike experiments where defects are typically isolated on the surface. The interface width, w, measures the surface roughness and is a good indication of the defect size. For all of our 50 ML simulations, the interface width remains below 3.0, in units of the ideal layer spacing ($a_0/2$). Compared to the size of the system (11 x 11, in units of the nearest neighbor distance, $a_0/\sqrt{2}$), the interface width is less than 20% of the length of the surface. Furthermore, most of the defects observed in these simulations are holes which tend to have less effect on the deposition of atoms near them than do large islands.

Another way that the small system size could affect the results would be if the surface roughness were to saturate during the deposition and growth of a thin film. Any finite system has a maximum roughness which is by definition smaller than that of an infinite system. Since the interface width from these MD simulations continues to increase throughout the deposition process, this limit has not been reached and thus the roughness of the film is not due to finite size effects.

One Cu/Cu(001) simulation has been performed with a larger system size (17 x 17) for comparison, using the slower deposition rate of 2 ps between depositions. The total number of atoms deposited in this 20 ML simulation corresponds to nearly 48 ML in the 11 x 11 system. With the larger system and slower deposition rate, this simulation required nearly 4 times as much computer time (29 weeks) to deposit 20 ML as the smaller 11 x 11 simulation did (8 weeks) to deposit 50 ML with 1 ps between depositions. The interface width results (not shown) are very similar to other Cu/Cu(001) results such as those in Figure 8. The size of the system apparently has no more influence on w than the set of random aiming points for the deposited atoms does in the simulation. The 11 x 11 system size is therefore sufficient to accurately describe the deposition process and film growth.

Results

Voids and vacancies in deposited film

The most stable adsorption site on a perfect fcc(001) surface is the fourfold hollow site. If there are defects in the surface, a fourfold hollow site may be missing one or more of its four supporting atoms and is then defined as an overhang (or incomplete) site. An atom in an overhang site is less energetically stable than one in a complete fourfold hollow site because it has fewer neighbors. Nevertheless, up to 15% of the atoms in a given layer remain in overhang sites after deposition instead of moving to fill the empty fourfold site below, due to interactions with neighboring atoms in the same layer.[7] Atoms first appear in overhang sites at θ_{tot} = 2-3 ML, although the empty sites present at this low coverage are eventually filled in

during further deposition. Overhanging atoms are not abundant until $\theta_{tot} \approx 10$ ML when large holes are found on the surface.

Overhanging atoms provide a mechanism for the formation of bulk vacancies in a thin film. An empty fourfold hollow site can be completely covered by four overhanging atoms in the layer above it to form a single bulk vacancy site. The total number of vacancies in a 50 ML film is presented in Table 2 for several simulations. While isolated bulk vacancies and small voids are found in the simulations, most of the vacancies are located in large voids with 30 to 150 adjacent bulk vacancies. Each of these voids extends vertically through 4 to 21 layers of the film and may contain from 1 to 18 vacancies (0.01 - 0.15 ML) in a single layer. The first bulk vacancies are located in layers 6 to 11 of the film and are created after deposition of anywhere from 8 to 23 ML. The presence of voids in a film can certainly affect its structural stability and other properties. However, voids are not visible from the surface and are not included in measurements of surface roughness. (We make a distinction between bulk voids and the holes which are still open to the surface and can be affected by further deposition events.)

In order to completely cover these large holes and form voids, many of the overhanging atoms are in sites with only one or two supporting atoms, instead of four as in the complete fourfold hollow site. As a depositing atom nears the surface, it is strongly attracted to those atoms within its interaction range. When it reaches a site with some minimum number of neighbors, the attractive force of those neighbors is sufficient to keep the atom in the site even though a nearby site may offer greater energetic stability. The cost of breaking the bonds in the atom's present site is too great for it to move to another site, i.e., the energetic barrier to

site change is too high. This is of course a function of the extremely low temperature of the simulation, since at higher temperature the thermal motion would increase the kinetic site hopping rate. Previous work[12] showed that there is no form of transient mobility on these surfaces and thus not even limited surface diffusion is possible at low temperature. Likewise, the void structure persists throughout the simulation because there is no excess energy available in the film to break bonds between neighboring atoms and allow the void to collapse.

This is also the reason for the observed formation of deep narrow voids. A depositing atom aimed into a hole rarely reaches the bottom. Instead it is attracted to an overhang site on the edge of the hole or along a side wall in the hole. This tends to decrease the opening at the top of the hole and increase the probability that the hole will be completely covered by overhanging atoms and become a void.

Multiatom rearrangements

At some point during the growth of a 50 ML film in each of our simulations, part of the surface structure abruptly collapses to produce a smoother surface. Holes in the surface are filled in (or covered) and islands disappear, resulting in fewer exposed layers after the multiatom event. The rearrangement appears to be initiated by one or more deposition events, according to careful analysis using visual animation. As an atom is deposited close to the edge of a deep hole in the surface, it may knock one or more nearby atoms out of their overhang sites and down into the hole. These atoms in turn may destabilize other overhanging atoms as they move to new adsorption sites, producing a cascade of atoms into the hole. When the rearrangement is finished, most of the atoms are in complete fourfold hollow sites and the deep hole is gone.

Several factors are required for a multiatom rearrangement event to occur. The first requirement is a rough surface, meaning a surface with defects such as holes or islands. The second requirement is a deposition event close to a defect which significantly destabilizes one or more neighboring atoms. A third and more subtle requirement involves the energetic barrier to the movement of many atoms. Atoms with fewer neighbors are typically easier to move since the total bond energy is smaller, even though for metals the strength of each bond increases as the total number of bonds decreases. A surface structure with many overhanging atoms missing two or even three supporting atoms, i.e., many atoms with fewer bonds to break, thus lowers the energy barrier for a rearrangement event and increases the probability that rearrangement will occur.

Support for these requirements comes from several additional calculations. Taking one simulation in which a rearrangement event occurred at θ_{tot} = 20.1 ML, we restarted the simulation at θ_{tot} = 20.0 ML with the same rough surface structure and varied the deposition conditions in an attempt to reproduce the rearrangement event. Figure 7 shows the results from restarting the simulation with identical simulation parameters, varying only the set of random aiming points for the deposited atoms. A rearrangement event was observed in two of the restarted deposition procedures, indicated by the sharp drops in the interface width in Figure 7, although the event proceeded somewhat differently in each case. In the remaining two simulations, no rearrangement was observed during deposition of a further 3 ML. Presumably such an event would occur at some later time, depending upon the random aiming points of the deposited atoms.

We have also restarted the same simulation at θ_{tot} = 20.0 ML with no further deposition and found that the surface structure did not change at all during 500 ps (corresponding to the time required for deposition of about 4 ML at the original deposition rate). The simulation was again restarted at θ_{tot} = 20.0 ML, this time with 10 ps between consecutive deposition events rather than 1 ps. Decreasing the deposition rate allows the surface more time to relax before the next deposition event, perhaps decreasing the probability of a rearrangement event. No multiatom rearrangement event occurred during deposition of a further 3 ML, but this is not conclusive of a change in the rearrangement probability with deposition rate since the same result was seen in two of the four simulations in Figure 7.

While the frequency of the multiatom rearrangement events may be influenced by the fast deposition rates necessary in MD simulations, there is nothing to suggest that these rearrangements do not occur in real systems. The three requirements detailed above can be satisfied in a low temperature experiment and we would expect multiatom rearrangements to occur, unless the actual rate is beyond the experimental time scale. The rearrangements take very little time (100 ps or less) and may not be directly observable. However, the effect of the rearrangements should be detectable.

Comparison of Cu and Pd

Figure 8 shows the interface width for one simulation of the deposition of 50 ML Pd/Pd(001) and one of 50 ML Cu/Cu(001). The simulation parameters are the same for both systems except for the set of random aiming points. As in the comparison of two Pd/Pd(001) simulations in Figure 2, there is no clear distinction between the two curves in Figure 8. Although it appears that Cu may grow more smoothly than Pd during deposition of the first

24 ML in Figure 8, this difference is not consistent for all of our simulations. These results indicate that any difference between Pd and Cu thin film growth at low temperature is small. Further conclusions cannot be reliably drawn from comparing the few available simulations, since there are large variations in the simulation results due to the random deposition process on the small surface area.

Consequences of multiple layers

The existence of two growth regimes is indicated, one for films with fewer than 5 to 10 layers and one for thicker films. The number of growing layers, i.e., the number of layers exposed on the film surface, greatly increases for $\theta_{tot} > 10$ ML. (There are only 2-5 growing layers for $\theta_{tot} < 5$ ML, increasing to 7 by $\theta_{tot} = 10$ ML, whereas the maximum number of exposed layers is 15-18 during deposition of 50 ML.) Furthermore, the interface width in general increases more quickly after deposition of 5-10 ML.

Multiple-layer events are found in these simulations that cannot occur at low θ_{tot}. For example, the multiatom rearrangements involve a number of layers as they modify the local surface structure. The absence of surface diffusion at low temperature makes such alternative atom transport mechanisms necessary for the growth of smooth films. Formation of large voids is another type of event that cannot occur until many layers have been deposited.

MD simulations of multiple-layer thin film growth are computationally intensive which prevents any meaningful statistical analysis of growth behavior. Instead we have studied the structural stability of the rough surface and looked for interesting events which may be representative of different growth mechanisms. While limited statistics may be possible for

deposition of 10 or 20 ML, the more interesting events do not occur until later in the deposition process.

Averaging the interface width over many runs would even out the effects of random deposition and give a clearer picture of the surface roughness over a large area. It might also determine if Pd/Pd(001) does grow more roughly than Cu/Cu(001) at low temperature as suggested in Ref. [6], although from our results we would expect any difference to be quite small. We note, however, that the conclusions from deposition of a single atom onto a pyramidal defect[6] do not necessarily apply to the sequential deposition of many atoms in MD simulations of thin film growth. In fact, we do not find well-defined pyramids (i.e., (111) facets) on the (001) surface during thin film growth by deposition of single atoms.

Comparison to experiment

The chosen temperature of 80 K ensures that site hopping on the clean fcc(001) surface does not occur on the timescale of a simulation or an experiment. However, other types of surface diffusion are possible during deposition and growth of a thin film, such as diffusion along islands or step edges or near a kink site, as well as interlayer diffusion processes. The activation barriers to diffusion may not be the same in each case, and in fact some could be quite small and therefore accessible at 80 K. Defect structures on the surface such as deep holes, overhanging atoms, and small fcc(111) facets can also affect the activation barriers to diffusion near the defects. For example, the activation barrier for site hopping on the (111) surface has been experimentally determined to be as low as 0.1 eV for some metals,[14] corresponding to a diffusion rate of one hop every microsecond at 80 K as compared to one hop every 10^5 years on the (001) surface.

An MD simulation cannot include diffusion events on the microsecond timescale, and thus a simulation at 80 K is equivalent to one at 0 K where *all* thermally activated diffusion is eliminated. However, this timescale *is* within the experimental range, and an experiment at 80 K may produce a smoother surface than one at 0 K due to these other types of diffusion. The result is that the MD simulations, although performed at 80 K, ideally should be compared to experiments performed at (or close to) 0 K.

There have been several experimental studies of deposition at low temperature for both Cu/Cu(100) and Pd/Pd(100). Intensity oscillations as a function of deposition time have been observed for Cu/Cu(100) at 77 K using RHEED[15] and at 100 K using helium atom beam scattering[16] and for Pd/Pd(100) at 100 K using LEED.[17] While some authors[15] interpret the presence of oscillations as an indication of at least quasi layer by layer growth, others[16] state that a few oscillations will be observed due to the correlation imposed on the random growth process by the fcc(100) lattice geometry. Hence it is not clear that the intensity oscillations indicate smooth film growth.

Repeating these experiments at lower temperatures should help resolve this question. If the oscillations are still present at extremely low temperature (below 10 K), then very likely they do not indicate layer by layer growth nor provide any information about the surface roughness. (Layer by layer growth requires efficient atom transport across the surface, and thermally activated diffusion is the only known transport mechanism during low-energy atom deposition.) On the other hand, if the oscillations disappear at lower temperature, then at 80 K long timescale diffusion processes are active which produce smoother films than predicted by the short timescale MD simulations. STM experiments near 0 K would provide

real space details about the surface roughness for direct comparison with the simulations, especially if the interface width could be calculated.

Conclusions

The structure of a thin metal film at low temperature is largely due to the stability of deposited atoms in overhang sites. Nearly all of the surface structure and growth mechanisms we describe for θ_{tot} > 5-10 ML are consequences of the presence of overhanging atoms during thin film growth: (1) surface roughness; (2) formation of voids; and (3) multiatom rearrangement events.

Dynamical features of thin film growth involve multiple layers of the film and many atoms in (1) multiatom rearrangement events and (2) formation of large holes and voids. The rearrangement events provide a mass transport mechanism which can be important especially in the absence of surface diffusion. However, such large-scale events will be difficult to model with other methods (e.g., kinetic Monte Carlo and statistical models). One consequence of these dynamical features is that the surface roughness determined by experiment may appear much more uniform since it is averaged over a large surface area and many deposition events.

It would be interesting to have experimental validation of the surface roughness (i.e., interface width) at temperatures close to 0 K for comparison with the MD simulation results. The choice of deposition rate should not affect the experimental results since no long time scale processes are expected to occur when all thermally activated diffusion is absent. Observation of the local surface structure before and after a multiatom rearrangement event would be particularly useful.

A related topic of interest is the growth of thin films by deposition of clusters rather than single atoms. MD simulation results for low-energy deposition of small clusters in the Pd/Pd(001) and Cu/Cu(001) systems will be presented in a forthcoming article.[18]

Acknowledgements

We thank Professor James W. Evans for helpful discussions. This work was supported by NSF grant CHE-9224884.

References

[1] M. Ohring, *The Materials Science of Thin Films*, (Academic Press, San Diego, CA, 1992).

[2] J. W. Evans, D. E. Sanders, P. A. Thiel, and A. E. DePristo, Phys. Rev. B **41**, 5410 (1990); H. C. Kang and J. W. Evans, Surf. Sci. **271**, 321 (1992).

[3] J.-K. Zuo, J. F. Wendelken, H. Dürr, and C.-L. Liu, Phys. Rev. Lett. **72**, 3064 (1994); H. Brune, Ch. Romainczyk, H. Röder, K. Kern, Nature **369**, 469 (1994); A. Zangwill, Mater. Res. Soc. Symp. Proc. **280** (*Evolution of Surface and Thin Film Microstructure*),121 (1993).

[4] J. A. Sprague and C. M. Gilmore, Mater. Res. Soc. Symp. Proc. **268** (*Materials Modification by Energetic Atoms and Ions*), 115 (1992); C. M. Gilmore and J. A. Sprague, Surf. Coat. Technol. **51**, 324 (1992); C. M. Gilmore and J. A. Sprague, Phys. Rev. B **44**, 8950 (1991).

[5] L. Yang and A. E. DePristo, J. Catalysis **149**, 223 (1994).

[6] D. M. Halstead and A. E. DePristo, Surf. Sci. **286**, 275 (1993).

[7] C. L. Kelchner and A. E. DePristo, "Molecular dynamics simulation of multilayer homoepitaxial deposition on fcc(100) metal surfaces," J. Vac. Sci. Tech. A (in press, March 1996).

[8] S. W. Rosencrance, J. S. Burnham, D. E. Sanders, C. He, B. J. Garrison, N. Winograd, Z. Postawa, and A. E. DePristo, Phys. Rev. B **52**, 6006 (1995); C. L. Kelchner, D. M. Halstead, L. S. Perkins, N. M. Wallace, and A. E. DePristo, Surf. Sci. **310**, 425 (1994); M. S. Stave and

A. E. DePristo, J. Chem. Phys. **97**, 3386 (1992); S. B. Sinnott, M. S. Stave, T. J. Raeker, and A. E. DePristo, Phys. Rev. B **44**, 8927 (1991); T. L. Wetzel and A. E. DePristo, "Structures and energetics of Ni_{24}-Ni_{55} clusters," J. Chem. Phys. (in press, March 1996).

[9] T. J. Raeker and A. E. DePristo, Int. Rev. Phys. Chem. **10**, 1 (1991).

[10] A. E. DePristo, in *Recent Advances in Density Functional Theory*, vol. 1, Part 1, ed. D. Chong, (World-Scientific, Singapore, 1996) ch. 6.

[11] J. W. Evans, Phys. Rev. B **43**, 3897 (1991).

[12] D. E. Sanders and A. E. DePristo, Surf. Sci. **254**, 341 (1991).

[13] C. Kittel, *Introduction to Solid State Physics*, (John Wiley & Sons, New York, 1986) ch. 5.

[14] H. Brune, H. Röder, C. Boragno, and K. Kern, Phys. Rev. Lett. **73**, 1955 (1994); M. Henzler, T. Schmidt, and E. Z. Luo, in *The Structure of Surfaces IV*, ed. X. Xie, S. Y. Tong, and M. A. Van Hove (World-Scientific, Singapore, 1994).

[15] W. F. Egelhoff, Jr. and I. Jacob, Phys. Rev. Lett. **62**, 921 (1989).

[16] H.-J. Ernst, F. Fabre, R. Folkerts, and J. Lapujoulade, J. Vac. Sci. Tech. A **12**, 1809 (1994); H.-J. Ernst, R. Folkerts, and J. Lapujoulade, Surf. Sci. Lett. **275**, L682 (1992).

[17] D. K. Flynn-Sanders, J. W. Evans, and P. A. Thiel, Surf. Sci. **289**, 75 (1993).

[18] C. L. Kelchner and A. E. DePristo, "Molecular dynamics simulation of multiple-layer thin film growth via cluster deposition," Nanostructured Materials (to be submitted).

Table 1. Data at end of 50 ML deposition for Pd/Pd(001), 11 x 11 system, 1 atom / 1 ps, 80 K.

		simulation A	simulation B
total layers	($\theta_j > 0$)	55	53
incomplete layers	($\theta_j < 1$)	35	24
exposed layers	($N_j > 0$)	12	8
average surface height ($\bar{j}$)		51.42 ML	50.45 ML
total bulk vacancies		157	61

Table 2. Total bulk vacancies (in atoms and in ML) after 50 ML deposition in an 11 x 11 system at 80 K. The time between consecutive depositions is given in the column headings.

	Pd/Pd(001) 1 ps, sim. A	Pd/Pd(001) 1 ps, sim. B	Pd/Pd(001) 2 ps	Cu/Cu(001) 1 ps	Cu/Cu(001) 2 ps
bulk vacancies	157	61	118	202	76
	1.30 ML	0.50 ML	0.98 ML	1.67 ML	0.63 ML

Figure Captions

Figure 1. Interface width, *w*, for Pd/Pd(001), 11 x 11, 1 atom / 1 ps, 80 K, simulation A. The top curve calculates *w* after each deposition event. Lower curves average *w* over 10, 100, 500, and 1000 deposition events (0.08, 0.83, 4.13, and 8.26 ML), respectively, and are shifted down for clarity. (All curves should lie exactly on the top curve.)

Figure 2. Interface width for Pd/Pd(001), 11 x 11, 1 atom / 1 ps, 80 K. Simulations were performed for two different sets of random aiming points for the deposited atoms.

Figure 3. Fraction of atoms in the first adsorbate layer after deposition of 1 ML for various deposition rates of Pd/Pd(001) and Cu/Cu(001), averaged over 11 simulations for each point. The Pd/Pd(001) data points are offset for clarity. Inset is the fraction of the third adsorbate layer which is filled after deposition of 3 ML for Cu/Cu(001).

Figure 4. Interface width for Pd/Pd(001), 11 x 11, 80 K, 1 ps and 2 ps between depositions.

Figure 5. Total system temperature. Each data point is averaged over the final timestep of 11 deposition events.

Figure 6. Temperature of top 10 adsorbate layers. Each data point is averaged over the final timestep of 11 deposition events.

Figure 7. Interface width for Pd/Pd(001), 11 x 11, 1 atom / 1 ps, 80 K. Simulation was restarted four times at 20.00 ML with the same parameters and a new initial random aiming point. (Solid line is the original simulation.)

Figure 8. Interface width for Pd/Pd(001) and Cu/Cu(001), 11 x 11, 80 K, 2 ps between depositions.

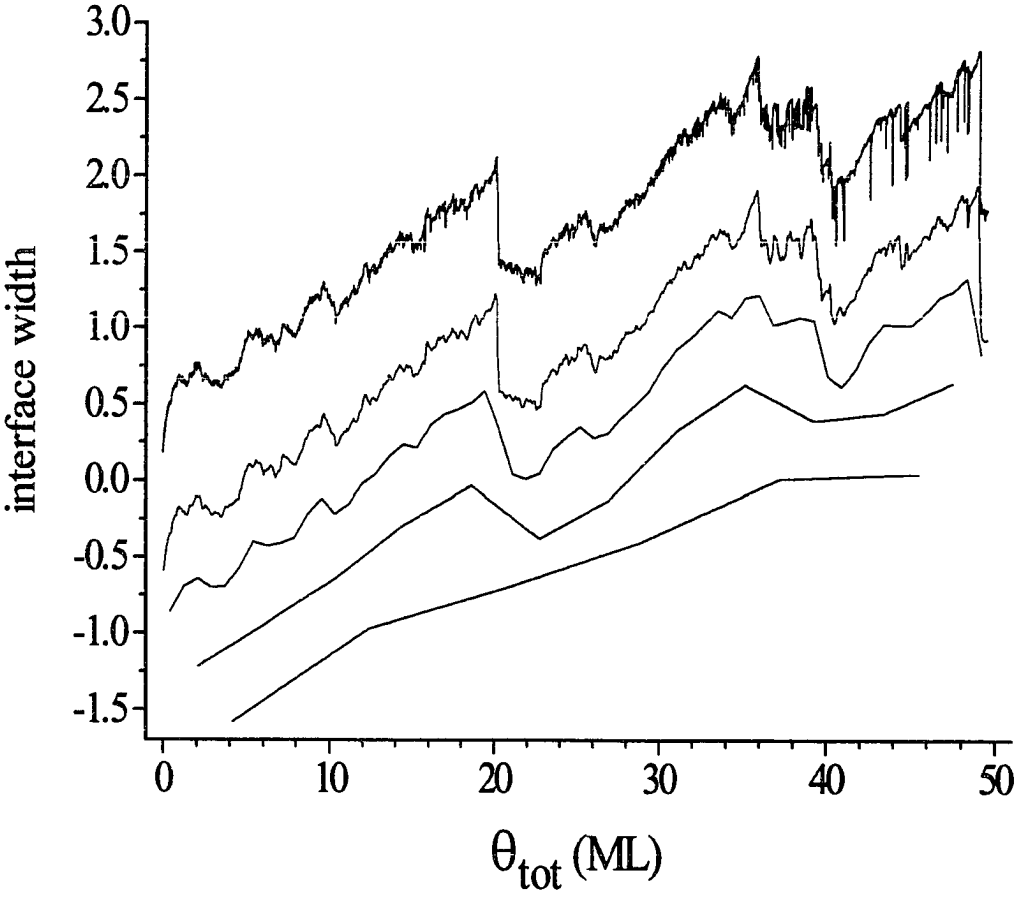
3.0
2.5
2.0
1.5
1.0
0.5
0.0
-0.5
-1.0
-1.5
interface width
0
10
20
30
40
50
θtot (ML)

Figure 1.

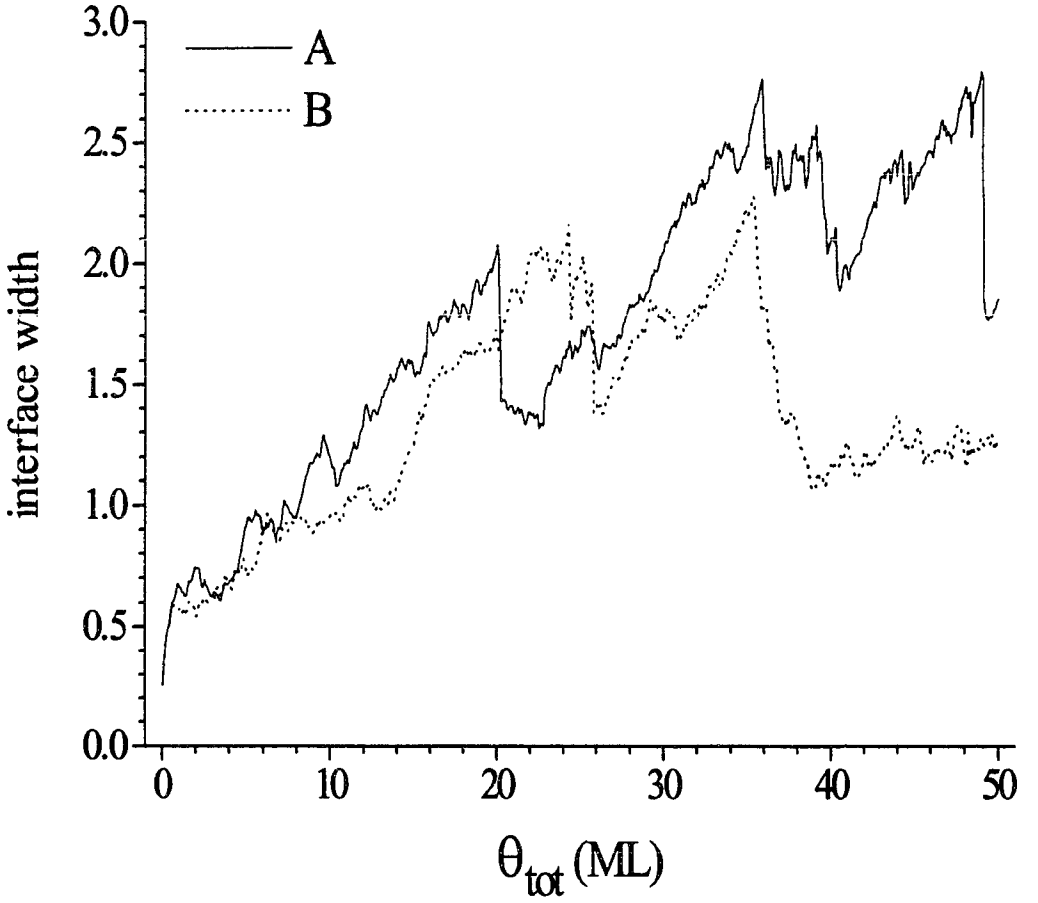

Figure 2.

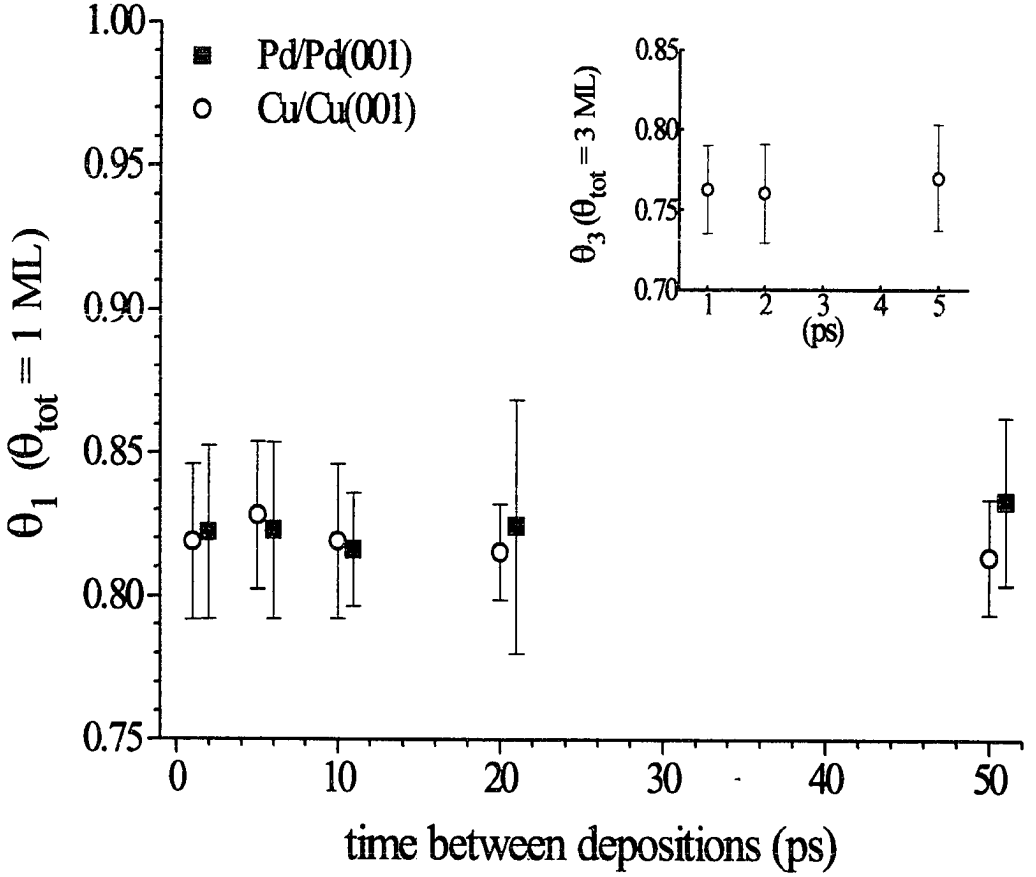
1.00
0.95
0.90
0.85
0.80
0.75
Pd/Pd(001)
Cu/Cu(001)
θ1 (θtot = 1 ML)
0
10
20
30
40
50
time between depositions (ps)
θ3(θtot = 3 ML)
0.85
0.80
0.75
0.70
1
2
3
4
5
(ps)

Figure 3.

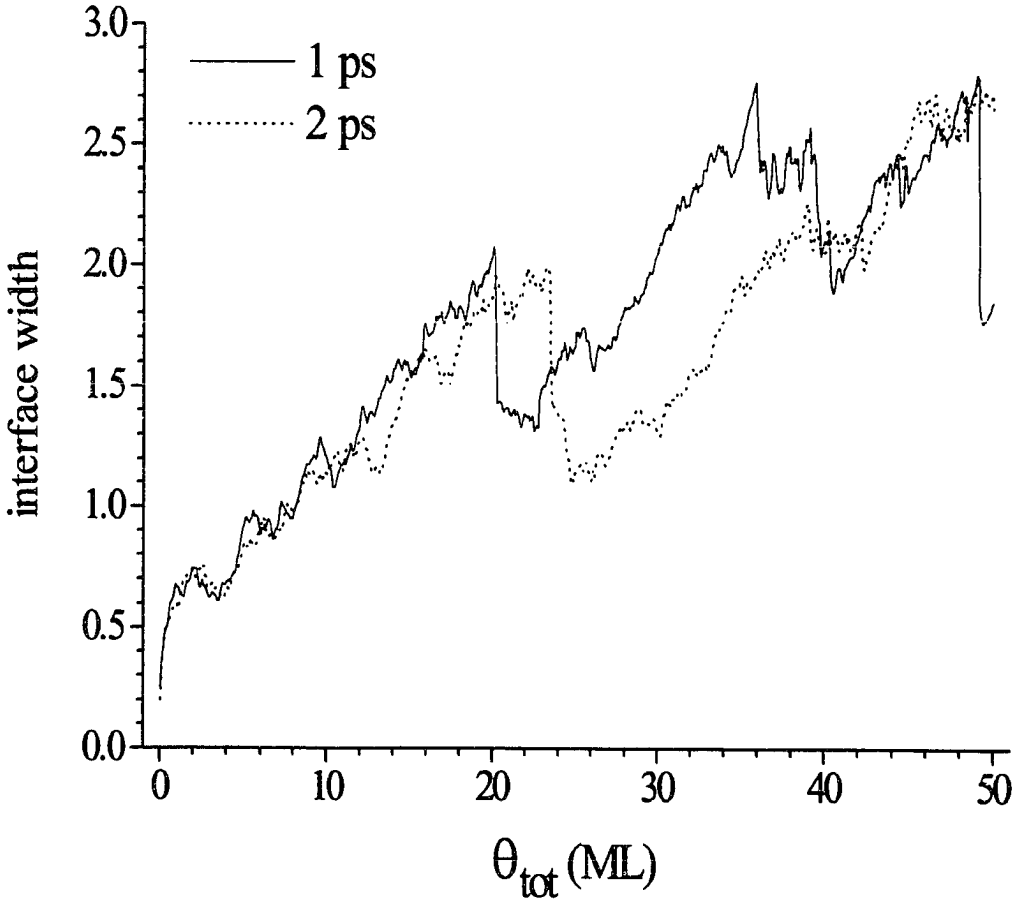
1 ps
2 ps
interface width
3.0
2.5
2.0
1.5
1.0
0.5
0.0
0
10
20
30
40
50
θtot (ML)

Figure 4.

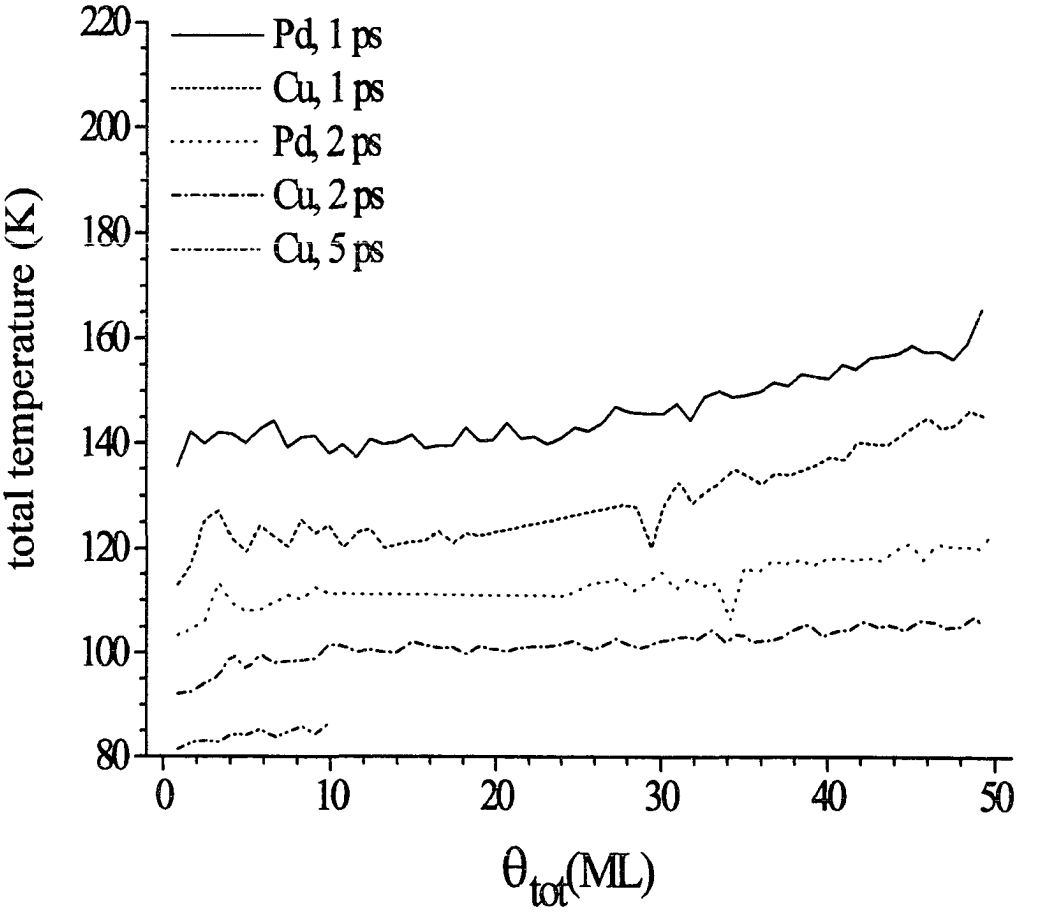
Pd, 1 ps
Cu, 1 ps
Pd, 2 ps
Cu, 2 ps
Cu, 5 ps
total temperature (K)
220
200
180
160
140
120
100
80
0
10
20
30
40
50
θtot(ML)

Figure 5.

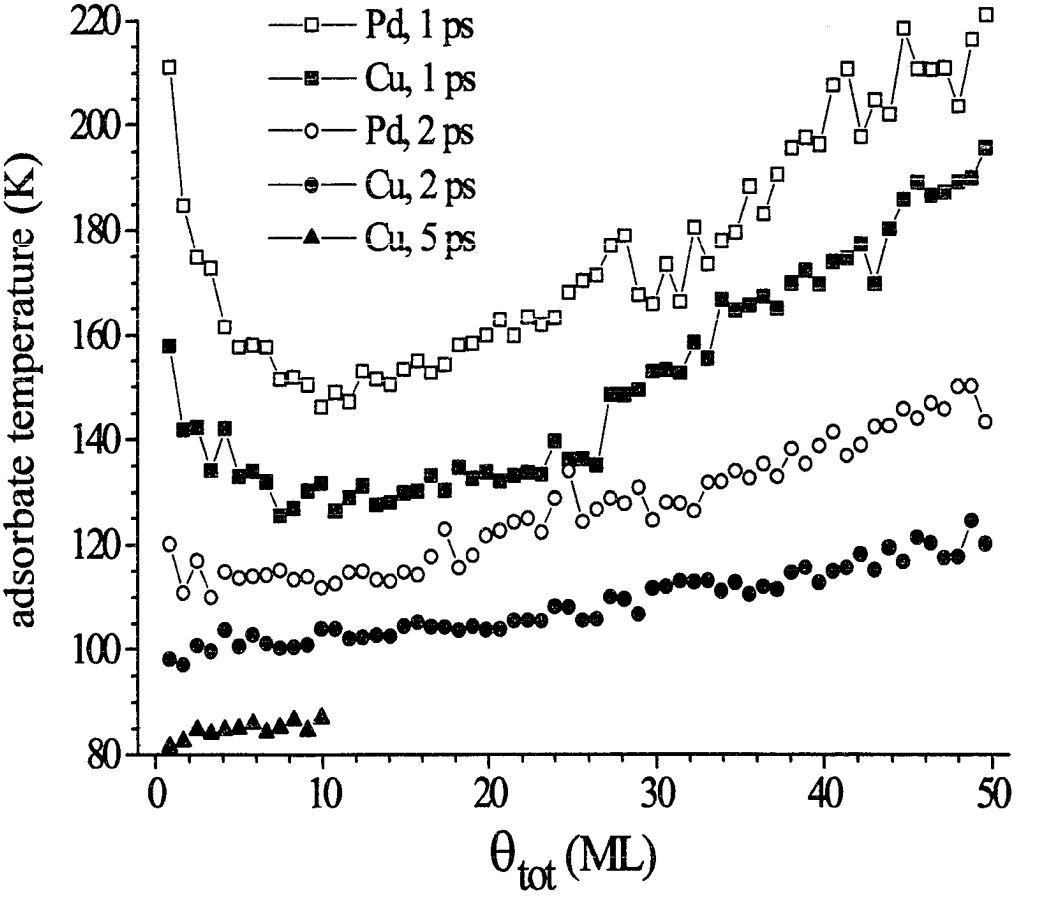
Pd, 1 ps
Cu, 1 ps
Pd, 2 ps
Cu, 2 ps
Cu, 5 ps
adsorbate temperature (K)
220
200
180
160
140
120
100
80
0
10
20
30
40
50
θtot (ML)

Figure 6.

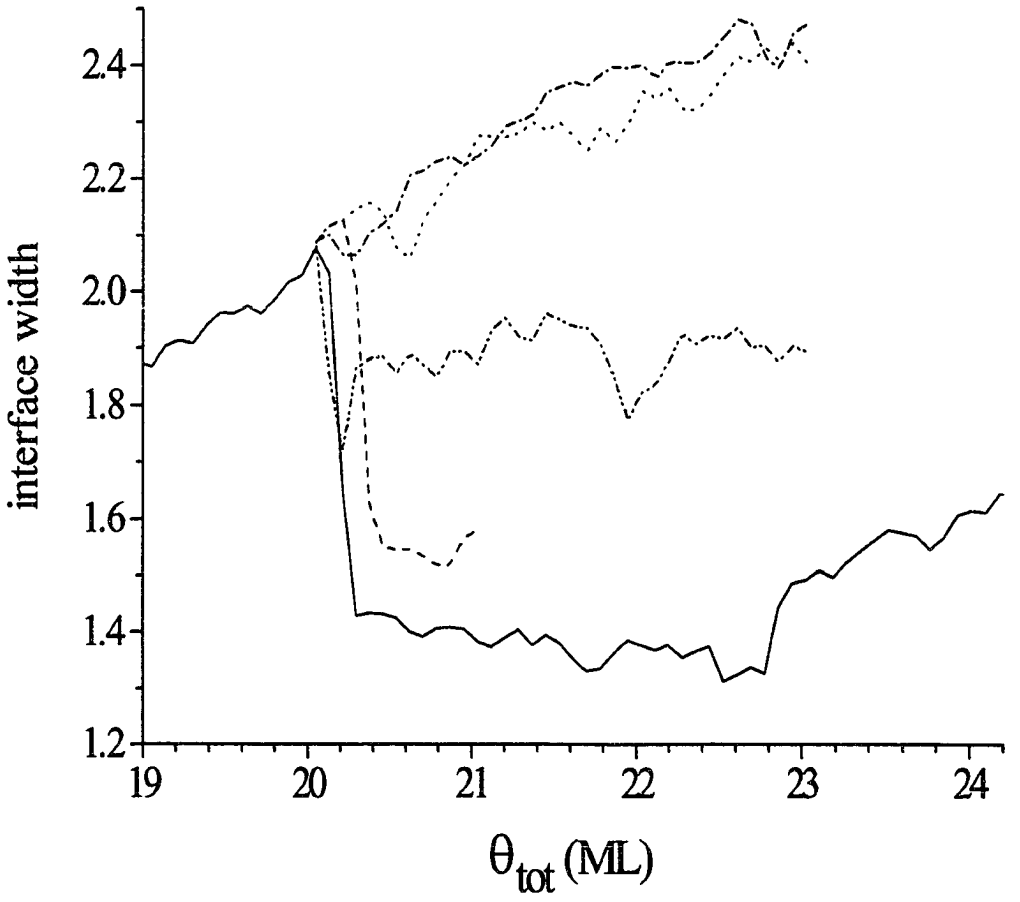

Figure 7.

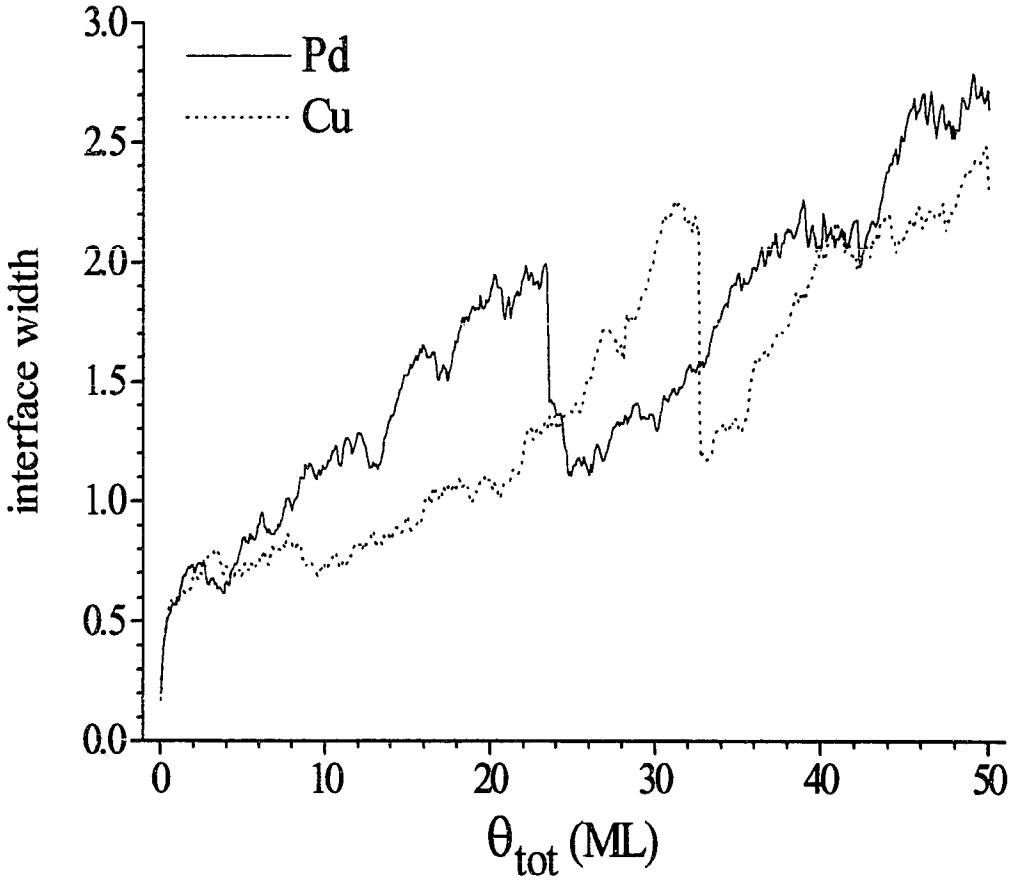

Figure 8.

MOLECULAR DYNAMICS SIMULATION OF MULTIPLE-LAYER THIN FILM GROWTH VIA CLUSTER DEPOSITION

A paper prepared for submission to Nanostructured Materials

Cynthia L. Kelchner and Andrew E. DePristo

Abstract

Molecular dynamics simulations permit multiple-layer thin film growth to be studied in detail, using reliable interatomic potentials for fcc metals from corrected effective medium theory. Results are presented for the homoepitaxial deposition of 20 ML on Pd(001) and Cu(001) at 80 K via deposition of 5- and 10-atom clusters, along with initial deposition results for 100-atom clusters. The growth of these thin films via low energy cluster deposition is much rougher than that of films grown via single atom deposition. The increased surface roughness can be attributed to the following factors: (1) most deposition events add atoms to two or more layers; and (2) the growth of (111) facets on the surface produces many partially exposed atoms. Neither of these features was observed during the deposition of single atoms. Thin films grown by deposition of larger clusters tend to be rougher than those produced by smaller clusters.

Introduction

Detailed study of the growth of thin films leads to further understanding and control of the deposition process and final structure of the film. This is important for many applications of

thin film technology since the mechanical, electrical, optical, and magnetic properties of the film can depend strongly on the film's structure.

One method of growing a thin film is to deposit single atoms under ultrahigh vacuum conditions to ensure a clean surface (e.g., molecular beam epitaxy). Experimental deposition techniques may deposit a range of small cluster sizes rather than single atoms as intended. The cluster size distribution depends on the experimental conditions (e.g., beam temperature) and can range from mostly monomers with a few dimers and trimers to larger clusters with very few monomers. The size of the deposited clusters can affect the growth mechanisms and final structure of a thin film. A few dimers deposited along with many monomers may or may not have a noticeable effect on the film structure. However, the sequential deposition of 10-atom clusters could produce quite a different film.

Some experimental techniques intentionally deposit clusters within a controlled size range, such as ionized cluster beam deposition (ICBD)[1] and energetic cluster impact (ECI)[2]. These methods seek to form compact, strongly adhering thin films by depositing accelerated cluster ions which locally heat the surface upon deposition. Molecular dynamics simulations[3,4] of ECI have shown that this excess heat can melt the cluster and local surface area, allowing lateral mobility of the cluster atoms as the cluster breaks up and annealing of any impact-created defects. The deposited clusters are generally large (1000 atoms or more) and have an initial kinetic energy of 1-10 eV per atom. Low kinetic energies lead to "soft-landing" of intact clusters on the surface, whereas high kinetic energies lead to crater formation in the surface upon deposition.[3]

Other experiments use low energy cluster beam deposition (LECBD) to produce "nanocrystalline structured" thin films.[5] This technique can lead to the formation of new phases by a random cluster stacking mechanism as the clusters are soft-landed on the surface. The resulting thin films are therefore strongly affected by the structure and properties of the original clusters. These cluster details do not affect the final film as much in ICBD or ECI, where the most important parameter is the initial energy per cluster atom.

Molecular dynamics (MD) can be used to study the growth of thin films in detail by following the motion of individual atoms as they are deposited and determining the various processes involved as the atoms adsorb on the surface. A number of MD simulations have been reported for deposition of a single cluster onto a clean surface,[6] but only a few theoretical studies, described below, have considered multiple-layer film growth via cluster deposition.

In two-dimensional MD simulations using a Lennard-Jones potential, Müller[7] found that the cluster energy per atom played an important role in the quality of the thin film. Low-energy clusters remained nearly intact upon deposition and produced "polycrystalline" films, whereas higher-energy clusters (energy per atom close to the atomic bond strength) produced homoepitaxial growth and very high energy clusters greatly damaged the surface. A three-dimensional (3D) simulation using the embedded atom method for Mo[3] resulted in similar conclusions and agreed with experimental results. Both of these simulations used one large cluster size, 91 atoms (≈700 in 3D) for Ref. [7] and 1043 atoms in Ref. [3]. A third multiple-layer simulation, this one of Si cluster deposition on Si(111),[8] studied the effect of the cluster size as well as the substrate and cluster temperatures and the initial cluster energy.

Combinations of these growth conditions were identified that produced the high surface diffusion and spreading of the cluster upon deposition considered necessary for epitaxial growth.

The present work studies the growth of thin films via the low energy deposition of small clusters. We compare the deposition of 10-atom clusters to previous results for the deposition of single atoms[9] during homoepitaxial thin film growth of metals, specifically Pd/Pd(001) and Cu/Cu(001) at 80 K. We also explore the effect of several different cluster sizes on the growth mechanisms and final structure of the thin films.

Simulation Procedure

The MD simulations use the simplest form of corrected effective medium (CEM) theory, known as MD/MC-CEM, which provides accurate interaction potentials for metals.[10, 11, 12] CEM theory determines the interaction energy of a system in any geometry by calculating the energy of each atom in a reference system plus correction terms for the difference in Coulomb and kinetic-exchange-correlation energies between the interacting system and the atom-in-reference system. This method has been extensively described elsewhere[10,11] including a recent critical review[12] and no further details are given here.

Periodic boundary conditions are used in the surface plane (in x and y). The square fcc(001) surface has four active layers and one fixed layer at the start of the simulation, with 11 x 11 atoms in each layer for most of the simulations. The surface is initialized from a Boltzmann distribution at 80 K. This low temperature was chosen to eliminate thermal surface diffusion. Except for the initial fixed layer which remains fixed and the lowest active layer (i.e., the one closest to the fixed layer) which is treated by Langevin dynamics to mimic a

constant temperature heat bath, all atoms follow Newton's equations throughout the simulation.

The geometry and atomic velocities of the depositing cluster are initialized separately before the first deposition event. The cluster is cut from the fcc bulk crystal and quenched to reach a stable structure, then relaxed at the specified cluster temperature. We chose a temperature of 100 K for convenience, since the cluster temperature has been observed to have little effect on the deposition process.[8] This procedure does not guarantee the minimum energy structure of the cluster but does find a low-energy, compact structure. Subsequent clusters in the deposition process use this same geometry, randomly rotated in space, and the same initial temperature distribution scaled to give the chosen cluster temperature.

One new cluster is placed out of the interaction range above the surface (+ z direction) with random x and y coordinates and a small initial kinetic energy of 0.25 eV directed toward the surface. (Both the coordinates and kinetic energy refer to the cluster's center of mass.) After a specified time, another cluster is placed above the surface and the deposition process is repeated until the desired number of clusters have been deposited.

The adsorption energy of a depositing cluster as it reaches the surface is simply that of one depositing atom multiplied by the number of atoms in the cluster, assuming that all of the atoms in the cluster bind directly to atoms already on the surface. The time required for this adsorption energy to dissipate throughout the system is also multiplied by the number of atoms in the depositing cluster. Thus an MD simulation of a thin film grown by deposition of small clusters requires the same amount of computational time as that of a thin film grown by deposition of single atoms. For deposition of large clusters, the computational time could be

reduced if one knew that only a fraction of the atoms in each cluster adsorb directly on the surface.

The morphology of the growing film can suggest possible mechanisms by which deposited atoms find stable adsorption sites on the surface. One way to measure the roughness of the surface is to calculate the interface width, w. The interface width is defined to be the standard deviation of the distribution of the exposed layers' height in units of the ideal layer spacing, and is calculated from the following equation:[13]

$$w^2 = \sum_{j=0}^{\infty} \left(j - \bar{j}\right)^2 N_j \qquad \textbf{Eq. 1}$$

N_j is the net number of exposed atoms in layer j where j=0 is the top substrate layer. The mean height of the surface is $\bar{j}$. The total coverage in monolayers (ML) is denoted by θ_{tot} in the rest of this article.

Deposition of 10-atom Clusters

Surface structure

In the vapor phase, the compact 10-atom cluster has vibrational and rotational motion due to its internal energy (temperature) as well as a net velocity directed toward the substrate due to its initial kinetic energy. The velocity of the cluster increases as it is attracted to the surface, and the cluster lands with some impact due to the strong adsorption energy (about 3 eV per atom). For the small total kinetic energy of 0.25 eV (i.e., 0.025 eV/atom), this impact is not enough to create defects or otherwise disrupt the structure of the substrate.

The depositing atoms can push into the top substrate layer during impact, particularly if a few atoms reach the surface before the rest of the cluster. Most of these atoms recoil out of the substrate as the cluster finds stable adsorption sites on the surface. However, we have observed exchange of cluster atoms with the substrate during the adsorption process. The final cluster structure is unchanged in these homoepitaxial systems, but this mechanism will be important when studying heteroepitaxy.

The cluster atoms must rearrange to fit into the fourfold hollow adsorption sites on the (001) surface. For the 10-atom clusters, this rearrangement is completed within 2-3 ps of the initial attraction to the substrate. The final structure of a 10-atom cluster deposited on a clean (001) substrate is usually three-dimensional with 1-2 atoms in the second adsorbate layer. All of the atoms in the second layer are in complete fourfold hollow sites created by the other cluster atoms. A cluster can also flatten into a single layer upon adsorption. The adsorbed clusters are fairly compact; the largest dimension in any direction is only four atoms for the 8-10 atoms found in the first layer.

When clusters are deposited on a rough surface containing islands and other defect structures, the adsorption process is not as simple. A depositing cluster is strongly attracted to the first atom within its interaction range, and on a rough surface this is often the top or side of an existing island. The cluster can adsorb onto the side of an island, adding atoms to about three layers of the structure. As the surface grows, the number and size of islands increase and the likelihood that a depositing cluster will reach the substrate quickly diminishes. The larger size of the cluster increases the probability that one or more of its atoms, and therefore the entire cluster, will be attracted to a nearby island during deposition rather than

continuing to move normal to the substrate. This results in large islands on the surface with deep channels between them. The channels are only 1-3 atoms wide at the base of the islands and are generally not filled in during further deposition.

The most striking feature of these rough surfaces is the formation of fcc(111) facets during thin film growth via cluster deposition. Each face of a perfect pyramid on the (001) surface is a (111) facet. For example, a 4-atom high pyramid has 16 atoms in the first (bottom) layer, nine in the second layer, four in the third layer, and one in the fourth (top) layer. This pyramid has a 4-atom high (111) facet on each of its four faces.

Figure 1 shows the structure of a (111) facet on the surface of a thin film. Figure 2 shows the same surface from the side, and a large (111) facet can be clearly seen on the right. For convenience, we have defined the minimum size of a (111) facet to be 3 atoms high and 2 atoms wide. The tallest (111) facets we have observed during deposition of 10-atom clusters are 12 atoms high and the widest are 6 atoms across. Most of the facets are only 4-5 atoms high and 3-4 atoms wide.

Depositing clusters often land on these (111) facets, and can either extend the facet (vertically and/or horizontally) or change the facet into some other structure. One or more atoms from a cluster may stick on the (111) facet while the rest of the cluster moves to nearby adsorption sites. These atoms can stay on the facet for tens to hundreds of picoseconds. While the diffusion rate on the (001) surface is negligible at 80 K, this is not true for the (111) surface where the activation barrier to diffusion is much smaller.[14] Thus the single atoms adsorbed on the (111) facet may not be in their final adsorption sites. An earlier study of single atom deposition on these pyramids[15] indicated that Pd atoms are more likely than Cu to

stay on the (111) facet for the first 5 ps after deposition. This difference was not observed to be significant in the current MD simulations.

Distinct (111) facets form only on a relatively flat surface. The (111) facets are observed as soon as 3-atom high islands are formed on the substrate ($\theta_{tot} \approx 1$ ML for most simulations of 10-atom cluster deposition). These facets grow as more clusters are deposited on and near them by adding atoms on the facet and by adding entire clusters to several layers on the facet which extends the facet laterally. As the surface becomes rougher, the (111) facets begin to disappear. It may be that the surface reaches a maximum number or size of (111) facets in a given area and cannot continue to grow by propagating the facets. Another possibility is that the random deposition process may deposit several clusters in such a way that they destructively interfere with the facet growth, e.g., distorting a (111) facet or simply covering it. The effect is that the (111) facets are covered by atoms adsorbed on the facet and by atoms in overhang sites near the top of the (111) facet.

An overhang site has been defined previously[9] as a fourfold hollow site that is missing one or more of its four supporting atoms. For the current MD simulations, we modify this definition to include only those fourfold hollow sites that are missing exactly one supporting atom. Sites that are missing two or more supporting atoms can often be more accurately described as sites on the (111) facet. (This was not the case during single atom deposition since (111) facets were not clearly formed.) An exception is made for overhanging rows, where most of the atoms are missing two supporting atoms.

The effect of overhanging atoms during thin film growth by cluster deposition is to enable growth beyond the (111) facet stage. Overhanging atoms are a consequence of the fact that

the depositing clusters are attracted to the islands on the surface and thus cannot deposit in the narrow gaps between the islands. The clusters land on the top or side of an existing island and many of the atoms remain in overhang sites or adsorb on the (111) facet in order to maintain the strong bonding within the cluster. This results in the next distinct stage of thin film growth, namely the disappearance of the (111) facets and gradual smoothing of the surface structure. This transition does not appear to occur at a specific θ_{tot} or interface width value.

The sides of the islands during this next stage of film growth are often vertical (100)-type faces at a 45° angle from the (111) facets. These vertical faces are created by overhanging atoms (not overhanging rows) at the corner of two (111) facets and can be more than six atoms wide.

Figure 1 shows an example of this vertical wall (or step) from the top (left side of figure). Other distorted structures are also observed due to edge dislocations formed on islands and other defects.

A multiatom rearrangement event may occur which covers some of the deep channels between islands by connecting the top few layers of the growing islands. These rearrangements are typically smaller than those seen during single atom deposition and do not fill the deep holes, leaving large voids in the film. Much of the surface is then smooth and (111) facets again begin to grow, repeating the cycle. The surface may also become smoother as depositing clusters gradually cover holes on the surface with overhanging rows and atoms, rather than by a specific rearrangement event. Note that these mechanisms for smoothing are localized, so that it is possible to find (111) facets growing on one section of the surface, such

as the top of a large island, even though another part of the surface is still very rough. This is one reason why it is so difficult to quantify the transition between (111) facet growth and other growth mechanisms.

The growth of a thin film can be illustrated by plotting the interface width as a function of coverage, as seen in Figure 3 for two Pd/Pd(001) simulations of 10-atom cluster deposition. Figure 3 shows many of the same features that were observed for deposition of single atoms.[9] For instance, the sudden decrease at θ_{tot} = 10 ML indicates a multiatom rearrangement event which smooths out the film surface. These types of events occur much earlier in the films grown by cluster deposition than those grown by single atom deposition. We have seen multiatom rearrangement events for coverages as low as 5 ML in the MD simulations of 10-atom cluster deposition. In contrast, the interface width during single atom deposition steadily increases for θ_{tot} < 20 ML with no large-scale multiatom events.[9]

The interface width of a thin film grown by cluster deposition is larger than that of a film grown by single atom deposition, indicating a rougher surface. In previous results[9] for single atom deposition of Cu/Cu(001) and Pd/Pd(001), the maximum interface width was 2.1 for θ_{tot} ≤ 20 ML. For 10-atom cluster deposition, the maximum interface width is 5.1 (in units of the ideal layer spacing). Table 1 shows the interface width at several coverages during deposition of single atoms and 5- and 10-atom clusters.

The deposition of clusters increases the surface roughness much more quickly than does single atom deposition. The maximum number of layers exposed on the surface (i.e., the number of growing layers) ranges from 14-25 for θ_{tot} ≤ 15 ML during thin film growth via 10-atom cluster deposition. The corresponding maximum during single atom deposition is only

6-12 exposed layers. Furthermore, during 10-atom cluster deposition the substrate is typically exposed until $\theta_{tot} \approx 6$ ML and can still be exposed at $\theta_{tot} = 15$ ML, whereas it is completely covered by $\theta_{tot} = 2$ ML during single atom deposition. This increased surface roughness during cluster deposition can be attributed to two factors: (1) most deposition events add atoms to two or more layers; and (2) the (111) facets have many partially exposed atoms. Neither of these features was observed during the deposition of single atoms.

The interface width is a useful tool to analyze a single simulation and to get an idea of the overall roughness of the system. Note, however, that the random nature of the deposition process in a small surface area can produce a large variation in interface width between any two simulations, as seen in Figure 3 and Figure 6. Detailed comparison of the interface width for two simulations is simply not meaningful unless they used the same random aiming points for the clusters. The random deposition effects can be diminished by either depositing over a very large surface area or averaging many small simulations. (This would also average out many of the interesting features of the interface width.) For this initial study of low energy cluster deposition, neither solution was deemed practical for these lengthy MD simulations.

System size effects

The size of the system can play an important role if it is small enough for the surface defects developed during thin film growth to interact with one another through the periodic boundary conditions. It has been determined[9] that a surface of 11 x 11 atoms is sufficient to study the growth of homoepitaxial thin films via single atom deposition. However, the deposition of small clusters in the present study induces rougher film growth than that of single atoms and the system size may influence the results.

The interface width of two MD simulations with a larger system size of 17 x 17 atoms is presented in Figure 4. This larger surface area allows each island to initially grow in a more isolated environment and produces more islands overall. Note that the interface width displays fewer sharp increases and decreases in Figure 4 than for the smaller 11 x 11 system in Figure 3, although the magnitude of w is similar for both system sizes. The lack of oscillations in w over a larger surface area is expected since the growth patterns due to the random deposition events are averaged out to some extent. (This difference due to the system size was not seen in single atom deposition results because the interface width was already fairly steady for the smaller system.)

This comparison can be quantified by fitting the interface width to a power law of the coverage: $w = A\theta^{\beta}$, where β is the growth exponent in accordance with the dynamic scaling theory.[16] The fitting parameters and the RMS deviation are listed in Table 2 for $\theta_{tot} \leq 10$ ML during deposition of 10-atom clusters of Pd/Pd(001) and Cu/Cu(001). The value of β varies widely for these simulations but the RMS deviation is quite similar for most of the smaller systems. The results for the first 17 x 17 simulation in Table 2 show a growth exponent at the lower end of the range for the 11 x 11 simulations, and the RMS deviation is a factor of two to six smaller than that for the 11 x 11 systems. The small RMS deviation indicates the relative uniformity of the growth for the larger system, i.e., fewer regions of sudden roughening or smoothing of the film surface during growth. The second 17 x 17 simulation has a rougher growth overall (larger β) but again shows no regions of sudden change in the surface structure in Figure 4, unlike the 11 x 11 simulations where such changes are seen for

coverages as low as 5 ML. The random events on the surface during deposition and growth are beginning to be averaged out even over this relatively small surface area of 17 x 17 atoms.

Comparison of Cu and Pd

For most of the Pd/Pd(001) simulations reported here, an identical MD simulation was done for Cu/Cu(001) including the same set of random aiming points for the depositing clusters. This permits the direct comparison of the results for these two metals. Figure 5 presents the interface width from one simulation for both Cu and Pd. The interface widths for Cu and Pd are indistinguishable for θ_{tot} < 5-10 ML for a given set of simulations, suggesting that any significant difference in the growth mechanisms for these two metals at low temperature does not appear until the thin film is well within the multiple-layer growth regime. While some of the simulations indicate that Pd grows more roughly than Cu by the time 15 ML have been deposited, other simulations indicate the opposite. The differences between Cu and Pd are not significant in the scope of the current analysis.

Cluster Size Effects

5-atom clusters

The deposition of 5-atom clusters produces somewhat different results than those discussed above for the 10-atom clusters. A compact 5-atom cluster deposited on a flat (001) surface with a small kinetic energy (0.25 eV total, or 0.05 eV per atom) typically flattens into a single layer such that all of the atoms adsorb directly on the surface. The adsorption energy of the cluster is thus five times that of a single atom, or roughly 15 eV.

This large amount of energy increases the mobility of the atoms as they reach the surface and results in a variety of final structures for the deposited cluster. When a small, compact cluster is deposited, several atoms may compete for the same adsorption site on the surface. An atom might not remain in the first stable site it finds since all of the atoms in the depositing cluster must find a stable adsorption site. (This is a decided contrast to the single-atom deposition process.[9]) The adsorption energy of a neighboring cluster atom may be partially transferred to that first-adsorbed atom and allow it to sample a larger number of sites. Similarly the impact of neighboring cluster atoms may transfer momentum to the first atom, in effect knocking the adsorbed atom out of the way for the next cluster atom to take its place. This "mobility" of the cluster atoms lasts for only 5-10 ps and is not seen at all for some deposited clusters.

The result of this increased mobility is evident in the final structure of the deposited clusters, in that the cluster does not necessarily remain intact once all of the atoms are adsorbed on the surface. In fact, one or all of the adsorbed cluster atoms may not be within a nearest neighbor distance of any other cluster atom. This does not occur as often for deposition of 10-atom clusters since the increased coordination of atoms in the larger cluster makes it more difficult for individual atoms to break away during adsorption. Also, some of the atoms in the larger cluster remain in new adsorption sites created in the second layer rather than adsorbing directly on the surface, decreasing both the total adsorption energy and the site competition of the cluster.

Fewer overhanging atoms are observed on the surface during deposition of 5-atom clusters, indicating that the empty fourfold hollow sites may be filled more efficiently than for

both larger cluster deposition and single-atom deposition. This is in agreement with the increased mobility of the small clusters during the adsorption process.

Overall, the deposition of smaller clusters can lead to a smoother surface than seen for the larger, 10-atom clusters. Figure 6 plots the interface width for two Pd/Pd(001) simulations of 5-atom cluster deposition, and one is noticeably smaller than that for 10-atom cluster deposition in Figure 3. The (111) facets are still observed during deposition of 5-atom clusters but they tend to be smaller than for the 10-atom cluster deposition. The smaller size of the 5-atom clusters increases the probability that they may reach the base of a hole or gap between islands without being attracted to the side walls as occurs for the 10-atom clusters. This may not decrease the surface roughness, however, since a cluster adsorbed high on a side wall can block lower exposed layers from the surface as effectively as one landing further down in the hole itself. Note that the smaller cluster size does not guarantee a smoother surface, as illustrated in Figure 6, since the effects of the random aiming points are still prominent due to the small surface area.

The size of the system (11 x 11 atoms) does not appear to influence the surface structure during deposition of 5-atom clusters. The islands and other surface structures are smaller than during deposition of 10-atom clusters and do not significantly interfere with one another through the periodic boundary conditions.

100-atom clusters

The deposition of a 100-atom cluster is in some respects simpler than that of the smaller 5-atom and 10-atom clusters. This large, spherically compact cluster has a rough diameter of nearly six atoms and results in atoms being added to at least four layers on the surface. The

adsorption energy plus the small initial kinetic energy (0.0025 eV/atom) of the cluster is not large enough to allow the cluster to flatten into a two-dimensional structure, as has been seen for simulations using high temperature or energetic cluster deposition.[3,7]

Deposition of the first 100-atom cluster on a clean (001) surface results in a single, 4- to 5-atom high pyramid with (111) facetted sides. The close-packed cluster atoms rearrange upon adsorption to match the fcc(001) structure of the substrate while retaining their high coordination within the cluster as much as possible. This rearrangement is complete within 5-7 ps of the cluster reaching the surface. Fewer than half of the cluster atoms adsorb directly on the surface. For example, the final structure of a 100-atom cluster deposited on a clean (001) surface consists of only about 35 atoms in the first adsorbate layer and 30 atoms in the second layer.

Subsequent clusters may add to the sides of this pyramid or adsorb on another clean area of the surface. On a rough surface, atoms along the sides of the depositing cluster may also adsorb on the islands. After a few clusters have been deposited, however, any exposed substrate area remaining in these MD simulations is not big enough for another cluster to reach the surface without being attracted to a nearby island. One deposited 100-atom cluster covers more than one-fourth of the 11 x 11 substrate surface area. Realistic MD simulations of thin film growth via deposition of 100-atom clusters would require a much large surface area (perhaps 50 x 50 atoms) to avoid effects from the periodic boundary conditions. Unfortunately, such a simulation is not practical at this time. Therefore we restrict our comments to the deposition process of a single 100-atom cluster and some general observations about the film growth process with these large clusters.

As a depositing 100-atom cluster adsorbs on the top few layers of a pyramid face, overhanging rows are formed to minimize the disruption to the cluster structure. This can result in several rows of overhanging atoms stacked on top of one another, forming an inverted (111) facet. Each atom in an overhanging row has only two supporting atoms, except for those on the ends of the row which can have three (or only one) supporting atoms. The overhanging rows are stabilized by nearest neighbors above them in the cluster rather than by supporting atoms in standard fourfold hollow sites on the surface. This avoids the bond-breaking within the cluster which would occur if the cluster atoms were to extend the (111) facet by adding to more layers of the pyramid.

A 100-atom cluster can immediately cover all or part of a hole in the surface if it happens to land on top of one. The stability of overhanging rows and the high coordination of most atoms in the cluster eliminate the need for a large structural rearrangement of the cluster upon adsorption. However, some rearrangements have been observed for 100-atom clusters. The most common structural change is caused by the cluster shearing along the (111) plane to move part of the cluster to a lower layer shortly after deposition.

Conclusions

The growth of thin metal films via low energy cluster deposition is much rougher than that of the corresponding films grown via single atom deposition. The increased surface roughness during cluster deposition can be attributed to two factors: (1) most deposition events add atoms to two or more layers; and (2) the growth of (111) facets produces many partially exposed atoms. Neither of these features was observed during the deposition of single atoms.

Thin films grown by deposition of larger clusters tend to be rougher than those produced by smaller cluster deposition. This is mostly due to the fact that larger clusters are more likely to be attracted to an existing island on the surface than to land in a hole or narrow gap between islands. Also, the atoms in larger clusters have a higher coordination and thus are more likely to retain the original cluster structure upon adsorption.

The growth behavior of a thin film in the multilayer regime cannot be simply extrapolated from the initial stages of deposition, in agreement with earlier results[9] for the deposition of single atoms. Likewise thin film growth via cluster deposition cannot be extrapolated from single atom deposition results, since deposition of a cluster can be a much more complicated event as seen in this and previous MD studies.[6] For example, the strong bonding within a cluster can affect the final structure of the cluster on the surface, as well as collisions between cluster atoms[8] as the cluster approaches the surface. The cluster size is also an important parameter and does not have a direct analogue in the deposition of single atoms. The explicit simulation of multiple-layer thin film growth via cluster deposition, using reliable interatomic potentials for metals, is therefore necessary to elucidate the growth mechanisms.

From these results, it is clear that the presence and size of clusters during deposition can greatly affect the final structure of a thin film as compared to deposition of single atoms. If high-quality thin films are desired, the low energy deposition of single atoms is shown to be preferred over deposition of small clusters. The MD simulations of cluster deposition presented here correspond to conditions in the LECBD experiments[5] which preserve some of the original cluster structure in the thin film.

Acknowledgements

This work was supported by NSF grant CHE-9224884.

References

[1] I. Yamada, G. H. Takaoka, H. Usui, and S. K. Koh, Mater. Res. Soc. Symp. Proc. **206** (*Clusters and Cluster-Assembled Materials*), 383 (1991); T. Takagi, *Ionized-Cluster Beam Deposition and Epitaxy* (Noyes, Park Ridge, NJ, 1988); I. Yamada, H. Usui, and T. Takagi, Z. Phys. D **3**, 137 (1986); I. Yamada, H. Takaoka, H. Usui, and T. Takagi, J. Vac. Sci. Tech. A **4**, 722 (1986).

[2] H. Haberland, M. Karrais, M. Mall, and Y. Thurner, J. Vac. Sci. Tech. A **10**, 3266 (1992).

[3] H. Haberland, Z. Insepov, and M. Moseler, Phys. Rev. B **51**, 11061 (1995).

[4] H. Haberland, M. Leber, M. Moseler, Y. Qiang, O. Rattunde, T. Reiners, and Y. Thurner, Mater. Res. Soc. Symp. Proc. **388** (*Film Synthesis and Growth Using Energetic Beams*), 207 (1995); H. Haberland, Z. Insepov, M. Karrais, M. Mall, M. Moseler, and Y. Thurner, Mater. Sci. Eng. B **19**, 31 (1993).

[5] P. Melinon, V. Paillard, V. Dupuis, A. Perez, P. Jensen, A. Hoareau, J. P. Perez, J. Tuaillon, M. Broyer, J. L. Vialle, M. Pellarin, B. Baguenard, and J. Lerme, Int. J. Mod. Phys. B **9**, 339 (1995); A. Perez, P. Melinon, V. Paillard, V. Dupuis, P. Jensen, A. Hoareau, J. P. Perez, J. Tuaillon, M. Broyer, J. L. Vialle, M. Pellarin, B. Baguenard, and J. Lerme, Nanostruct. Mater. **6**, 43 (1995); V. Dupuis, J. P. Perez, J. Tuaillon, V. Paillard, P. Melinon, G. Guiraud, J. P. Dupin, A. Perez, L. Thomas, B. Barbara, and B. Bouchet, Scr. Metall. Mater. **33**, 1563 (1995); J. D. Bielefeld and R. P. Andres, Mater. Res. Soc. Symp. Proc. **317** (*Mechanisms of Thin Film Evolution*), 155 (1994).

[6] L. Rongwu, P. Zhengying, and H. Yukun, Phys. Rev. B **53**, 4156 (1996); Z. Insepov, M. Sosnowski, G. H. Takaoka, and I. Yamada, Mater. Res. Soc. Symp. Proc. **316** (*Materials Synthesis and Processing Using Ion Beams*), 999 (1994); H.-P. Cheng and U. Landman, J. Phys. Chem. **98**, 3527 (1994); W. D. Luedtke and U. Landman, Phys. Rev. Lett. **73**, 569 (1994); A. Miyamoto, R. Yamauchi, and M. Kubo, App. Surf. Sci. **75**, 51 (1994); H. Haberland, Z. Insepov, and M. Moseler, Z. Phys. D **26**, 229 (1993); H. Hsieh and R. S. Averback, Phys. Rev. B **45**, 4417 (1992); C. L. Cleveland and U. Landman, Science **257**, 355 (1992); P. Blandin, C. Massobrio, and J. Buttet, Mater. Res. Soc. Symp. Proc. **278** (*Computational Methods in Materials Science*), 249 (1992).

[7] K.-H. Müller, J. Appl. Phys. **61**, 2516 (1987).

[8] R. Biswas, G. S. Grest, and C. M. Soukoulis, Phys. Rev. B **38**, 8154 (1988).

[9] C. L. Kelchner and A. E. DePristo, "Molecular dynamics simulation of multilayer homoepitaxial deposition on fcc(100) metal surfaces," J. Vac. Sci. Tech. A (in press, March 1996); C. L. Kelchner and A. E. DePristo, "Molecular dynamics simulations of multilayer homoepitaxial thin film growth," Surf. Sci. (to be submitted).

[10] S. W. Rosencrance, J. S. Burnham, D. E. Sanders, C. He, B. J. Garrison, N. Winograd, Z. Postawa and A. E. DePristo, Phys. Rev. B **52**, 6006 (1995); C. L. Kelchner, D. M. Halstead, L. S. Perkins, N. M. Wallace, and A. E. DePristo, Surf. Sci. **310**, 425 (1994); M. S. Stave and A. E. DePristo, J. Chem. Phys. **97**, 3386 (1992); S. B. Sinnott, M. S. Stave, T. J. Raeker, and A. E. DePristo, Phys. Rev. B **44**, 8927 (1991); T. L. Wetzel and A. E. DePristo, "Structures and energetics of Ni_{24}-Ni_{55} clusters," J. Chem. Phys. (in press, March 1996).

[11] T. J. Raeker and A. E. DePristo, Int. Rev. Phys. Chem. **10**, 1 (1991).

[12] A. E. DePristo, in *Recent Advances in Density Functional Theory*, vol. 1, Part 1, ed. D. Chong, (World-Scientific, Singapore, 1996) ch. 6.

[13] J. W. Evans, Phys. Rev. B **43**, 3897 (1991).

[14] R. Kunkel, B. Poelsema, L. K. Verheij, and G. Comsa, Phys. Rev. Lett. **65**, 733 (1990).

[15] D. M. Halstead and A. E. DePristo, Surf. Sci. **286**, 275 (1993).

[16] L. M. Sander, in *Solids Far From Equilibrium: Growth Morphology and Defects*, ed. C. Godrèche (Cambridge University Press, Cambridge, 1991); F. Family and T. Vicsek, J. Phys. A **18**, L75 (1985).

Table 1. Range of interface width at several coverages for all simulations of deposition via single atoms and two different cluster sizes. (These values include 5, 4, and 8 simulations for single atom, 5-atom, and 10-atom cluster deposition, respectively. Results from both Cu and Pd are included.)

	single atom	5-atom	10-atom
5 ML	0.7 - 0.9	1.0 - 1.6	1.7 - 3.1
10 ML	0.7 - 1.2	1.5 - 3.1	2.0 - 4.3
15 ML	0.9 - 1.5	2.4 - 3.3	1.3 - 5.1

Table 2. The interface width is fit to $w = A\theta^{\beta}$ for deposition of 10 ML by 10-atom clusters. The time between depositions is listed in the first column and shows little effect on the results. Averaging w over the four simulations on the smaller surface for each metal yields the fitting parameters given in the "averaged w" row. The RMS deviation from the fit is also listed.

11 x 11 surface							
Pd/Pd(001)	A	β	RMS	Cu/Cu(001)	A	β	RMS
10 ps	0.702	0.626	0.180		0.975	0.487	0.333
10 ps	1.094	0.332	0.191		1.286	0.234	0.240
20 ps	0.902	0.462	0.229		1.073	0.418	0.242
30 ps	0.889	0.753	0.190		0.791	0.712	0.122
averaged w	0.883	0.562	0.098		1.037	0.458	0.092
17 x 17 surface							
10 ps	0.984	0.368	0.051				
10 ps	0.793	0.602	0.137				

Figure Captions

Figure 1. Top view of Cu/Cu(001) surface at θ_{tot} = 6 ML during deposition of 10-atom clusters. A (111) facet and a (100)-type vertical wall can be seen. There are 10 adsorbate layers growing and the substrate is still exposed.

Figure 2. Side view of the surface in Figure 1.

Figure 3. Interface width during deposition of 10-atom clusters of Pd/Pd(001), 11 x 11, 80 K. (Calculated after each deposition event.)

Figure 4. Interface width during deposition of 10-atom clusters of Pd/Pd(001), 17 x 17, 80 K. (Calculated after each deposition event.)

Figure 5. Interface width during deposition of 10-atom clusters of Cu/Cu(001) and Pd/Pd(001), 11 x 11, 80 K. All simulation parameters are identical.

Figure 6. Interface width during deposition of 5-atom clusters of Pd/Pd(001), 11 x 11, 80 K. (Calculated after each deposition event.)

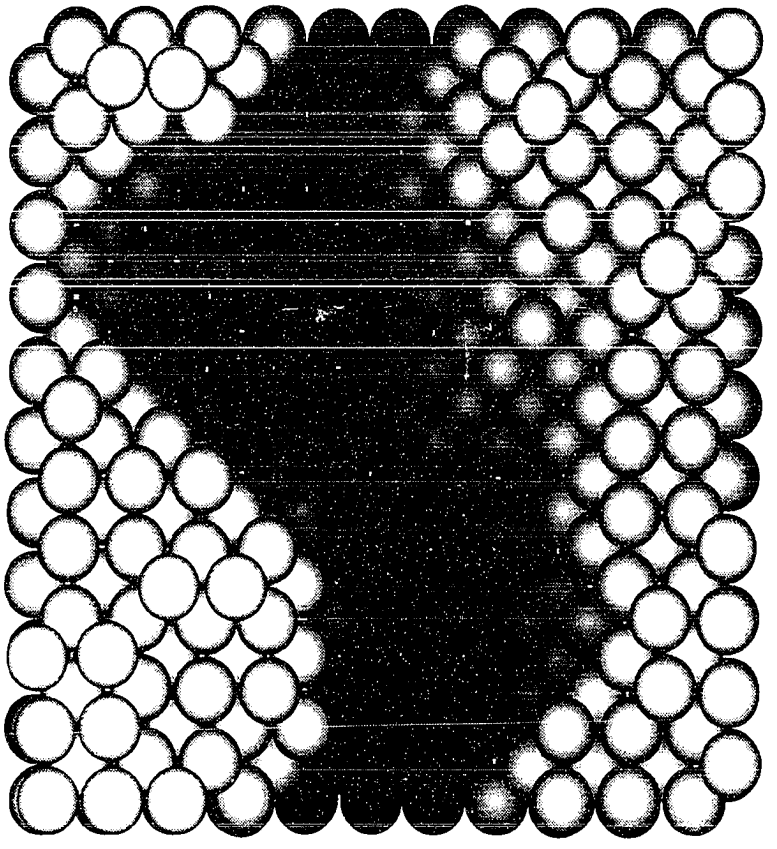

Figure 1.

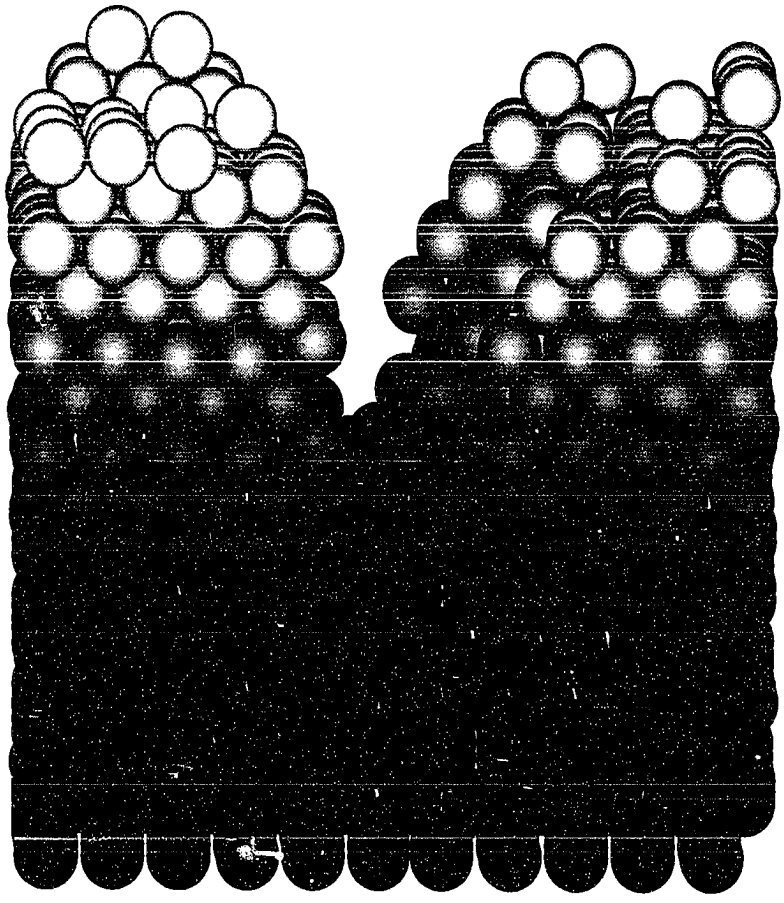

Figure 2.

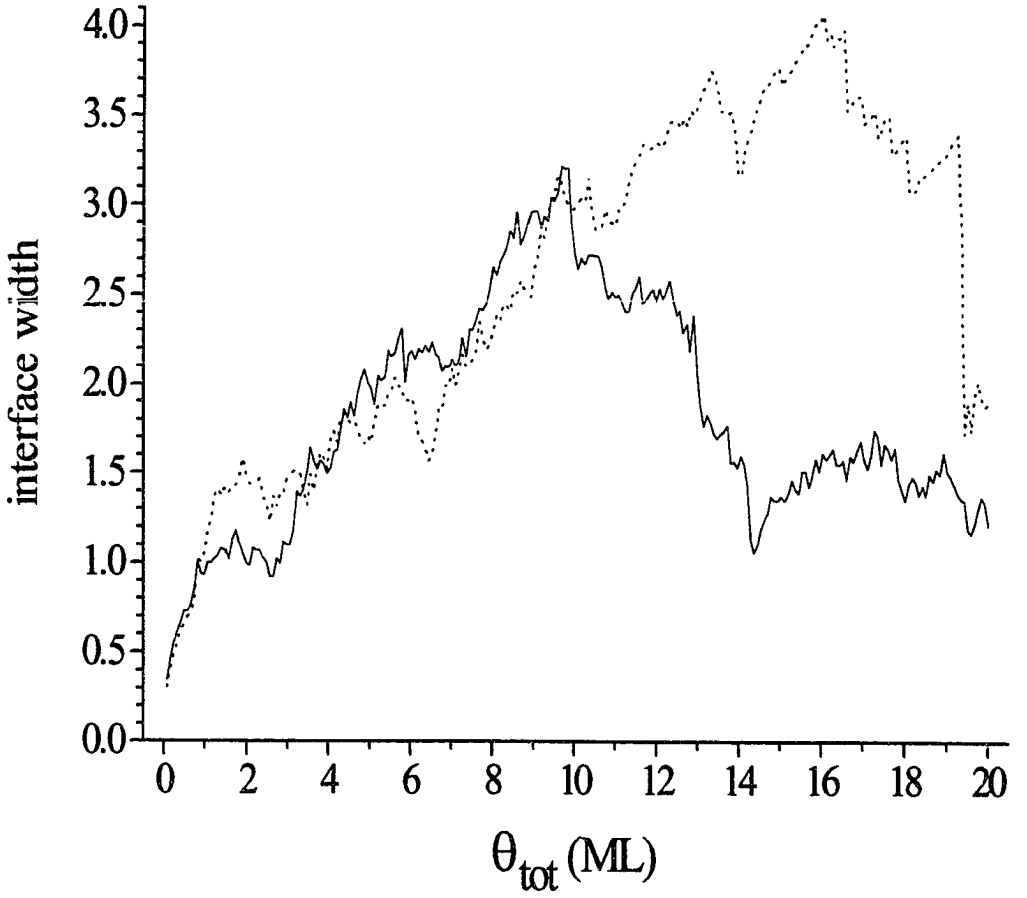
interface width
4.0
3.5
3.0
2.5
2.0
1.5
1.0
0.5
0.0
0
2
4
6
8
10
12
14
16
18
20
θtot (ML)

Figure 3.

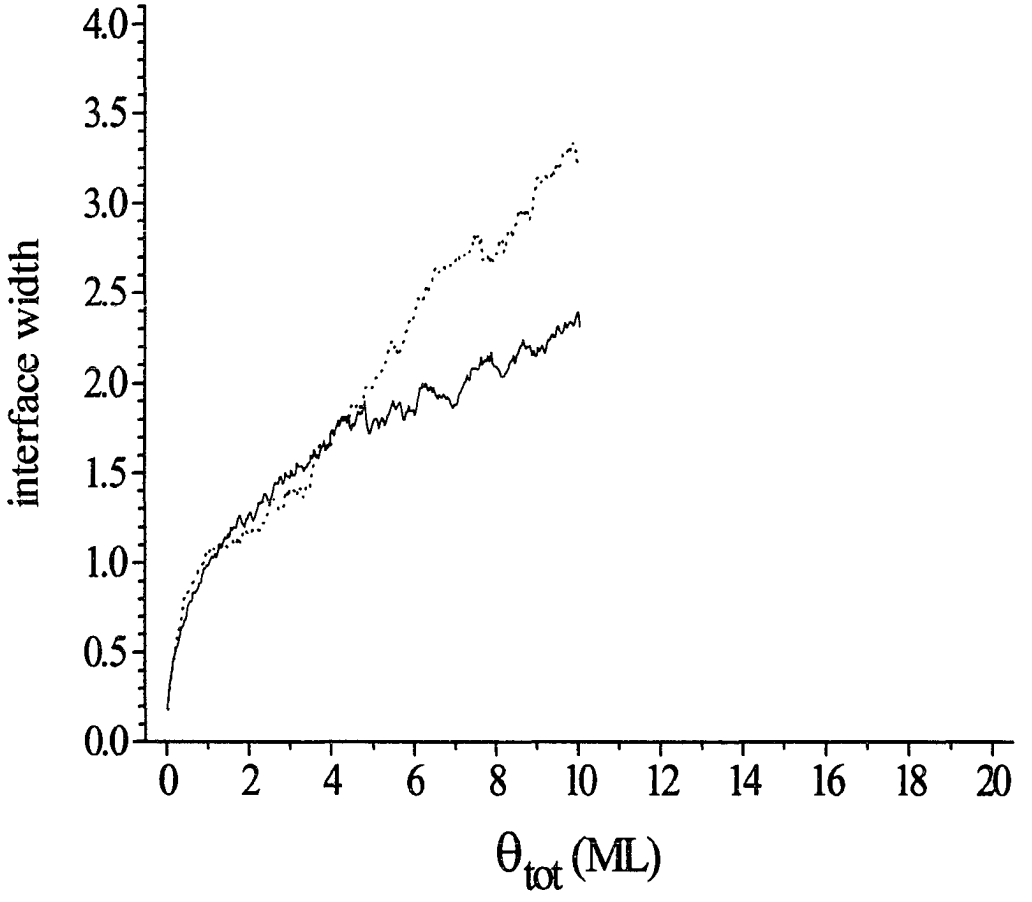
interface width
4.0
3.5
3.0
2.5
2.0
1.5
1.0
0.5
0.0
0
2
4
6
8
10
12
14
16
18
20
θtot (ML)

Figure 4.

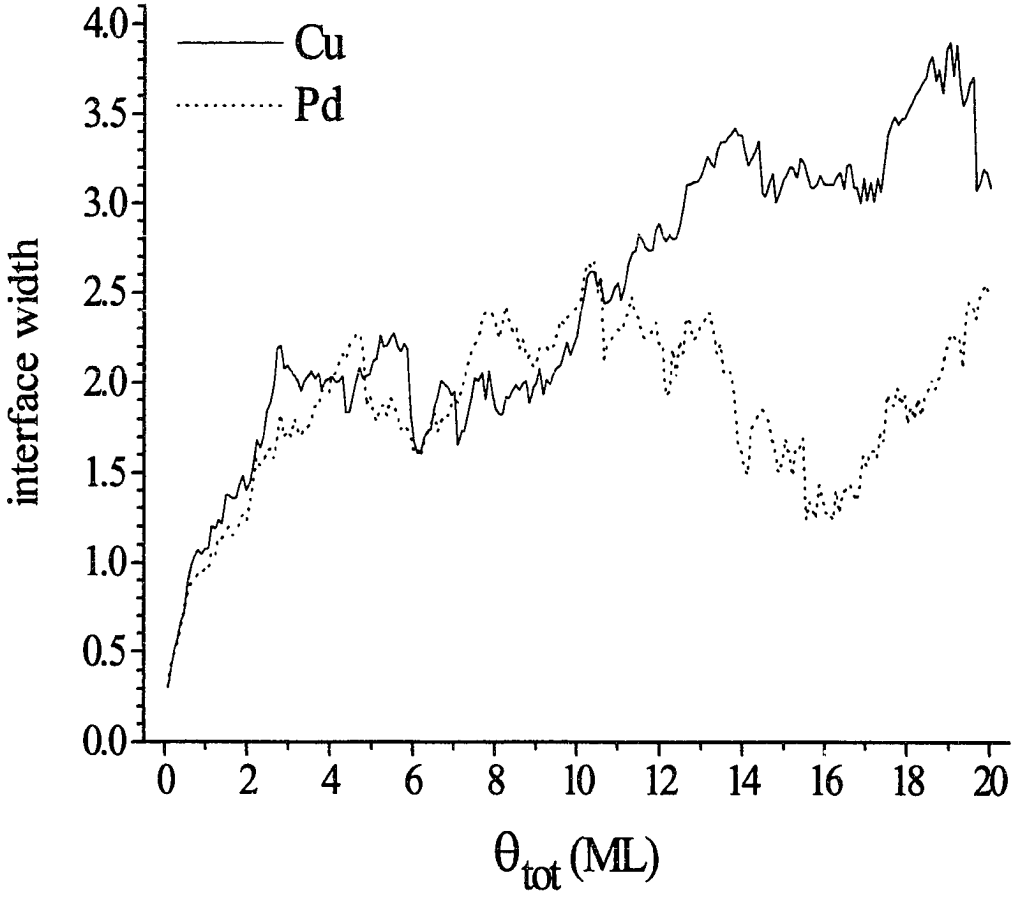
Cu
Pd
interface width
4.0
3.5
3.0
2.5
2.0
1.5
1.0
0.5
0.0
0
2
4
6
8
10
12
14
16
18
20
θtot (ML)

Figure 5.

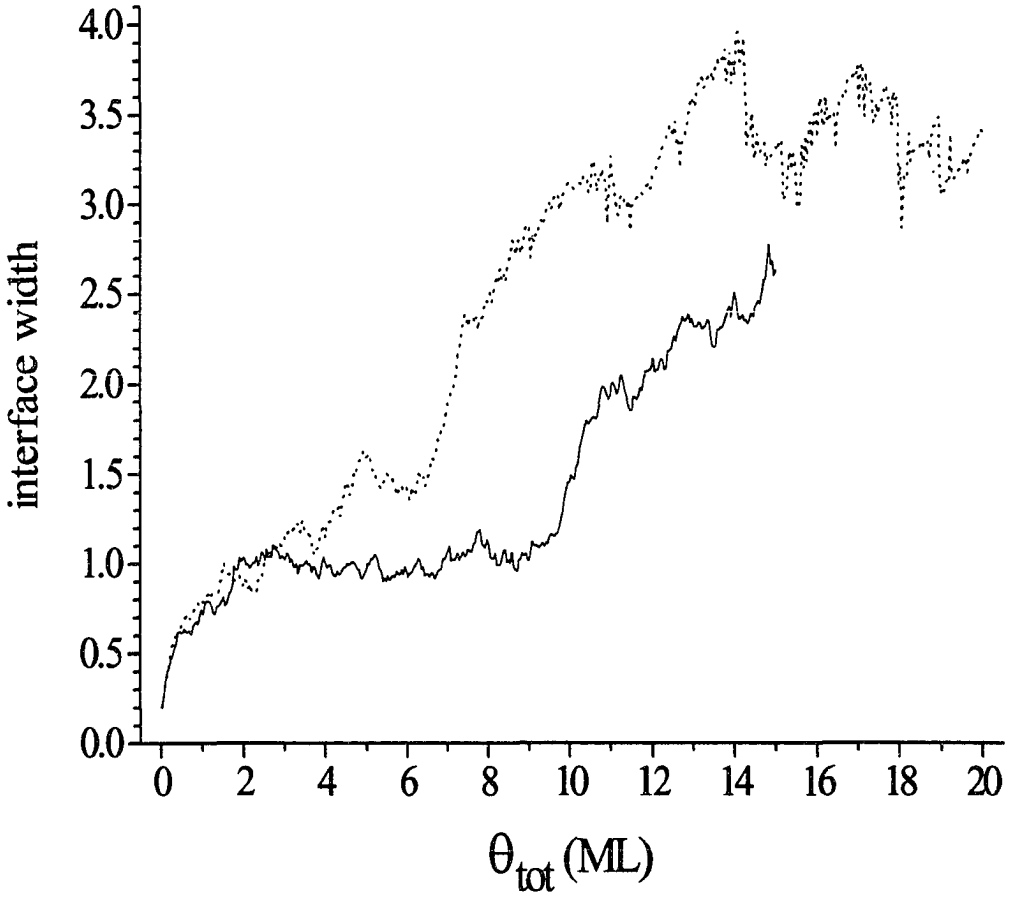
interface width
4.0
3.5
3.0
2.5
2.0
1.5
1.0
0.5
0.0
0
2
4
6
8
10
12
14
16
18
20
θtot (ML)

Figure 6.

GENERAL CONCLUSIONS

In this dissertation, the growth of multiple-layer homoepitaxial thin metal films has been studied in detail using molecular dynamics (MD) simulations with reliable interatomic potentials. This work represents the first such simulations of multiple-layer thin film growth by deposition of single atoms and also by deposition of low energy clusters. Related studies have focused on the initial stages of deposition and growth (up to 3 layers) for single atom deposition[1] or the deposition of a single cluster of atoms.[2] However, the growth behavior of a thin film in the multilayer regime cannot be simply extrapolated from the initial stages of deposition since, as shown in this work, the growth mechanisms can change with the thickness of the film.

Likewise thin film growth via cluster deposition cannot be extrapolated from single atom deposition results, since deposition of a cluster can be a much more complicated event as seen in this and previous MD studies.[2] The cluster size has also been shown to be an important parameter that does not have a direct analogue in the deposition of single atoms. The explicit simulation of multiple-layer thin film growth via cluster deposition is therefore necessary to elucidate the growth mechanisms.

Two significant features are observed during the growth of 50-layer thin films by deposition of single atoms of Pd on Pd(001) and Cu on Cu(001) at 80 K. First, the overhang sites on the surface can be stable, in contrast to the common view that only complete fourfold hollow sites are stable on the fcc(001) surface. This can greatly increase the surface roughness by allowing defects in the growing surface. Most growth models do not include defects of any kind. Second, multiatom rearrangement events occur during growth. These fill

or cover deep holes in the surface and thus tend to decrease the local surface roughness. Such multiatom processes are not included in any of the current growth models.

The structure of a thin metal film grown by single atom deposition at low temperature is largely due to the stability of deposited atoms in overhang sites. Nearly all of the surface structure and growth mechanisms described for $\theta_{tot} > 5$-10 ML are consequences of the presence of overhanging atoms during thin film growth: (1) surface roughness; (2) formation of voids; and (3) multiatom rearrangement events.

The growth of thin metal films via low energy cluster deposition is much rougher than that of the corresponding films grown via single atom deposition. The increased surface roughness during cluster deposition can be attributed to two factors: (1) most deposition events add atoms to two or more layers; and (2) the growth of (111) facets produces many partially exposed atoms. Thin films grown by deposition of larger clusters tend to be rougher than those produced by smaller cluster deposition. Furthermore, the atoms in larger clusters have a higher coordination and thus are more likely to retain the original cluster structure upon adsorption.

Dynamical features of thin film growth involve multiple layers of the film and many atoms in (1) multiatom rearrangement events and (2) formation of large holes and voids. The rearrangement events provide a mass transport mechanism which can be important especially in the absence of surface diffusion. One consequence of these local dynamical features is that the surface roughness determined by experiment may appear much more uniform since it is averaged over a large surface area and many deposition events.

References

[1] Y. Li, T. J. Raeker, and A. E. DePristo, Phys. Rev. B **50**, 14742 (1994);
G. Bilalbegovic and A. E. DePristo, Surf. Sci. **302**, L299 (1994);
T. J. Raeker and A. E. DePristo, Surf. Sci. **317**, 283 (1994);
S. Liu, Z. Zhang, J. Nørskov, and H. Metiu, Surf. Sci. **321**, 161 (1994);
J. C. Hamilton, M. S. Daw, and S. M. Foiles, Phys. Rev. Lett. **74**, 2760 (1995).
C. M. Gilmore and J. A. Sprague, J. Vac. Sci. Tech. A **13**, 1160 (1995);
J. A. Sprague and C. M. Gilmore, Surf. Coat. Technol. **65**, 71 (1994);
J. A. Sprague and C. M. Gilmore, Mater. Res. Soc. Symp. Proc. **268** (*Materials Modification by Energetic Atoms and Ions*), 115 (1992);
C. M. Gilmore and J. A. Sprague, Surf. Coat. Technol. **51**, 324 (1992);
C. M. Gilmore and J. A. Sprague, Phys. Rev. B **44**, 8950 (1991);
T. D. Andreadis, M. Rosen, M. I. Haftel, and J. A. Sprague, Mater. Res. Soc. Symp. Proc. **202** (*Evolution of Thin Film and Surface Microstructure*), 283 (1991);
M. Villarba and H. Jonsson, Phys. Rev. B **49**, 2208 (1994);
M. Breeman, G. T. Barkema, D. O. Boerma, Surf. Sci. **307-309**, 526 (1994);
P. Stoltze and J.K. Nørskov, Phys. Rev. B **48**, 5607 (1993).

[2] L. Rongwu, P. Zhengying, and H. Yukun, Phys. Rev. B **53**, 4156 (1996);
H. Hsieh and R. S. Averback, Phys. Rev. B **45**, 4417 (1992);
Z. Insepov, M. Sosnowski, G. H. Takaoka, and I. Yamada, Mater. Res. Soc. Symp. Proc. **316** (*Materials Synthesis and Processing Using Ion Beams*), 999 (1994);
H.-P. Cheng and U. Landman, J. Phys. Chem. **98**, 3527 (1994);
C. L. Cleveland and U. Landman, Science **257**, 355 (1992);
A. Miyamoto, R. Yamauchi, and M. Kubo, App. Surf. Sci. **75**, 51 (1994);
P. Blandin, C. Massobrio, and J. Buttet, Mater. Res. Soc. Symp. Proc. **278** (*Computational Methods in Materials Science*), 249 (1992).

ACKNOWLEDGEMENTS

I would like to thank Dr. Andrew E. DePristo for his guidance and support as my major professor. It has been a long road, and his encouragement has been appreciated.

I have also received encouragement and recognition in the form of a graduate student award from the American Vacuum Society (AVS). The 1995 Nellie Yeoh Whetten Award affirmed that my research topic and results were important and interesting to a wider audience, just at the inevitable stage of my research where I was beginning to doubt its value. I am grateful to the AVS for sponsoring such awards.

Finally, I would like to thank my husband, Scot, for all his support and much-needed distractions. We have kept each other sane while writing our respective theses at the same time.